Characterizing Pathways of Groundwater Recharge and Discharge in a Geologically and Topographically Complex Watershed

by

Reid Dauphinee

Submitted in partial fulfilment of the requirements
for the degree of Master of Applied Science

at

Dalhousie University
Halifax, Nova Scotia
December 2024

Dalhousie University is located in Mi'kma'ki, the
ancestral and unceded territory of the Mi'kmaq.
We are all Treaty people.

TABLE OF CONTENTS

LIST OF TABLES

LIST OF FIGURES

ABSTRACT

Groundwater is an increasingly important source of drinking water for many Canadian and First Nations communities. However, groundwater-surface water interactions and the effects of climate change on groundwater recharge remain poorly understood, especially in cold regions with complex geology and topography. This study focuses on the Christmas Brook watershed and connected fault aquifer system, which supplies water to Eskasoni First Nation, Nova Scotia, Canada. The objectives are to quantify the sources and flow pathways of streamflow and groundwater recharge feeding the pumping wells, informing watershed management in low mountain settings. Water sampling, hydrochemical mixing analysis, hydrometric monitoring, and groundwater modelling were used to achieve these objectives.

A total of 134 samples were analyzed for ions, isotopes, and metals. Stream gauging stations were installed at the highland wetland outlet and lowland watershed outlet. Level loggers were placed in highland bedrock and wetland observation wells. A weather station (Davis Instruments) in the highland area provided data for comparison with a lowland ECCC station 3 km away. Hydrochemical results show that groundwater contributes 27 ± 15% of streamflow at the downstream station, increasing downstream and during spring and fall. The remaining 73 ± 15% originates from the wetlands and lakes in the headwaters. A MODFLOW6 groundwater model with particle tracking indicates that streamflow infiltration contributes 60% of pumping well water, while local fractured rock recharge accounts for 40%. Wetlands and the area around the wells are critical for groundwater recharge and streamflow generation. These findings enhance understanding of groundwater-surface water interactions, supporting collaborative water management and climate change research in low mountain regions.

ACKNOWLEDGEMENTS

I would like to express my gratitude to my supervisor, Dr. Lauren Somers, for her support, mentorship, and the opportunities she has provided throughout my research. I also thank my committee members, Fred Baechler and Dr. Barret Kurylyk, for their valuable input and feedback. I am grateful to my labmates, Jacob Steel and Amber Dort, for their friendship and support, as well as to past and present members of the Somers Hydrologic Change Lab for their assistance in both the lab and field. I would also like to acknowledge Richard Winston of the United States Geological Survey (USGS) and the team at Eskasoni Fish and Wildlife Commission (EFWC) for their contributions. Finally, these results are a testament to the unwavering support I have received from my friends and family.

CHAPTER 1 – INTRODUCTION

1.1 Importance and Threats to Groundwater Resources

1.1.1 Global and Local Importance of Groundwater Resources

Groundwater is an essential resource, providing approximately a quarter of all the water used by humans worldwide (United Nations, 2022). Groundwater also plays a significant role in supporting aquatic ecosystems, especially during periods of drought, when baseflow (groundwater discharge to streams) provides a resilient and consistent water source due to its delayed and dampened response to climate variations compared to surface water systems (Griebler & Maria, 2015). Beyond their use for drinking water and agriculture, groundwater and springs are also a vital recreational and spiritual resource in many cultures and communities (Blackstock, 2001). Given the slow replenishment and potential for contamination, a preventative approach to groundwater management is critical to ensure it remains a sustainable resource for future generations (Government of Canada, 2017).

Groundwater serves as the primary domestic water source for 30% of Canadians, and its importance is even more pronounced in rural areas (Government of Nova Scotia, 2023). In Nova Scotia, groundwater is a crucial resource, particularly in rural areas where it forms most (90+%) of the domestic water supply through both private and public wells. The province's groundwater quality is generally considered good given limited agricultural or industrial activities. However, challenges remain regarding natural heavy metal contamination and water quantity challenges. Anthropogenic pollutants such as fertilizers, pesticides, road salt, and hydrocarbons pose threats to groundwater quality. Additionally, natural groundwater contamination from geologic strata (i.e., geogenic contamination) is a major concern, with elevated levels of arsenic, iron, manganese, and salinity frequently reported in some regions (Nova Scotia Museum, 2017). Although

natural filtration during groundwater flow through geologic materials offers some protection against certain pollutants, this benefit is limited in areas with thin till cover and shallow water tables (Nova Scotia Museum, 2017; U.S. Geological Survey, 1999). Effective management and protection of Nova Scotia's groundwater is essential to prevent long-term contamination and ensure this vital resource remains safe and abundant.

1.1.2 Threats to Sustainable Groundwater Use

Sustainable groundwater use is threatened by over-extraction, contamination and climate change. Over-extraction of groundwater is a critical issue worldwide, particularly in arid and semi-arid regions where it has led to alarming depletion rates, increased water costs, land subsidence, and seawater intrusion (Jia et al., 2020). The depletion of groundwater not only compromises water availability but also disrupts the ecological balance of nearby aquatic ecosystems, as reduced groundwater flow to streams diminishes the habitat and resources essential for native plant and animal species (de Graaf et al., 2019). Global-scale analysis indicates that the declines in groundwater levels associated with reaching environmental flow limits are unexpectedly small, with only minor reductions required to impact streamflow (de Graaf et al., 2019). These small declines suggest that environmental flow limits may be exceeded before significant groundwater depletion occurs, a phenomenon that varies depending on the specific groundwater–surface water interactions. As climate change and rising food demands intensify, the urgent need for sustainable groundwater management practices becomes increasingly evident to prevent long-term damage to both human and natural systems (Alley, Reilly, & Franke, 1999).

Groundwater contamination from anthropogenic and geogenic sources is also a major threat to sustainable groundwater use. Major groundwater contamination from anthropogenic sources includes nitrates and heavy metals like lead, which can leach from agricultural and industrial sites, areas of natural mineralization, and outdated water supply systems (Lasagna, De Luca, & Franchino, 2016; Podgorski & Berg, 2020;

Karthikyan & Lakshmanan, 2011). Additionally, geogenic contaminants like fluoride, uranium, and salinity are naturally occurring in certain geologic formations (e.g., granitic and volcanic bedrock), possibly reaching harmful levels in groundwater sources (Zhang et al., 2022; Kurwadkar, Kanel, & Nakarmi, 2020). In coastal regions, sea level rise (SLR) and the associated risk of saltwater intrusion are threatening many high-quality coastal aquifer systems (Costall et al., 2020; Hauer et al., 2021). In Atlantic Canada, over 140,000 people were living within less than 5 MASL as of 2021 (Government of Canada, 2024), many of whom depend on groundwater for their drinking water, illustrating the local importance of this issue.

Climate change poses a significant threat to groundwater resources by altering recharge rates, increasing the frequency of extreme weather events, and exacerbating the effects of groundwater extraction (Stigter et al., 2022). Shifts in temperature and precipitation patterns can lead to reduced groundwater recharge, particularly in regions already vulnerable to water scarcity. These changes jeopardize the sustainability of groundwater resources, with potentially severe consequences for both ecosystems and human populations reliant on these reserves (Klove et al., 2014).

In cold regions, climate change is causing major shifts in snow-dominated hydrological systems, which play a crucial role in regulating seasonal water availability in many montane regions (Barnett, Adam, & Lettenmaier, 2005). Warmer temperatures lead to reduced snow accumulation (increased precipitation as rain) and earlier snowmelt, disrupting the timing and magnitude of streamflow and groundwater recharge (Stewart, Cayan, & Dettinger, 2005; Cochand, Therrien, & Lemieux, 2018). This shift increases the risk of hydrologic drought during the summer months, further exacerbating water scarcity issues in regions dependent on snowmelt-fed rivers and aquifers (Nygren et al., 2020).

1.2 Groundwater Processes in Low Mountains

1.2.1 Importance of Mountain Groundwater Resources

Mountains and highlands play a crucial role in providing water resources to downstream regions. Due to orographic effects, mountains often receive increased precipitation relative to their adjacent lowlands and experience reduced evapotranspiration (ET). Furthermore, many mountain regions store water as snow in the winter and release it during drier periods, helping to buffer seasonality of precipitation (Goulden & Bales, 2014; Viviroli et al., 2007). Viviroli et al. (2020) predict that by 2050, around 1.5 billion people living in lowlands will be critically dependent on mountain runoff. Recent studies have emphasized the importance of groundwater in sustaining mountain streamflow and downstream water resources (Andermann et al., 2012; Galleani et al., 2011; Liu, Williams, & Caine, 2004; Xiao et al., 2023). Prioritizing headwater conservation is important because the quality and quantity of water in mountains is propagated downstream to lowland regions (Barnett et al., 2005; Finger et al., 2012; Stewart et al., 2005; Vörösmarty et al., 2005).

Low mountain regions like the Appalachians of eastern North America also play an important role in water supply (Fernandez & Zegre, 2019) but have typically been less studied than high mountain systems. Low mountain regions often exhibit orographic precipitation but typically experience a more moderate climate with lower precipitation rates and less seasonal variability compared to high-mountain regions (Pepin et al., 2022). Low mountain regions are more likely to have hybrid nival-pluvial hydrologic system, whereas high-mountain hydrology is often dominated by snowmelt and, in some cases, glaciers (Cochand, Therrien, & Lemieux, 2018). Additionally, low mountains typically have more and/or denser vegetation and therefore more ET, further influencing hydrological processes differently than the often sparse, high-altitude vegetation of high mountains (Somers & McKenzie, 2020).

1.2.2 Groundwater Recharge

Groundwater recharge is the process by which water from precipitation and surface sources infiltrates the subsurface to replenish aquifers. In low mountain regions, recharge occurs through infiltration of rain and snowmelt, as well as interactions with surface water bodies. Environmental factors such as topography, climate, vegetation, geology, and soil properties all play a role in regulating recharge (Goulden & Bales, 2014; Maule & Stein, 1990; Tetzlaff et al., 2014).

Vegetation impacts recharge by influencing soil moisture retention, evapotranspiration rates, and root depth, which affects how much water infiltrates to deeper soil layers and ultimately to the water table. Forested areas, for instance, may reduce recharge through higher evapotranspiration rates, while grassy or sparse vegetation cover can enhance infiltration by allowing more water to reach the subsurface (Jasechko et al., 2014; Evaristo & McDonnell, 2017).

The complex topography of high and low mountain regions alike influences groundwater recharge. Several studies have shown observable orographic effects over low mountains (Smith & Barstad, 2003; Minder et al., 2008). For example, a study from northern England showed orographic effects on rainfall distribution over the Pennine uplands (Burt & Ferranti, 2012). Meanwhile, slope and aspect influence snow accumulation, melt, and ET (Hock et al., 2019; Somers & McKenzie, 2020). Valleys, lower slope areas and leeward slopes tend to accumulate more snowpack and therefore more potential snowmelt recharge (Hood & Hayashi, 2015; Dunn, Langan, & Colohan, 2001).

Mountains, and cold regions generally exhibit strong hydrologic seasonality, driven by snow accumulation and melt (Viviroli et al., 2007). Several previous studies have found that winter precipitation is particularly important for groundwater recharge in mountains and cold regions. Jasechko et al. (2014) found that arid and temperate climates consistently have winter groundwater recharge exceeding that of summer. An isotopic study in central Canada indicated that snowmelt is the primary source of groundwater recharge (Jasechko et al., 2017). Several studies using oxygen-18 to partition stream

water sources in forested watersheds have reported snowmelt contributions ranging from 20% to 50% of streamflow during the spring melt period even when snow accounts for less than 30% of precipitation (Jenicek & Ledvinka, 2020; Miller, Lyon, & Miller, 2020; Li et al., 2021). In northern climates, dynamic groundwater storage is affected by the timing of snowmelt. Furthermore, seasonally frozen ground is a control on aquifer recharge (Nygren et al., 2020; Tetzlaff et al., 2014). These results indicate that small changes to winter recharge dynamics may have a larger overall impact on groundwater flux than the same change in summer months.

Geologic properties and soil type are additional controls on groundwater recharge, influencing how quickly water infiltrates and disperses through subsurface layers. Higher hydraulic conductivity generally allows water to flow more freely through the geologic matrix, promoting increased recharge under favorable conditions such as sufficient precipitation and unsaturated soil (Healy, 2010). Areas with high hydraulic conductivity are typically associated with sandy soils or fractured geological formations, while clay-rich soils and unfractured bedrock have lower hydraulic conductivity, restricting groundwater flow and reducing recharge potential (Fronzi et al., 2021). As depth increases, hydraulic conductivity often decreases due to compaction and reduced fracture frequency, limiting recharge to shallow, more permeable layers (Gleeson et al., 2016). Surficial deposits can act as collectors, slowly feeding recharge zones in deeper, faulted areas, which often rely on fractures to enhance vertical groundwater flow (Zarate et al., 2021). Additionally, groundwater flow can be anisotropic, with particle orientation promoting horizontal flow over vertical flow, which can influence recharge patterns (Aquilina et al., 2023).

In addition to recharge within mountains, mountain regions often provide groundwater recharge to adjacent lowland aquifers. Although definitions vary in the literature, Markovich et al (2019) define mountain front recharge (MFR) as any recharge originating within the mountain block (distinguished by its thin confining layer and elevated topography relative to the surrounding lowland) that enters a basin aquifer. MFR can then be broken down into two components: surface MFR and mountain block recharge (MBR). Surface MFR is the infiltration of mountain stream water into lowland

aquifers where the stream crosses the mountain front and encounters more permeable sediments. MBR is groundwater inflow to the lowland aquifer from an adjacent mountain block. Few studies have examined the extent to which MFR processes exist, or their importance, in low mountain environments.

1.2.3 Mountain Aquifers

Low-mountain aquifers, typically found in valley and foothill regions, include two main types: alluvial aquifers and fractured rock aquifers. Alluvial aquifers are generally unconfined, consisting of coarse-grained sediments such as gravel and sand that facilitate groundwater flow (Soulsby et al., 2000). In contrast, fractured rock aquifers, often in bedrock-dominated areas, rely on fractures and fault zones to transmit water, resulting in more localized and variable flow patterns (Larkin & Sharp, Jr., 1992). The physical landscape of low mountains, characterized by steep topography, creates significant hydraulic gradients that enhance recharge through fractures and permeable soils during snowmelt and rainfall events. Seasonal changes, such as snowmelt in spring or episodic rainfall, strongly influence water table dynamics. These events can temporarily increase hydraulic connectivity between surface water (e.g., streams, wetlands) and underlying groundwater, allowing for exchanges that may not occur under normal conditions (Cochand, Therrien, & Lemieux, 2018). This connectivity highlights how headwater systems and downstream aquifers are closely linked, with upland recharge areas playing an essential role in maintaining groundwater flow to lower elevation aquifers.

1.2.4 Fault Aquifers

Faults and fracture zones are common in mountain regions and can significantly influence groundwater flow (Allen & Nott, 2021). Faults are the fractured zones at the contact of two rock bodies which have moved relative to one another. Fault types include thrust, strike-slip, normal, transform, bedding plane detachment, and crustal structure

zones. Fault zone geology can be simplified into three features: the fault core, the damage zone and the prolith (undamaged host rock). The fault core can have a hydraulic conductivity up to seven orders of magnitude greater than the damage zone and a sharp transition from fault core to damage zone. The damaged zone can have permeability up to five orders of magnitude higher than the prolith and a gradual transition usually exists from the damage zone to prolith (Caine, Evans, & Forster, 1996; Karasaki et al., 2011).

Faults can act as either conduits or barriers to groundwater flow. They may facilitate the lateral movement of water through the fractured zone at a faster rate than the surrounding matrix, while the fault core (characterized by high deformation, fine material, and high compaction) can obstruct perpendicular flow but facilitate parallel flow (Moore & Walsh, 2021; Scibek, Gleeson, & McKenzie, 2016). These preferential pathways enable increased exchange between surface water and groundwater by allowing surface water to infiltrate more easily into the fractured zones of the fault, while groundwater can discharge more readily to surface water bodies, enhancing the interaction between the two systems. Additionally, fractures and fine-grain particulates in fault zones offer more surface area for groundwater to dissolve minerals, which can increase dissolved solids and potentially pose a risk to human health by increasing metal concentrations in the groundwater (Fronzi, et al., 2021).

Faults and associated damage zones can create viable aquifers in otherwise low-permeability rocks. For example, crystalline rocks (i.e., igneous, metamorphic) are generally thought to be poor aquifers due to their low porosity and permeability. However, the process of geologic faulting and deformation can increase these properties. In mountain settings, basement fracturing is often the source of spring water and is evidence of deep flow circulation via thermal monitoring (Bense et al., 2013). Several studies across North American mountain ranges indicate crystalline rock acting as conduit-barrier systems (Ball et al., 2010; White & Burbey, 2007). Roques et al. (2014) conducted a study in France with results indicating that sub-vertical faults act as the primary connection between adjacent aquifers.

While the role of fault systems in fluid hydrocarbon transfer and geotechnical assessments has been extensively studied, only a small subset of research has focused on

the impact of fault structures on groundwater flow (e.g., Fronzi et al., 2021; Scibek, Gleeson, & McKenzie, 2016). Faulted areas can have more complex and variable head gradients due to the combined effects of enhanced flow paths and barriers created by faults. Furthermore, a fault acting as a barrier may not be evident until groundwater abstraction takes place, further hindering our understanding of fault aquifer systems (Bense et al., 2013). Leray et al. (2013) suggest that monitoring temperature and environmental tracers in complex hard rock and faulted aquifers can be used to further predict flow paths and increase certainty in transit times.

1.2.5 Groundwater-Surface Water Interactions

The interactions between streams, lakes, wetlands, and groundwater are complex yet vital to the water balance of a watershed. Groundwater-surface water interactions are increasingly recognized as critical aspects of riparian zone ecosystems (Steiness et al., 2019). In humid climates, streams often gain water from the underlying groundwater system because the high recharge and resulting hydraulic gradients of the surrounding fluvial plain directs groundwater flow towards the stream channel, creating natural zones of groundwater discharge (Woessner, 2000; Boulton et al., 2010; Hester et al., 2020). In areas surrounding lakes, the water table gradient controls groundwater seepage to and from the lake. Flow systems with low hydraulic gradients tend to exhibit localized flow patterns (Fetter, 2001). Similarly, smaller watersheds often have localized flow systems, which may not capture larger-scale hydrogeologic processes (Cowie et al., 2017).

Groundwater discharge to surface water bodies, known as baseflow, often sustains streamflow during dry and warm periods, supporting water resources and ecosystems. Baseflow recession during hydrograph analysis refers to the exponential decay of flow after a precipitation event. As the water table drops during dry periods, so does the rate of groundwater discharge to surface water bodies (Liu, Williams, & Caine, 2004; Somers et al., 2019). In mountain regions, several studies suggest that groundwater can contribute as much as ~60% to streamflow even during peak discharge in the melt season, although

this contribution is highly variable in different settings (Andermann et al., 2012; Galleani et al., 2011; Liu, Williams, & Caine, 2004; Xiao et al., 2023).

Surface water infiltration into groundwater can be a key mechanism for aquifer recharge in areas with hydrologic connectivity between streams, wetlands, lakes, and underlying aquifers. In low-mountain regions, this process is heavily influenced by both the permeability of surficial deposits and the underlying bedrock. For instance, alluvial and valley aquifers allow significant infiltration from adjacent water bodies, contributing to local groundwater storage (Liu, Williams, & Caine, 2004; Soulsby, Malcolm, & Malcolm, 2000). Wetlands serve an important role as natural recharge zones, where water temporarily pools and percolates slowly into the subsurface, enhancing groundwater levels during wetter periods (Tromp-Van Merveld, Peters, & McDonnell, 2007). Natural wetlands, particularly peatlands, which cover around 15% of the boreal land area (boreal biome; Helbig et al., 2020), provide valuable ecosystem services such as water retention during storm events, reducing flood impacts and maintaining baseflow (Acreman & Holden, 2013). Their high porosity and significant storage capacity make them crucial for sustaining groundwater recharge (Findlay & Kadykola, 2016). Understanding these wetland functions is essential for predicting hydrological responses to climate change or potential restoration actions (Kimmel, Kull, & Mander, 2008).

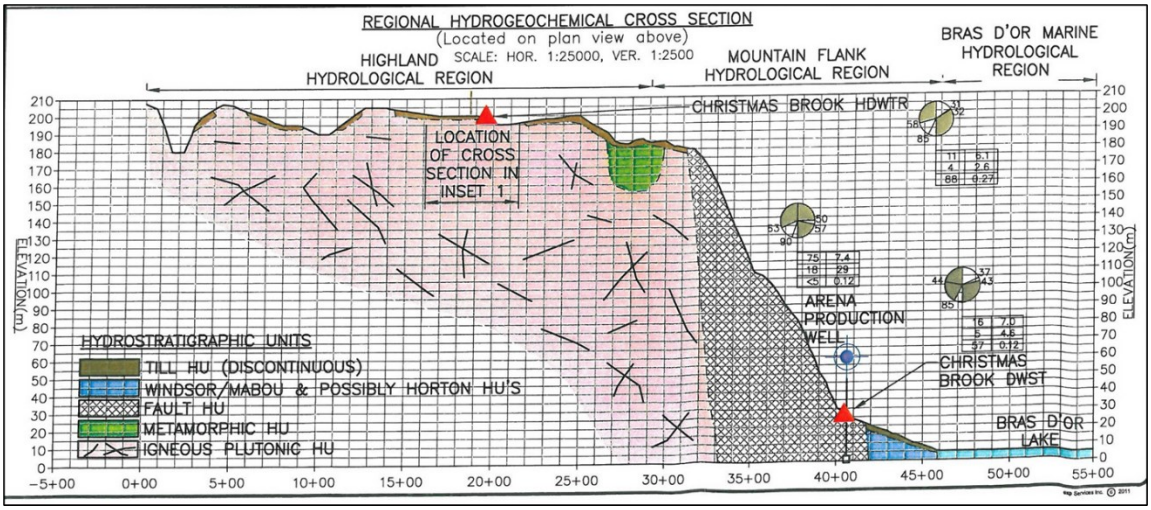

Figure 1: Conceptual figure - regional hydrochemical cross-section: A simplified cross-sectional representation of the Boisdale Hills study site.

1.2.6 Potential Climate Change Impacts

The direction and magnitude of changes in mountain groundwater storage remains poorly understood. Several studies indicate that projected changes in temperature, ET, and precipitation will impact groundwater recharge in mountain regions (Mountain Research Initiative EDW Working Group, 2015; Somers & McKenzie, 2020; Goulden & Bales, 2014; Samways et al., 2024). Projected temperature increases are nearly ubiquitous, but there is still high uncertainty regarding future precipitation trends and magnitude in many regions (Stocker et al., 2015). Furthermore, heterogeneous soil, geology, relief and land cover make it difficult to quantify not only the magnitude but even the direction of future precipitation and recharge trends (Kurylyk, MacQuarrie, & Voss, 2014; Stigter et al., 2022).

In many montane catchments, and cold regions generally, the primary source of groundwater recharge is snowmelt and a shift from snow to rain is projected to change the seasonality of recharge. For example, Cochand, Therrien, & Lemieux (2018) used a groundwater flow model to simulate the impacts of climate change on surface and subsurface flows in a low mountain watershed in Quebec, Canada. Simulations showed an increase in winter groundwater levels and a decrease in hydraulic head and streamflow during the summer. Furthermore, this decrease in solid precipitation may be accompanied by earlier snowmelt recharge and increased seasonal drought. However, Mackay et al., (2020) found that environments that experience high volumes of rain recharge with adequate storage can partially equalize or maintain stream flow through periods of drought.

Additionally, changes in seasonal soil freezing can significantly impact groundwater recharge and discharge processes. Kurylyk, MacQuarrie, and Voss (2014) modeled the dynamic freeze-thaw cycles in unconfined aquifers in New Brunswick, Canada, demonstrating that winter precipitation could still be released as groundwater before summer low-flow periods. This is influenced by the timing of subsurface freezing and thawing, which dictates how and when water infiltrates into the subsurface and contributes to streamflow. For instance, frozen soil reduces infiltration capacity due to

pore blockage, delaying recharge until soil thawing occurs. As highlighted in a study by Evans et al. (2018), the timing of these freeze-thaw processes can shift groundwater discharge to streams, creating a lag effect and impacting seasonal water availability. Furthermore, increased winter precipitation coupled with frozen topsoil conditions can exacerbate flood risks as surface runoff dominates when infiltration is limited.

1.3 Knowledge Gaps

Adequate management and protection of groundwater resources relies on an understanding of groundwater recharge pathways and interactions with surface waters. These processes shape the climate change and contamination risks to aquifers. In montane watersheds with complex topography and geology, these interactions remain poorly understood. Observation wells in mountains are scarce, and our understanding of montane hydrogeology has been limited by this data scarcity (Somers & McKenzie, 2020). Accessible, low mountain regions may provide an opportunity to characterize physical hydrological processes which can provide insights to other low and high mountain areas.

Atlantic Canada has also received little research attention in terms of groundwater-surface water interactions with hard rock aquifers despite high dependence on groundwater for drinking water. Furthermore, Atlantic Canada is near (or in some areas past) the tipping point between snow and rain-dominated hydrology, (Schnorbus, Werner, & Bennett, 2012) making it an interesting setting to consider groundwater recharge pathways and potential climate change impacts. Improved process understanding is needed to facilitate source water protection and climate change adaptation.

1.4 Research Objectives

The overarching goal of this research is to improve our understanding of recharge pathways and groundwater-surface water interactions in cold, montane watersheds with complex topography and geology. The focus of this study is on Christmas Brook watershed in the Eskasoni Mi'kmaq community, Cape Breton, Nova Scotia, Canada, which provides a representative and accessible study site to achieve this goal in partnership with the community. This study will improve our understanding of how the montane uplands support water resources. The specific objectives are to:

1. Quantify the contributions of different sources and areas within the watershed to streamflow and fault-groundwater recharge, using tracer-based modeling to evaluate hydrological processes.

2. Characterize groundwater flow paths to the fault aquifer and assess the relative contributions of different flow pathways within the watershed.

3. Integrate the findings from Objectives 1 and 2 to improve understanding of hydrological dynamics in the watershed and develop actionable recommendations for source water protection and watershed management.

To achieve these objectives, end member mixing analysis (EMMA) was first applied to quantify the proportion of streamflow coming from different sources/areas within the watershed. Hydrochemical signatures were used to infer connections between the groundwater and surface water systems. A numerical groundwater flow model, calibrated to field data, was then developed to characterize the subsurface flow paths to the fault aquifer used for drinking water supply. The results from Objectives 1 and 2 were compared to provide a holistic understanding of the integrated hydrological system and to offer recommendations for source water protection in a cold montane watershed with complex geology.

CHAPTER 2 – METHODS

2.1 STUDY SITE

Eskasoni (from We'kwistoqnik - where the fir trees are plentiful) is the largest Mi'kmaq community in Nova Scotia, with a population exceeding 4,700 people (Governemnt of Canada, 2021). The community is in Cape Breton (Unama'ki [oo-nah-MAH-gee] - Land of Fog) at the base of the Boisdale Hills and stretches over 8 kilometers along the coast of the Bras D'Or Lake. Eskasoni relies on groundwater pumped from a fault aquifer along the base of the Boisdale Hills for their municipal water supply. We focus on the Christmas Brook watershed which contains two production wells that penetrate the fault aquifer (Figure 1).

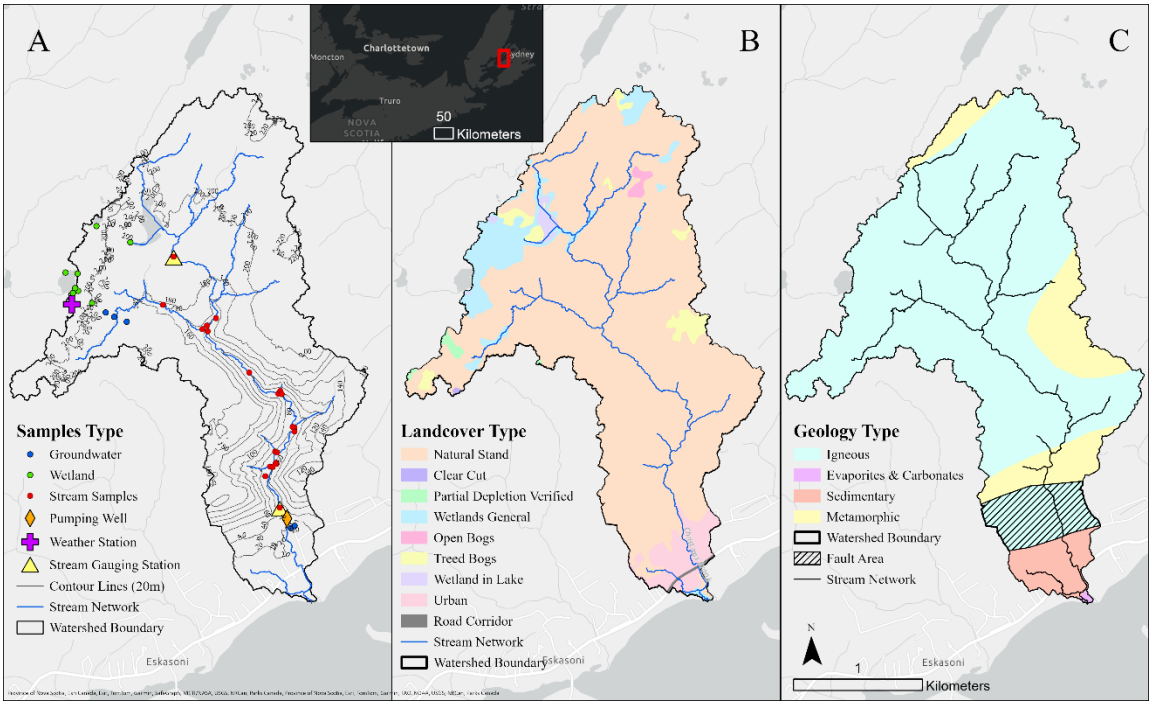

Figure 2: Watershed map with instrument and sample locations (a), land cover classification from the Nova Scotia Forest Inventory (b), and geology (c). Map inset shows site location relative to Nova Scotia, Canada.

2.1.1 Geology and Soil

The geology of the Christmas Brook watershed is complex and includes several different formations. The lowland plateau (area between the Bras D'Or lake and the transition slope) mainly comprises the Grantmire Formation of the Lower Horton Group (Barr & White, 2017) with minor exposures of the basal Windsor Group (Boehner & Giles, 2008; Boehner, Adams, & Giles, 2003). The Grantmire Formation is characterized by interstratified layers of red conglomerate, sandstone, calcareous siltstone and sandstone, minor grey shale, and scattered pedogenic limestone concretions. The Windsor Group comprises siltstones, carbonate rocks and evaporites and is typically highly deformed (Barr & White, 2017). These sedimentary rocks are generally gently dipping but steepen in proximity to fractured basement rock.

Farther inland, the beginning of the transition slope is underlain by a strip of the Boisdale Hills Pluton comprising coarse-grained hornblende granodiorite which is typically cataclastic and sheared and underlies younger local sedimentary rock of the Grantmire formation (Raeside & Barr, 1990). Moving further up the mountain flank, a thin strip of the Benacadie Brook Formation (Late Proterozoic clastic-volcanic-carbonate unit) cuts across the middle of the watershed. Its composition is metamorphosed sedimentary rock comprising metasiltstone and quartzite with the rare occurrence of volcanic rock. In other areas of the Boisdale Hills, minor occurrences of pink calcareous siltstone, and ferruginous quartzite are present (Barr & White, 2017).

The highland plateau portion of the watershed, including the wetlands, is underlain by the Shunacadie Pluton, comprised of medium-grained biotite granodiorite dating to approximately 564 Ma (Raeside & Barr, 1990). The composition is like that of the Boisdale Hills pluton; however, the Shunanacadie pluton is less fractured and sheared in general.

The fault and damage zone and associated aquifer cuts across the lower part of the watershed. The exact boundaries are unknown, but the outcrops and previous hydrogeological investigations have provided an approximate fault zone extent shown in

Figure 1. In the fault zone, precipitation water infiltrates rather rapidly, restricting the interaction time with the atmosphere.

Surficial geology within the Christmas Brook watershed is dominated by glacial till, organic deposits, and minor fluvial deposits, reflecting its glacial history. The lowland plateau and transition slope are primarily covered by a thin veneer of glacial till, with variable thickness and composition. The tills in this region are predominantly sandy loam with a stony matrix, corresponding to the Thom soil group, and exhibit good drainage (Agriculture Canada, 1981). Along the highland plateau, extensive wetlands are underlain by thick accumulations of organic deposits, classified as Peat soils. These organic deposits are stone-free, poorly drained, and occupy depressional topography, forming the dominant surficial material in the wetland areas.

In some areas, particularly along the Christmas Brook channel, fluvial deposits consisting of sand and gravel are present. These deposits are typically localized and associated with post-glacial reworking of sediments by stream processes. Additionally, minor colluvial deposits occur along steep slopes near the transition from the lowlands to the Boisdale Hills, composed of a mixture of angular rock fragments and finer material derived from slope processes.

2.1.2 Landcover

Hardwood dominated Acadian Forest covers much of the Christmas Brook watershed, specifically at the lower elevations and within the river valley. Acadian forests often occur in low-land coastal fringes and deep, sheltered valleys (Government of Canada, 2022). Mature Acadian Forests include a mixture of hardwoods and softwoods; however, individual stands can vary (i.e., pure hardwood valleys). These forests are rich in shade tolerant undergrowth; small trees, shrubs, ground-plants, lichens, and mosses. When undisturbed, mature stands can live 300+ years (e.g., the Grande Anse Valley; Government of Canada, 2024).

Boreal Forest and wetlands dominate the higher elevation peneplain area of the Christmas Brook watershed. Boreal Forests are cold weather forests, dominated by conifers and found within acidic, nutrient rich soils (Alberta Forest Products Association, 2024). Compared to the Acadian Forest, the Boreal Forest has fewer species (Government of Canada, 2024). Dense canopy cover and acidic soil prevent extensive undergrowth. A notable characteristic of these forests is their relatively short life cycle, reaching 150 years under ideal conditions, or 50-100 years under typical conditions (Government of Canada, 2024).

2.1.3 Climate

Cape Breton Island has a temperate, coastal climate (maritime boreal climate). This climate is characterized by variable weather, warm summers, cold snowy winters, and moderate precipitation (Government of Canada, 2022). Being positioned between the Gulf of St. Lawrence and the Atlantic Ocean, the island experiences rapid changes in weather (winter thaws, fog, and snowfall of 300-400 cm/yr.; Government of Canada, 2022). During the study period (2022-2023), summer (June-August) had an average daily temperature of 17.9°C, with extremes of 29°C. Winter (December-February) had an average daily temperature of -1.1°C, with lows below -10°C (Eskasoni First Nation automatic weather station Nova Scotia; Government of Canada, 2024) (Government of Nova Scotia, 2023). Annual precipitation averages 1,500 mm/yr on Cape Breton Island with Eskasoni receiving 1586 mm/yr during the study period (with 22 days of missing data; Government of Nova Scotia, 2023). Baechler, Cross, & Baechler (2019) observed that the island's climate is changing, with precipitation decreasing by approximately 300 mm, and temperatures rising by approximately 0.8°C since the 1980s.

2.1.4 Bras d'Or Lake

Christmas Brook drains to Bras d'Or Lake, and the study watershed is within the Bras d'Or Lake Biosphere Region. Bras d'Or Lake has three channels connecting the lake to the ocean, the Great and the Little Bras d'Or Channels in the north and the man-made St. Peters Canal in the south. Freshwater runoff and saline ocean water mix within the lake; the average salinity near East Bay is 20.5 g/kg (Petrie & Bugden, 2002). Due to the flow restriction within the lakes, the average tidal amplitude observed at Eskasoni is approximately 5 cm. Furthermore, the tidal maximum is lagged by 4.5 hours, and tidal peak is reduced compared to the ocean (Petrie & Bugden, 2002). Non-tidal factors, particularly changes in atmospheric pressure (the barometric influence), can cause water levels in the Bras d'Or Lakes to fluctuate by as much as 50 cm, approximately 10 times the effect of tidal variations (Petrie & Bugden, 2002). When high atmospheric pressure builds over the lakes, it pushes water towards lower-pressure areas, typically in the open ocean, causing a drop in lake water levels. Conversely, when pressure drops over the lakes, water levels rise as water flows in from higher-pressure areas. The current rate of sea-level rise within the lakes is 36.7 cm/century, the projected water level rise by 2100 is 75 cm and the rate increase could be as high as 115 cm/century (Shaw et al., 2006).

2.1.5 Indigenous Protected and Conserved Area and Source-Water Protection

Our study area is within Eskasoni First Nation, and the research was conducted in collaboration with the Eskasoni Fish and Wildlife Commission (EFWC) and Bras d'Or Lake Biosphere Region Association. EFWC is leading the development of an Indigenous Protected and Conserved Area (IPCA) which overlaps with the study area. Concurrently, a new source water protection plan is being developed for Eskasoni's groundwater supply. This study aims to build hydrological understanding to support both initiatives, and therefore, some background on these initiatives is provided. IPCAs are defined as "lands and waters where Indigenous governments have the primary role in protecting and conserving ecosystems through Indigenous laws, governance and knowledge systems"

(The Indigenous Circle of Experts, 2018). The IPCA project aims to protect a large portion of the Boisdale Hills above Eskasoni First Nation to manage activities (e.g., forestry) which may impact water quality, flooding, and ecology, while preserving natural space for cultural and recreational activities (Nash, 2021).

All IPCAs are built upon 3 foundational characteristics; they are indigenous led, include a long-term commitment to conservation, and elevate indigenous rights and responsibilities. Indigenous-led conservation initiatives reflect the individual needs of the respective nation, where indigenous governments have the primary role in determining objectives, boundaries, and governance, accompanied by transparent negotiations. Long-term commitment to conservations stems from the Indigenous peoples' view on multi-generational stewardship, protecting lands and waters for future generations. "Elevate rights and responsibilities" refers to the physical and spiritual connection indigenous people share with the land. They have the right to benefit from the land and all that it offers, with the corresponding duty to care for and respect the land, relating back to the previous point of multigenerational conservation (The Indigenous Circle of Experts, 2018). Many traditional activities depend on water, the ability to access good water greatly impacts these activities and the surrounding environments (Assembly of First Nations, 2021). In turn, the Indigenous government must work with their people to achieve a balance between conservation and cultural goals.

2.2 Data Collection

Extensive field data was collected in the Christmas Brook watershed, primarily between July 5th, 2022, and July 1st, 2023, with some additional field measurements conducted in July of 2024. Field data included continuous meteorological, streamflow and groundwater levels across the topographic gradient of the catchment and four synoptic water sampling campaigns. The principles of ownership, control, access, and possession (OCAP) were followed in collecting and analyzing environmental data. The OCAP principles were established to protect the collection and use of First Nations data (First Nations Information Governance Centre, 2023). OCAP principals were applied in

the current study through a data sharing plan with mutual access to field data between Dalhousie University and EFWC. Furthermore, during fieldwork campaigns, Dalhousie, EFWC, and community guardians staff all participated in data collection.

2.2.1 Meteorologic/Hydrometric Data

Meteorological data for this study was collected from two weather stations located at different elevations within or near the catchment area. The EFWC station (Davis Instruments GroWeather, Cabled, Metric 6820CM), positioned on the highland plateau at approximately 200 meters elevation, began collecting data on January 28th, 2023 (Figure 1a). Data from the Environment and Climate Change Canada (ECCC) weather station at Castle Bay Beach, located at sea level approximately 3 km from the watershed, provided additional lowland meteorological information. The ECCC station has been operational since before the study period, though it has some missing data. Both stations automatically recorded temperature, relative humidity, liquid precipitation, and snow depth at hourly intervals, and I was responsible for downloading the data.

2.2.2 Stream Discharge Data

Two stream gaging stations were installed on Christmas Brook in July 2022: one at the watershed outlet, attached to a concrete channel which was formerly dammed, and the other where the main stem of Christmas Brook leaves the plateau wetlands (Figure 1a). These stations each house a pressure transducer (Solinst Levelogger™) which measures water level at a 15-minute interval, and a barometric pressure transducer (Solinst Barologger™) was also installed to monitor the barometric pressure at the same time step for barometric compensation. A staff gauge was also installed for easy stage reference. Stream flow was manually measured regularly with an electromagnetic current meter (OTT MFPro). Stream flow measurements were used to establish a power function rating curve and convert stage to discharge data.

2.2.3 Groundwater Observations Wells

The Christmas Brook watershed has six highland bedrock monitoring wells (drilled in 2011), two shallow monitoring wells in the plateau wetlands (one installed in 2011, and one installed in 2022), two lowland monitoring wells (drilled 2004) and two lowland pumping wells (drilled in 1984 and 2020) for municipal water supply (Figure 1a). The monitoring well specifications are shown in Table 1 in the Results section.

The highland bedrock monitoring wells were drilled in three sets of two: MW1A and MW1B, MW2A and MW2B, MW3A and MW3B, each set having one deep and one shallow well. The shallow bedrock wells (MW1A, MW2A, and MW3A) were drilled to depths of 6.70 m, 6.40 m, and 4.57 m, respectively (terminated in shallow bedrock). These deeper wells (MW1B, MW2B, MW3B) were drilled to depths of 17.10 m, 16.91 m, and 15.54 m, respectively (terminated in intermediate bedrock). These six wells all have a screen length of 1.52 m and PVC casing. The two wetland porewater monitoring wells (PNA and PNC) were installed by manually pushing or auguring into the peat. PNA was installed in 2011 and has a screen 2.7 m long. PNC was installed July 6th, 2022, using a hand auger with a 1.5 m screen. The lowland bedrock monitoring wells (MW4 and MW5) were drilled in 2004, following an oil spill in the neighborhood (no contamination was detected). MW4 was drilled to a depth of 60 with casing diameter of 6 inches. Between 0-12 ft, the lithology was brown, gravely, till and bounders; between 12-60 ft, the lithology changed to brown, hard, coarse grained, sand and gravel. A water level logger was installed in MW4 in August 2023.

Two production wells were drilled within the Christmas Brook watershed on Arena Road near the outlet. The first production well (PW1) was completed in 1984. During drilling, the top 4.9 meters was overburden consisting of silt, clay, gravel, and boulders. The well was drilled to a depth of 26.2 m, the well was cased to a depth of 24.7 m, followed by the screen. The screen was stainless steel with a nominal diameter of 203 mm, a length of 2.44 m, and a No. 60 slot size (Nolan, Davis & Associates Limitted, 1984). The second production well (PW2) was drilled in 2020. At this location, the overburden consisted primarily of silty sand and gravel, with a thickness of 1.8 m. A 0.4

m borehole was drilled to a depth of 1.8 meters below ground surface (mbgs). This was followed by a 0.3 m borehole to 24 mbgs and a final 0.25 m borehole to 91.5 mbgs. The well was cased to a depth of 24 mbgs with a steel conductor equipped with a drive shoe. The bottom remained open to the total depth.

2.2.4 Water Sampling and Analysis

Water samples were collected for stable water isotopes ($\delta^{18}O$, $\delta^{2}H$), major ions and trace metals during four field campaigns (July and November 2022, May and July 2023). Three samples were taken at each sampling location: a 250 ml plastic bottle for ions, a 60 ml amber glass bottle for isotopes, and a 10 ml plastic vile for metals. All sampling containers were rinsed three times before collecting the sample. Wells were purged for 5 minutes prior to monitoring well sampling using an inertial pump. The metals samples were filtered in the field with a 0.2um syringe filter.

The sampled waters included groundwater (sampled from 6 observation wells near the headwaters, 2 shallow wells in the peatland and from the two production wells), the main stem of Christmas Brook (corresponding to higher-order streams), tributaries to Christmas Brook (corresponding to lower-order streams), springs, ponds and lakes (which are only been present in the peatland). Precipitation was also sampled via a precipitation collector which was designed and installed following criteria outlined by the International Atomic Energy Agency (IAEA, 2011). At each sample location, the coordinates were recorded with a GPS, and temperature, conductivity, dissolved oxygen and pH were recorded using a YSI water quality meter. In cases of concentration values below the detection limit or invalid measurements (i.e., negative values), values were replaced with half of the detection limit (Helsel, 2005).

The isotope samples were analysed at the CERC Ocean Laboratory, and the ions and metals were analysed at the Centre for Water Resource Studies Laboratory, both at Dalhousie University. Stable water isotopes were analysed with a Picarro L2130 water

isotope analyser which uses the cavity-ring-down spectrometry technique. The precision for $\delta^{18}O$ is <0.05 permil and <0.2 permil for $\delta^{2}H$.

The metals samples were analysed using a Thermo Scientific iCAP-RQ Inductively Couple Plasma Mass Spectrometer following EPA Method 200.8 and Standard Methods 3125 for sample preparation and analysis. The anions samples were analysed using a Thermo Scientific Aquion Ion Chromatograph following EPA Method 300.0 for sample preparation and analysis. All reported metals values were compared to Health Canada's water quality guidelines (Health Canada, 2023).

2.2.5 Ion Charge Balance

Charge balance error (CBE) was calculated as a check on ion concentration data quality. In natural aqueous solutions, the total positive charge from cations should balance the total negative charge from anions, meaning the sum of the cation charges minus the sum of the anion charges should equal zero (Fetter, 2001):

$$\sum cations - |\sum anions| = 0 \qquad [1]$$

The cations in this study include Ca^{2+}, Na^{+}, Mg^{2+}, and K^{+}, while the anions include SO_4^{2-}, Cl^{-}, CO_3^{2-}, and HCO_3^{-}. The CBE is calculated by converting ion measurements from ppm to mEq/L and then using the following equation for each sample:

$$CBE = \frac{\sum cations - |\sum anions|}{\sum cations + |\sum anions|} \times 100 \qquad [2]$$

A positive CBE indicates an excess of cations, while a negative CBE indicates an excess of anions. An acceptable threshold for CBE is within 5%, exceeding this range could be a result of laboratory error or an unaccounted dissolved species (i.e., major ion; Fetter, 2001).

2.3 Geospatial Analysis

The Christmas Brook watershed was delineated with the hydrology toolbox in ArcGIS based on the Nova Scotia 1-meter resolution Lidar digital elevation model (DEM) (Government of Nova Scotia, 2020). Landcover was characterized using the Nova Scotia Forest Inventory Vector Land Use Layer for Cape Breton (Government of Nova Scotia, 2021). Landcover was predominantly natural forest stand but also consisted of small areas of clear-cut or partial depletion (clear-cut residual > 25 % of crown closure), wetland, beaver flowage, open bogs, treed bogs, and lake. According to the Nova Scotia Forest Inventory, the dominant tree species within the Christmas Brook watershed are Balsam Fir, Black Spruce, Red Maple, Sugar Maple, White Spruce, White Birch, and Yellow Birch (in order of dominance).

2.4 End-Member Mixing Analysis (EMMA)

We applied EMMA to Christmas Brook to quantify the contributions of different catchment waters to streamflow. Hydrologic tracer studies are among the most widely used and well-established techniques for characterizing flow systems (e.g., recharge, flow paths, residence time, discharge measurements; Cao et al, 2020; Schilling et al, 2023). Tracers can be either natural or artificial, including dissolved solids, gases, temperature, and dyes. It is essential that a tracer be conservative—remaining unchanged over time and space—and easily measurable. Tracer-based studies are particularly effective in mountain environments (remote, difficult-to-access sites), where only periodic synoptic sampling may be possible (Tetzlaff et al., 2014; Brunner, Therrien et al., 2017; Somers & McKenzie, 2020; Benischke, 2021).

Groundwater often exhibits a distinct ionic signature compared to surface water due to prolonged interaction with mineral-rich geology. Similarly, the stable water isotopic composition ($\delta^{18}O$ and $\delta^{2}H$) of groundwater differs from that of surface water due to atmospheric exposure and associated isotopic fractionation. Consequently, surface

water isotope signatures can vary considerably (Benischke, 2021). Relevant processes regulating the relative $\delta^{18}O$ and $\delta^{2}H$ composition include phase changes that affect water above or near ground surface (in this case evaporative fractionation), as well as simple mixing. Thus, isotopes can be used for differentiating groundwater sources and near surface flow paths (Blumstock et al., 2015).

2.4.1 Tracer Selection

Correlation analysis was used to characterize the relationship between the different potential tracers and identify those which reliably separate the different water types. Pearson's correlation coefficient (r) measures the strength and direction of a linear relationship between two variables. A value of 1 (or -1) represents a perfect correlation while 0 indicates no correlation. A correlation matrix was computed for all potential ion and isotope tracers. Bivariate plots were used to individually assess the relationship between ion/isotope pairs. These plots allowed visualization of water chemistry relationships, checking for their ability to cluster waters of different sources, linearity and presence of any outliers. Five major ions (Ca^{2+}, Na^{+}, Mg^{2+}, K^{+}, Cl^{-}) and both isotopes ($\delta^{18}O$ and $\delta^{2}H$) were ultimately selected for the EMMA analysis.

2.4.2 Ion Ratios and Seasonal Variability

Ion ratios, such as Na^{+}/Ca^{2+}, Na^{+}/Cl^{-}, and Ca^{2+}/Mg^{2+}, were analyzed to explore seasonal changes in water chemistry and to infer potential influences from groundwater and surface water interactions. The data was assessed to identify seasonal variation and to investigate the relationship between ion concentrations, hydrological conditions, and geologic influences in the study area.

2.4.3 Two End-Member Mixing Analysis

A two-end member EMMA was conducted using the framework developed by Christophersen & Hooper (1992). EMMA uses the chemical signatures of source components (i.e., end members) to determine their contribution to a mixed chemical signature, often streamflow (Christophersen & Hooper, 1992). This simplest form of EMMA can be expressed as a mass balance with two sources, their tracer concentrations, and a mixture (Cook, 2020; Pardo et al., 2022):

$$m = f_1 v_1 + f_2 v_2 \quad [3]$$

where m represents the concentration of the mixed water, f_1 and f_2 are the fractions of mixture derived from sources 1 and 2, and v_1 and v_2 are concentrations of conservative tracer in end-member 1 and 2, respectively.

Rearranging Equation 3 leads to the conventional mixing equation below. In our mixing analysis, groundwater discharge and wetland lakes/porewater were identified as the two end members contributing to streamflow. Equation 4 is applied to field water chemistry data with the underlying assumptions that mixing is conservative ($f_1 + f_2 = 1$) and that the end member signatures are stable in space and time.

$$f_1^* = \frac{Q_g}{Q_s} = \frac{m - v_2}{v_1 - v_2} \quad [4]$$

In this equation, f^*_1 is the estimated fraction of groundwater in the stream mixture, Q_g is the groundwater flow to the stream, and Q_s is the total stream flow. This equation can be applied to individual measurements or their averages but will carry high uncertainty unless the values of v_1 and v_2 are much farther apart than their associated uncertainties (Kirchner, 2023). We apply this equation to individual water samples in our analysis.

In EMMA, the number of tracers used must be equal to, or greater than, the number of end members minus one (i.e., a minimum of two tracers is needed to distinguish between three end members). In the case that more than two tracers are used, an optimization procedure or principal components analysis (PCA) can be used to interpret the data. PCA can be used in EMMA to reduce the dimensionality of the data to a few principal components (PCs). Water samples can then be recast in PC space to assess the water chemistry signature at a lower number of dimensions. Often two

eigenvalues can capture 80-90% of the variation (Christophersen & Hooper, 1992; Hooper, 2003; Liu et al., 2008). For two end-member systems, data should plot linearly in PC space with the end-members plotting at the extremities, enclosing the other data (non-end-members should fall along a mixing line between the end-members).

We implemented the EMMA following the procedure outlined by Christophersen & Hooper (1992) as follows:

1. Concentration data was retained for five major ions and two isotopes (Ca^{2+}, Na^{+}, Mg^{2+}, K^{+}, Cl^{-}, ^{18}O, ^{2}H)
2. The data was standardized (Z-score standardization) to reduce the influence of variation within individual ions.
3. A principal component analysis (PCA) was performed on the dataset for all 7 tracers and PCs were selected to account for the greatest amount of variability.
4. The concentration of end members is projected into PC space.
5. The extent to which the end members encapsulate the target data (stream-water) was examined within PC space, and end members were chosen which best bound the stream data.
6. The EMMA equation was applied (Equation 4) to determine the proportional contribution of end members to each mixed stream water sample.

Burns et al. (2001) highlights the importance of comparing hydro-chemical and isotope tracer modelling with hydrometric measurements to verify the physical capability of the model results. Therefore, we compare and complement the EMMA results with hydrometric observations, baseflow separation and groundwater modelling (described below).

2.4.4 Uncertainty Analysis

A Monte Carlo error propagation approach was used to quantify the uncertainty in the results of the mixing model. For each sampling period, 1000 iterations were used to

randomly select end-member concentrations from the observed distributions and then used to calculate the mixed proportions. The results of the 1000 iterations were aggregated and represented as standard deviation error envelopes around the end-member contributions reported for the stream composition at the downstream gauging station.

2.5 Baseflow Separation

Baseflow separation was performed on the downstream streamflow record for July 2022 to July 2023 to assess groundwater contribution to streamflow and provide a comparison for the mixing analysis results. Several methods exist for baseflow separation using streamflow records (Mao et al., 2024; Li et al., 2021). Seven commonly-used methods were considered including:

1. HYDSEP-LM: This method uses linear interpolation to separate baseflow and is generally less sensitive to small changes in flow (Eckhardt, 2008; Burkey, 2024).
2. HYDRUN: A non-linear separation method that allows dynamic adjustments. This method is more responsive to high-flow events and is suitable for watersheds where baseflow and event-flow interact closely (Tang & Carey, 2017).
3. Digital filtering methods; Lyne-Hollick filter method (DF-F1), Chapman filtering method (DF-F2), Chapman and Maxwell filtering method (DF-F3), Boughton-Chapman filtering method (DF-F4), Eckhardt filtering method (DF-F5). These methods vary in filter strength and sensitivity, making them suitable for different use cases. The filtering methods increase in intensity; DF-F1 is a low-pass filter with a fixed cutoff frequency, while DF-F5 is a high intensity filter (less noise, slower recession, slower response, and high baseflow allocation) using multiple filtering parameters (Nathan & McMahon, 1990; Chapman, 1999).

The different methods require different numbers of filter parameters (typically 1-3) which can be difficult to estimate. Furthermore, the results of the different methods vary

widely in terms of the baseflow indices (BFI) the produce. We therefore selected a baseflow separation method by taking the following steps for each method:

1. Start by selecting filter parameters from literature based on the hydrologic context.
2. Sensitivity analysis: Vary the filter parameters to assess if the model is highly sensitive to the filter parameter(s) (Eckhardt, 2004), which could indicate that a different baseflow method may be more suitable given our uncertainty in the parameters. Sensitivity plots for each method were generated by varying their coefficients across ranges established in the literature (Eckhardt, 2004; Mao et al., 2024; Bosch et al., 2017). When assessing these plots, it was noted that if the response curves showed minimal variation, selecting a median or default coefficient value (e.g., 0.95) provided reasonable smoothing without obscuring important flow details. Conversely, highly variable response curves indicated high sensitivity, necessitating the selection of a coefficient (k) that most accurately represented the known hydrological characteristics of the stream.
3. Visual inspection: Plot streamflow and baseflow to see how well the baseflow aligns with the natural variation of the stream. Separations which indicate too much (i.e., streamflow >~70% baseflow) or too little baseflow (i.e., streamflow <~20% baseflow) were ruled out.
4. Comparison to other methods: Cross-validate with other baseflow separation methods using Baseflow Index (BFI) to look for which methods represent the median.
5. Consider hydrological principles: Ensure that the hydrograph and equation constants maintain physical reasonableness.

Ultimately, DF-F3 (Chapman and Maxwell) was chosen as the most appropriate baseflow separation method. The BFI was calculated and then the baseflow separation amount was compared to the hydrochemical mixing model and outflow from the groundwater flow model. This comparison will help assess groundwater contributions to

streamflow, particularly during low-flow periods. If the model estimates align, it will increase confidence in the groundwater flow model parameters.

Additionally, a flow duration curve (FDC) was generated using the discharge data from the lowland gauging station. An additional estimate of BFI was calculated using the flow that is exceeded 90% of the time (Q_{90}) and the mean daily flow ($Q_{mean;}$ Nathan & McMahon, 1990):

$$BFI \approx \frac{Q_{90}}{Q_{mean}} \quad [5]$$

2.6 Hydrogeologic Modelling

We applied a groundwater flow model of the Christmas Brook watershed to investigate flow paths and the recharge area for the production wells withing the fault aquifer. The model was calibrated using field data, and a sensitivity analysis was conducted to characterize the reliability of the results.

2.6.1 Software Overview

A steady-state hydrogeological model of the Christmas Brook watershed was prepared using MODFLOW6 (Langevin et al., 2017) to characterize groundwater flow paths, fault aquifer recharge and groundwater transit times. The Model Muse graphical user interface (Winston, 2024) was used to prepare MODFLOW input files. MODFLOW6 is an efficient and widely used groundwater modelling software. MODFLOW has been used to evaluate groundwater-surface water interactions, the effects of discontinuities on groundwater level, and the effects of climate change on groundwater resources (e.g. Ntona et al., 2022; Li et al., 2011; Malekinezhad & Banadkooki, 2018). This software can simulate groundwater flow, groundwater-surface water interface, and solute transport. The MODFLOW6 solver uses a generalized control-

volume finite-difference (CVFD) approach, where cells are hydraulically connected to surrounding cells (Langevin et al., 2017). The data for model development and calibration were obtained from provincial databases, contractor reports, and multiple field campaigns.

2.6.2 Model Domain

A structured uniform model grid was created with cell size 50 m by 50 m. The model top is the ground surface as defined by a Lidar DEM with 1 m horizontal resolution downloaded from the GeoNova Provincial LiDAR database (Government of Nova Scotia, 2020). The model domain has three layers; Layer one extends from the ground surface down 10 m below ground surface (m bgs), representing soil and unconsolidated sediments. Layer two extends from 10 to 65 m bgs to represent fractured rock and the third layer extends from 65 m bgs to 200 m below sea level and represents intact bedrock. These layer depths are based on the geological information from well logs and assumptions based on professional judgement. The fault aquifer is represented as a zone of higher hydraulic conductivity that crosses the lower area of the Christmas Brook watershed (Figure 2). An equivalent porous medium approach was used to simulate groundwater flow through fractured bedrock. Layers one and two were set to be convertible (confined or unconfined) while Layer 3 was confined.

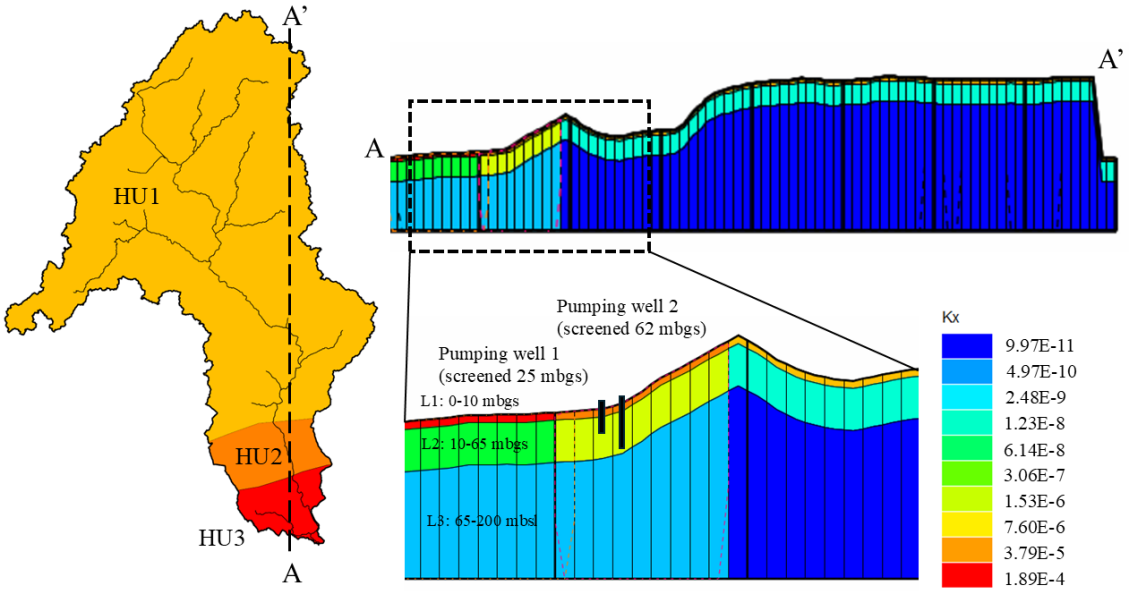

Figure 3: Model domain showing the three hydrogeologic zones: HU1 represents the in-tact granodiorite, HU2 represents the fault aquifer and HU3 presents the lowland sedimentary rock. Dashed line A-A' coincides with a pumping well location; the cross-section view shows the three model layers and their thicknesses. L1 represents an unconsolidated surficial layer, L2 represents fractured bedrock and L3 represents in-tact bedrock. The magnified cross section view (bottom right) better shows all 9 hydrogeologic units (3 zones, 3 layers) in the vicinity of the fault aquifer, and the colours indicate the K produced by the automated model calibration in m/s. K_y is equal to K_x, and K_z is equal to $K_x/10$.

2.6.3 Boundary Conditions

The lateral and bottom boundaries of the model domain are no-flow boundaries in accordance with the watershed divide, and reduced flow at depth (Andserson, Hunt, & Woessner, 2015). A recharge boundary (RCH package) of constant flux was applied across the domain at the top of the water table. Initial recharge flux was estimated, using Equation 6, from Nova Scotia baseflow data by Kennedy et al. (2010).

$$R_B = P \times r \qquad [6]$$

In this equation, R_B represents the recharge (mm), P is mean annual precipitation (mm), r is recharge ratio from Kennedy et al. (2010).

The small lakes in the wetland are represented using the lake package (LAK) and a single cell at the watershed outlet was assigned a specified head boundary (CHD package) condition to represent Bras D'Or Lake and allow a small amount of groundwater discharge directly to the lake (rather than to Christmas Brook). Neither saltwater intrusion, nor tidal influence were considered at the lake boundary. The stream network was simulated using the stream flow routing (SFR) package; the pumping wells were represented with the well package (WEL).

2.6.4 Initial Conditions

A transient spin-up was employed to establish initial head conditions that would facilitate steady-state model convergence (R. Winston, personal communications, 2024). The following procedure was applied: (1) the initial groundwater heads were set equal to model top/surface; (2) a transient stress period of length 1,000,000 seconds with 100-time steps was run; (3) the final simulated heads from the transient run were used as the initial condition for the steady-state simulation to facilitate convergence.

2.6.5 Model Calibration and Sensitivity Analysis

Hydraulic conductivity and precipitation were then manually calibrated using a one-factor-at-a-time calibration approach to adjust initial parameters to best fit the observed groundwater heads from piezometers, observation wells, and baseflow (minimum observed stream flows) within the model domain. The hydraulic conductivity was assumed to be anisotropic in the vertical direction with $K_x = K_y = 10K_z$. However, due to a lack of detailed data to quantify the degree of anisotropy, an isotropic assumption was made in the absence of more specific field information. This assumption can be revisited in future work as more data on fault orientations and hydraulic properties become available. Finally, hydraulic conductivity was calibrated using the Model-

Independent Parameter Estimation and Uncertainty Analysis (PEST; Doherty, 2018) to optimize fit to the observed data.

Following calibration, a sensitivity analysis was performed within MODFLOW6 to assess how the selected model parameters impact the conclusions of the study. Hydraulic conductivity in all layers was increased and decreased by one order of magnitude and the recharge values were varied by +100 mm and -60 mm (Kennedy et al., 2010). The results were compared to the calibrated model and assessed using two performance metrics : root mean square error (RMSE) and percent bias (PBIAS). RMSE is a measure of the difference between observed and predicted values, where lower values indicate better model performance. PBIAS is used to assess the model's tendency to over- or under-predict, with values closer to zero indicating minimal bias.

2.6.6 Particle Tracking

The MODPATH particle tracking utility for MODFLOW was applied to the calibrated groundwater flow model to characterize groundwater flow paths through the watershed and fault aquifer. Both backward and forward particle tracking were used to assess dominant recharge pathways and residence times of water in the subsurface. Forward particle tracking is advantageous for identifying recharge areas and understanding the overall contribution of water sources to an aquifer, offering a comprehensive view of flow paths and distribution. In contrast, backward (reverse) tracking is effective for tracing contaminant pathways and identifying sources or sinks but tends to focus on concentrated paths, potentially missing diffuse recharge areas.

For backwards particle tracking, 24 particles which terminated at a rectangle around the pumping wells were tracked backwards to their origin. Multiple simulations were run; particles were specified to pass through and stop at weak sources and sinks to better show the particle origins. For forwards particle tracking, four groups of nine particles were launched in different areas of the watershed including two groups in the plateau wetlands and two groups in the steep transition slope. The particles were first

launched at the model top, and their flow paths were simulated for 25 years in a transient (but quasi steady state) simulation. Next the particles were launched near the top of layer 2 (fractured bedrock) and were tracked for 100 years. Particles were specified to stop and weak sources and sinks to show where they discharge to the stream or pumping well.

CHAPTER 3 – RESULTS

3.1 FIELD DATA COLLECTION

3.1.1 Hydrometric Data Collection

According to the ECCC Castle Bay Meteorological Station (lower elevation station; climate ID 8201780), the average air temperature during 2022 was 8.1°C. The total precipitation received that year was 1586 mm. The maximum depth of snow (daily average) was 47.6 cm, recorded February 15th, 2023, at the highland station. Meteorological data was compared between the lower (ECCC Castle Bay) and upper (EFWC Davis) meteorological stations between the period of overlap from February 1st, 2023, to January 31st, 2024 (1 year; Figure 3). Over the study period, the highland station received 143.7 mm (18.8%) more precipitation than the lowland station. Most of this difference occurs during extreme precipitation events in July and August. The upper station was also 1.4°C colder and had 1.1 cm higher average snow depth than the lower station during the 2022-2023 winter.

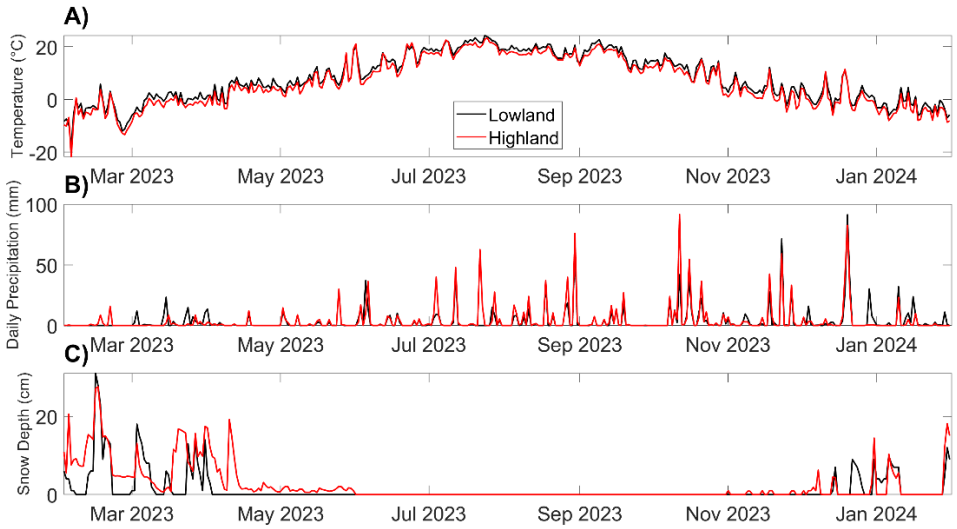

Figure 4: Comparison of highland (red) and lowland (black) meteorologic station data; (A) average daily temperature, (B) total daily precipitation, (C) snow depth.

Notable hydrometric events during the study period include Hurricane Fiona on September 24th, 2022, which brought 108 mm of precipitation, and Hurricane Lee on September 16th, 2023, with 61.1 mm of precipitation. Another significant event was an unnamed tropical storm on January 16th, 2023, during which Environment and Climate Change Canada issued wind warnings in Cape Breton County. This storm resulted in 65.7 mm of precipitation between January 14th and 16th. Additionally, several snowstorms and snowfall warnings occurred in February and March 2023.

The two stream gauging stations recorded streamflow between July 5, 2022, and July 5, 2023 (Figure 4). At the lower station, daily average flow values ranged from 0.005 m^3/s to 4.55 m^3/s, with a mean of 0.20 m^3/s. At the upper station, daily average flow values ranged from 0.0045 m^3/s to 5.95 m^3/s, with a mean of 0.158 m^3/s. Both stream gauging stations showed flashy hydrographs with rapid increases in streamflow during storm events, with the highest observed levels occurring on the same days. At the lower station, the second-highest observed stage was 1.57 meters in December 2022, and at the upper station, it was 0.49 meters during the same month. Notably, artificial spikes were observed at both stations on September 24, 2023, which were excluded from this analysis.

Field measurements revealed that the highest stage recorded during manual discharge measurements was 0.505 meters at the lowland station in May 2023 and 0.314 meters at the highland station in July 2022. These stages are significantly lower than the highest observed stages during storm events, indicating that the discharge values derived using the rating curves likely involve extrapolation beyond the range of calibration. This introduces uncertainty in the discharge estimates, particularly for extreme flow events.

The rating curves used for discharge calculation were developed using a power function fit. For the lowland station, the fit equation was $y = 1.1043 * x^{3.4262}$, with an RMSE of 0.0050 and an R^2 of 0.9766. For the highland station, the fit equation was $y = 260.6299 * x^{6.0577}$, with an RMSE of 0.0024 and an R^2 of 0.9992. While these curves provide an appropriate relationship within the measured data range, their application to higher flows—such as those observed during storms—is less certain. The maximum

stages observed during storm events exceeded the highest measured stages used to develop the rating curves, reaching 1.57 meters at the lower station and 0.49 meters at the upper station in December 2022. This extrapolation assumes that the stage-discharge relationship holds for higher flows, but the potential for significant error increases at these extremes. Future work should focus on collecting high-flow discharge measurements to refine the rating curves and reduce uncertainty in discharge estimates for extreme events.

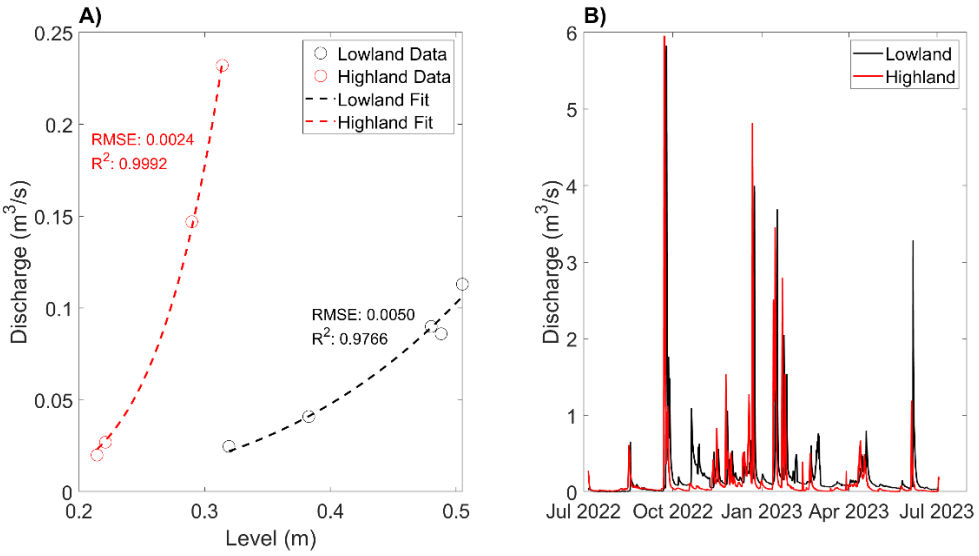

Figure 5: (A) Rating curves generated for both stream gauging stations. The power function for the upstream station was $y = 373.79x^{6.3527}$, and the power function for the downstream station was $y = 0.9316x^{3.2064}$. (B) The continuous discharge data obtained by transforming level data via the rating curves.

3.1.2 Groundwater Levels in Observation Wells

Groundwater levels (hydraulic heads) were recorded continuously between July 6th, 2022, and July 5th, 2023, in MW1a, MW2a, MW3a, MW3b, PNA and PNC (Figure 5, Table 1). Non-continuous spot measurements of groundwater levels were also recorded for MW2b and MW3b during quarterly field trips. Monitoring wells MW1A and MW1B had the deepest water tables relative to ground surface (1.452 mbsg and 2.140 mbgs,

respectively) followed by MW2 (0.584 mbgs) then MW3 (0.291 mbgs) (Figure 2). MW1A showed the most variable head, ranging from 2.72 mbgs to 0.51 mbgs. The wetland wells (PNA and PNC) had water tables consistently near ground surface. Groundwater level was recorded in MW4 (near the pumping wells) continuously between August 31st, 2023, and March 13th, 2024, with an average water table depth of 6.94 mbgs (not shown in Figure 5 due to non-overlapping time period).

Temporal groundwater fluctuations are largely a reflection of the precipitation and stream discharge temporal patterns (Figure 5). Variation in the water table in PNA and PNC porewater wells was muted compared to the bedrock monitoring wells (MWs). The MW1 plot showed an upward hydraulic gradient (higher head at higher elevation), consistent with groundwater flowing downward, whereas MW2 and MW3 exhibited downward hydraulic gradients (higher head at lower elevation), indicating groundwater flowing upward (Table 1).

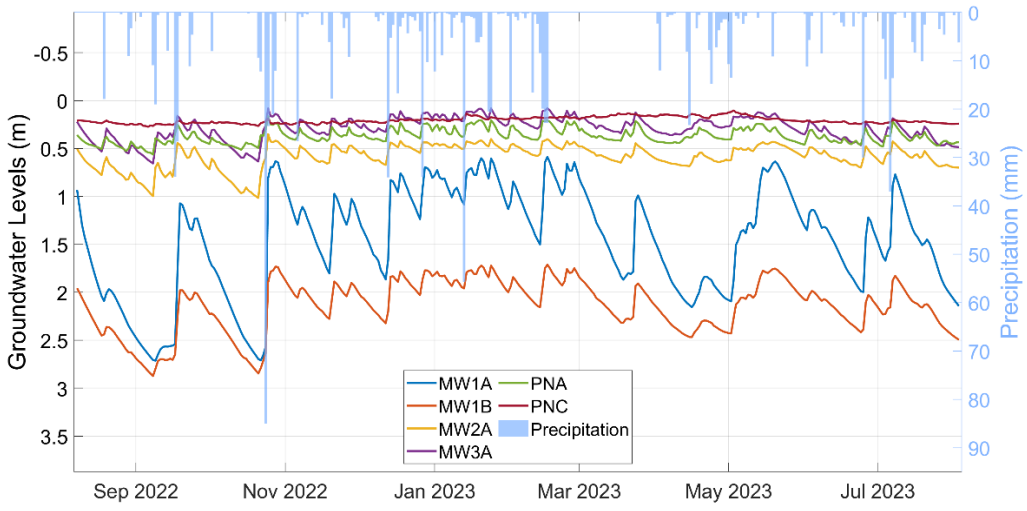

Figure 6: Groundwater levels (left axis) as depths below ground surface in bedrock monitoring wells and wetland wells with daily average precipitation values (right axis).

Table 1: Summary of hydraulic head and vertical gradients at each well. Highlighted cells represent values from spot measurements since continuous logger data was not deployed. The depth of the water table at time of drilling has been included from a report by EXP Services (2011).

Well ID	Ground Surface Elevation (masl)	Well Bottom Elevation (masl)	Screen Length (m)	Screened Material	Average Depth of Water Table (m, loggers)	Depth of Water Table in 2011 at Time of Drilling (m)	Average Head (m)	Vertical Flow Direction
MW 1A	194.16	187.46	1.52	Fractured bedrock	1.452	1.15	192.71	-0.070 (downward)
MW 1B	194.12	177.02	1.52	Fractured bedrock	2.140	1.94	191.98	
MW 2A	192.32	185.92	1.52	Fractured bedrock	0.584	0.55	191.74	0.001 (upward)
MW 2B	192.33	175.42	1.52	Fractured bedrock	0.579	0.57	191.75	
MW 3A	196.86	192.29	1.52	Fractured bedrock	0.291	0.22	196.57	0.014 (upward)
MW 3B	196.95	181.41	1.52	Fractured bedrock	0.233	0.32	196.72	
MW 4	19.34	0.93	unknown	Fault damage zone bedrock	6.935	N/A	9.41	No multi-level data available for these wells
PNA	200.04	197.29	2.7	Peat	0.371	1.28	196.92	
PNC	201.44	198.84	2.6	Peat	0.205	N/A	201.24	

3.2 Water Chemistry Sampling

A total of 134 water samples were collected during four synoptic water sampling campaigns in July and November 2022, as well as May and July 2023, and analyzed for major ions and stable water isotopes. An additional 13 precipitation samples were sporadically collected throughout the year and analyzed exclusively for isotopes.

3.2.1 Major Ions

On average, groundwater had the highest ionic concentrations, followed by stream water samples, and then the wetland porewater/lake samples. There were a few exceptions to this pattern; for instance, aluminum, iron, and bromide concentrations were highest in mainstream and tributary samples. Major ion concentrations are somewhat dependant on discharge rate (Figure 6). At the upper streamflow station, Cl, HCO_3, Ca, Mg, and DIC have increased concentrations measured during low-flow periods (<0.025 m^3/s), and all samples approach a plateau (or minor fluctuations) as flow exceeds 0.05 m^3/s. Similarly, at the downstream location, Cl, Na, and Ca are highest during low-flow conditions and plateau as flow exceeds 0.2 m^3/s, apart from HCO_3, which slightly increases before rejoining the trend. The remaining ions appear to be chemo-static, with concentrations unaffected by discharge rate.

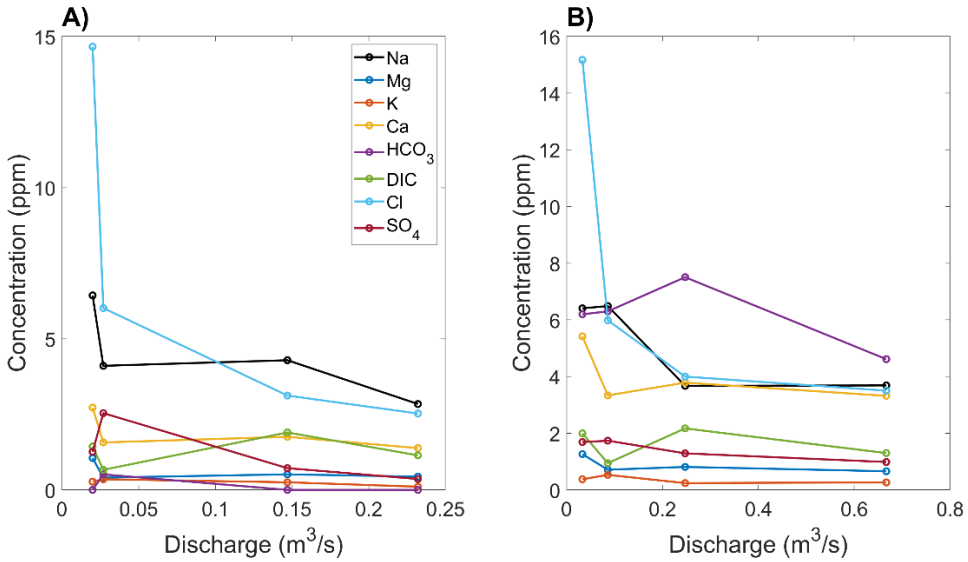

Figure 7: Ion concentration discharge relationships for the upstream gauging station (A) and downstream gauging station (B). See Figure 1a for gauging station locations.

The major ion chemistry of the water samples clustered by water source (groundwater, wetlands, tributaries and main stream) within a piper plot (Figure 7). Surface water samples were generally in the middle of the plot with no dominant water type, consistent with being a mixed signal. A few of the tributary samples had cations within the sodium and potassium group, and anions of the sulphate type ($Na^+ + K^+$ - SO_4^{2-} type). Therefore, the predominant tributary hydrogeochemical facies are split between mixed water type and sodium chloride type ($SO_4^{2-} + Cl^-$). The groundwater samples primarily have cations of the calcium type and anions of the bicarbonate type (Ca^{2+} - HCO_3^- - CO_3^- type). Therefore, the predominant groundwater hydrogeochemical facies are of the magnesium bicarbonate type. The groundwater samples demonstrate that weak acids exceed strong acids and that alkaline earths exceed alkalies. The wetland samples from both porewater and from wetland ponds have cations predominantly in the sodium potassium group and anions of the sulphate type ($Na^+ + K^+$ - SO_4^{2-} type). Therefore, the predominant wetlands hydrogeochemical facies are of the sodium chloride types. The wetland samples demonstrate that strong acids exceed weak acids and that alkalies exceed alkaline earths. The ionic order from the July 2023 samples was Na^+, Ca^{2+}, Cl^-, HCO_3^-, Mg^{2+}, SO_4^{2-}, K^+ for surface waters, Ca^{2+}, HCO_3^-, Cl^-, Na^+, Mg^{2+}, SO_4^{2-},

K^+ for groundwater and Na^+, Cl^-, Mg^{2+}, Ca^{2+}, SO_4^{2-}, K^+ for wetlands (no CO_3^{2-} present in samples).

Only two precipitation samples from July 2023 were included in the Piper plot. These samples, collected from both the top cone and accumulated bottom water of the precipitation collector, plotted as bicarbonate type and sodium potassium type, with overall chemical facies bordering mixed water and sodium bicarbonate type. The unusual chemistry for this region could result from environmental contamination - dust deposition from a nearby gravel road and prolonged residence time in the collector are likely contributors. Compared to stream and groundwater samples, precipitation ion concentrations were lower, as expected for this system.

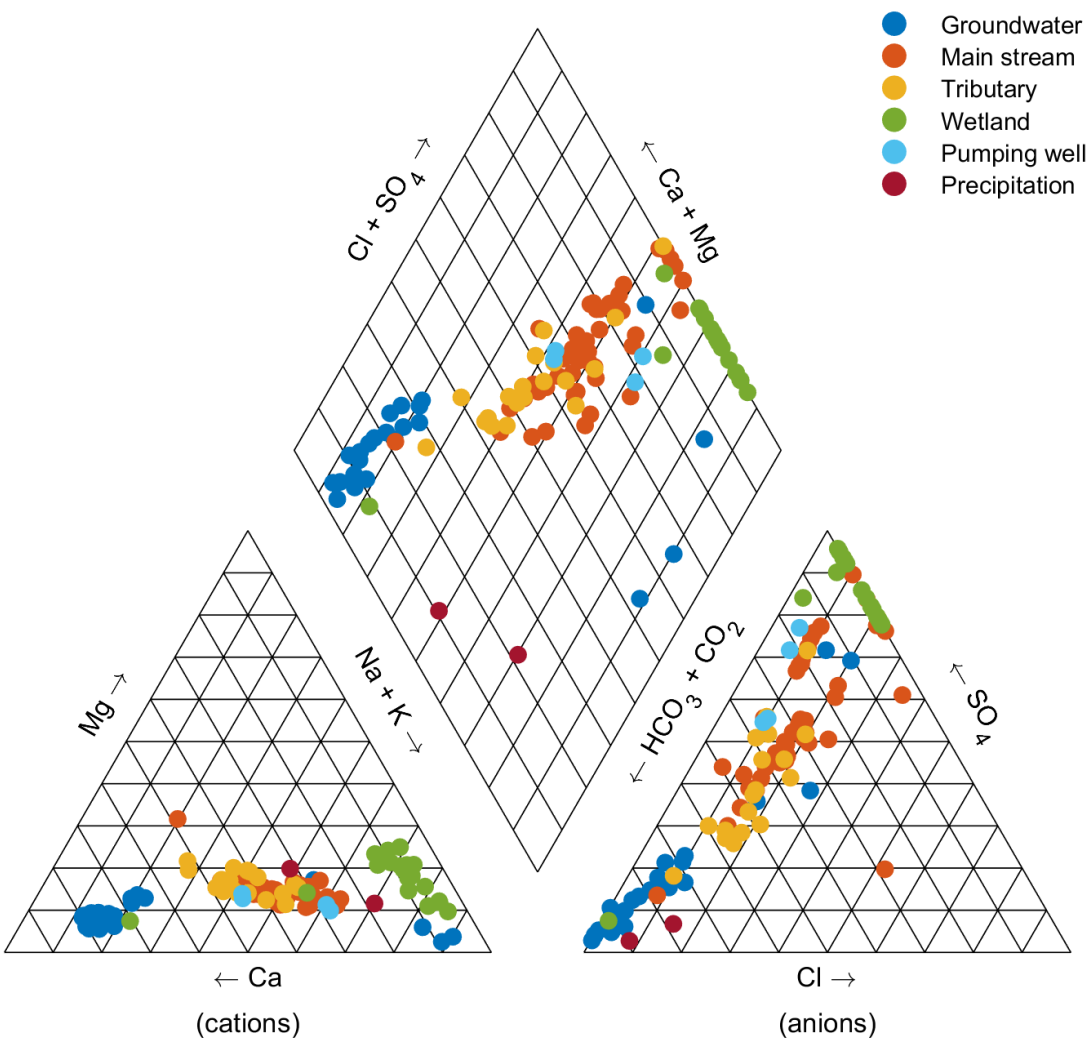

Figure 8: Piper diagram of major ion samples for all field campaigns

The charge balance error was calculated for each sample and averaged for each sampling campaign; the median percent charge balance errors for the four sampling campaigns were +19.7%, +7.1%, +23.4%, and +5.2% for July, November 2022, May and July 2023, respectively. Appendix 4 provides the complete charge balance error calculations.

Ion concentrations and ratios at the downstream gaging station exhibited distinct seasonal variations (Table 2). In November, concentrations of Cl^-, Na^+, Ca^{2+}, and Mg^{2+} were highest, likely due to low-flow conditions that increased the proportion of groundwater discharge and limited dilution from surface runoff, attributed to reduced

precipitation in the preceding week. In contrast, ion ratios spiked in May (Na^+/Ca^{2+}, Na^+/Cl^-) and July (Ca^{2+}/Cl^-, Ca^{2+}/Mg^{2+}, K^+/Cl^-), suggesting increased contributions from surface water during snowmelt or spring rains, as well as changes in water-rock interactions and evaporation during the warmer months.

Table 2: Ion concentrations (ppm) at the downstream gaging station for each field campaign.

Major Ions	July 2022	November 2022	May 2023	July 2023
Ca^{2+}	3.79	5.42	3.33	3.32
Mg^{2+}	0.81	1.26	0.71	0.66
Na^+	3.67	6.41	6.49	3.69
K^+	Below detection limit	0.38	0.53	0.26
Cl^-	4.00	15.17	5.98	3.50
HCO_3^-	7.504	6.1953	6.2991	4.61
SO_4^-	1.29	1.69	1.74	0.98

Metal concentrations in the water samples were generally within the accepted Guidelines for Canadian Drinking Water Quality – Summary Tables (Health Canada, 2023), with many concentrations falling below detection limits. However, a few exceptions were noted. Specifically, 12 manganese (Mn) samples exceeded the guideline value of 0.12 mg/L, with 11 of these coming from upland bedrock monitoring wells (particularly MW2 and MW3) and one from the upland gauging station. Additionally, arsenic (As) concentrations exceeded the guideline value of 0.010 mg/L in four samples, all taken from MW2B during different field campaigns. Lastly, one lead (Pb) sample, collected from the upstream gauging station in July 2023, exceeded the guideline value of 0.005 mg/L. Metals were not analyzed for precipitation samples. Complete lab results, including metal concentrations and respective guideline values, are provided in Appendix 3.

3.2.2 Stable Water Isotopes

The stable water isotopic ratios in precipitation, surface water and groundwater varied seasonally. Precipitation isotopic data collected between August 2022 and July 2023 is used to produce a site-specific meteoric water line based on an ordinary least squares regression. The site-specific water line is compared to the global meteoric water line (GMWL; Rozanski et al.,1992), and a published local meteoric water line (LMWL) for Truro, NS from (Gibson et al., 2020) in Figure 8. When compared to the GMWL, the average d-excess and LC-excess of precipitation samples is 11.37‰ and 1.40‰, respectively.

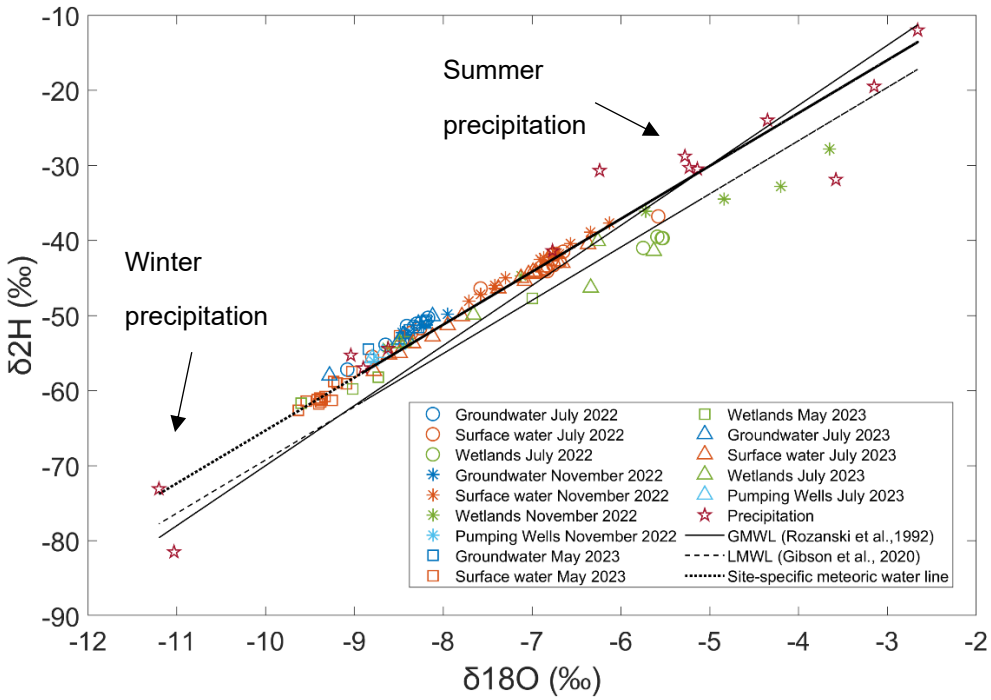

Figure 9: Dual isotope plot showing isotopic composition of all samples and the GMLW (Rozanski et al., 1992), LMWL at Truro (Gibson et al. 2020), NS and OLSR water line which is based on a regression to precipitation samples collected and Christmas Brook.

Precipitation samples range between -10 and -80‰ in δ^2H and between -2 and -11‰ in $\delta^{18}O$, with average values of -40.74‰ and -6.51‰, respectively. Precipitation samples are more enriched in the summer and fall months and more depleted in the early spring and winter. Most samples plotted above both the GMWL and the LMWL. Additionally, most samples plot closest to the site-specific water line, although the site-specific line is not well constrained given the limited number of precipitation samples obtained.

Groundwater samples are generally more depleted, with average δ^2H and $\delta^{18}O$ values of -52.65‰ and -8.45‰, respectively. Pumping wells show slightly more depleted values compared to bedrock monitoring wells, -55.18‰ and -8.68‰, respectively. Surface water signatures vary substantially throughout the year, generally grouping by sampling campaign, with averages of -49.21‰ and -7.74‰ for δ^2H and $\delta^{18}O$, respectively. However, the May 2023 surface water samples are notably more depleted, with average values of -60.15‰ and -9.28‰, respectively. These depleted samples differ from the other surface water campaigns, aligning more closely with winter precipitation and groundwater samples. Meanwhile, samples from July 2022/2023 and November 2022 are more enriched. Wetland samples are generally enriched compared to all other sample types (excluding precipitation), with wetland surface water being more enriched than wetland porewater. Average wetland δ^2H and $\delta^{18}O$ values are -45.51‰ and -6.77‰, respectively. Individual trendlines for sample types reveal that groundwater has the steepest slope, while surface water has the shallowest slope, indicative of evaporitic influence.

3.3 Mixing Analysis

3.3.1 Correlation Analysis and Tracer Selection

The correlation analysis showed strong correlations between several ionic concentrations and/or isotope ratios (Figure 9), indicating which tracers are most

conservative or which may be particularly useful for end member separation in the mixing analysis. Figure 9 shows the complete correlation matrices, and hydrochemical bivariate plots are provided in the Appendix 1. Consistently, high correlation coefficients were noted between Ca^{2+}-HCO_3^-, δ^2H-$\delta^{18}O$, Ca^{2+}-Mg^{2+}, Na^+-Cl^-, and K^+-DIC across sampling events, while Na^+, SO_4^{2-}, and Cl^- had lower correlation coefficients, except with each other. DIC and HCO_3^- mostly showed low correlation coefficients and more scatter in bivariate plots and were interpreted to be less conservative than other ions. Therefore, SO_4^-, DIC and HCO_3^- were excluded from the mixing analysis.

A

	Na	Mg	K	Ca	HCO_3	DIC	SO_4	Cl	^2H	^{18}O
Na	1									
Mg	0.72	1								
K	0.74	0.67	1							
Ca	0.87	0.78	0.78	1						
HCO_3	0.89	0.83	0.79	0.99	1					
DIC	0.82	0.74	0.93	0.92	0.92	1				
SO_4	0.59	0.38	0.34	0.32	0.38	0.29	1			
Cl	0.70	0.53	0.65	0.62	0.63	0.63	0.77	1		
^2H	-0.63	-0.55	-0.66	-0.44	-0.50	-0.60	-0.69	-0.78	1	
^{18}O	-0.67	-0.57	-0.66	-0.49	-0.53	-0.62	-0.68	-0.78	0.98	1

B

	Na	Mg	K	Ca	HCO_3	DIC	SO_4	Cl	^2H	^{18}O
Na	1									
Mg	0.49	1								
K	0.16	0.70	1							
Ca	0.19	0.81	0.78	1						
HCO_3	0.17	0.77	0.78	0.99	1					
DIC	0.04	0.50	0.81	0.77	0.80	1				
SO_4	0.77	0.41	0.05	0.11	0.06	-0.14	1			
Cl	0.86	0.37	-0.09	-0.08	-0.13	-0.25	0.71	1		
^2H	-0.43	-0.51	-0.71	-0.54	-0.52	-0.65	-0.40	-0.24	1	
^{18}O	-0.36	-0.46	-0.68	-0.51	-0.49	-0.60	-0.34	-0.20	0.98	1

C

	Na	Mg	K	Ca	HCO_3	DIC	SO_4	Cl	^2H	^{18}O
Na	1									
Mg	0.78	1								
K	0.72	0.77	1							
Ca	0.79	0.93	0.72	1						
HCO_3	0.75	0.91	0.70	0.96	1					
DIC	0.51	0.71	0.72	0.78	0.75	1				
SO_4	0.03	-0.04	-0.02	-0.23	-0.13	-0.41	1			
Cl	0.43	0.24	0.38	0.11	0.16	0.00	0.72	1		
^2H	0.36	0.46	0.60	0.51	0.50	0.57	-0.19	0.20	1	
^{18}O	0.22	0.36	0.43	0.42	0.41	0.47	-0.30	-0.01	0.95	1

D

	Na	Mg	K	Ca	HCO_3	DIC	SO_4	Cl	^2H	^{18}O
Na	1									
Mg	0.72	1								
K	-0.02	0.05	1							
Ca	0.39	0.84	0.00	1						
HCO_3	0.29	0.79	0.28	0.92	1					
DIC	0.23	0.68	0.30	0.84	0.88	1				
SO_4	0.43	0.27	0.72	-0.04	0.09	0.09	1			
Cl	0.95	0.52	-0.01	0.14	0.04	0.04	0.50	1		
^2H	-0.35	-0.37	0.58	-0.26	-0.03	-0.07	0.14	-0.27	1	
^{18}O	-0.38	-0.43	0.56	-0.33	-0.09	-0.14	0.11	-0.29	0.98	1

Figure 10: Correlation classification results from correlation matrices of hydrochemical (Ca^{2+}, Na^+, Mg^{2+}, K^+, SO_4^{2-}, Cl^-, DIC, HCO_3^-) and isotopic ($\delta^{18}O$, δ^2H) parameters using Pearson's correlation coefficient r. Green cells represent $1 > r \geq 0.9$ and $-1 < r \leq -0.9$ (very strong correlations), yellow cells represent $0.9 > r \geq 0.7$ and $-0.9 < r \leq -0.7$ (strong), white cells represent $0.7 > r > 0.3$ and $-0.7 < r < -0.3$ (moderate), and red cells represent $0.3 \geq r \geq -0.3$ (weak).

3.3.2 End Member Mixing Analysis

PCA was used to reduce the dimensionality of the dataset integrating different tracers to characterize the hydrochemistry. The first principal component explained

69.8%, 54.2%, 55.0%, and 42.2% of the variance, and two principal components explained 85.5%, 81.1%, 76.4%, and 67.8% of the variance for July 2022, November 2022, May 2023 and July 2023, respectively. Water samples cluster by water type in PC space (Figure 10). The sample types were broadly clustered into three primary groups in relation to PC1 and PC2: wetlands, streams, and groundwater. The wetlands (including ponds and porewater) and groundwater generally form non-overlapping clusters and are interpreted as the main end members, while the stream samples (including main stream and tributary samples) generally fall in between, representing a mixed signature. The May 2023 sampling campaign is an exception where the mixed samples do not fall in a line between wetland and groundwater. This may be due to a third unaccounted for end member (e.g., a large snowmelt influence), and therefore the mixing analysis results for May 2023 are likely unreliable. For the two sampling campaigns when the pumping wells could be sampled, the hydrochemical signature of the pumping wells is distinct from the other groundwater wells in November 2022 but similar to the other groundwater wells in July 2023.

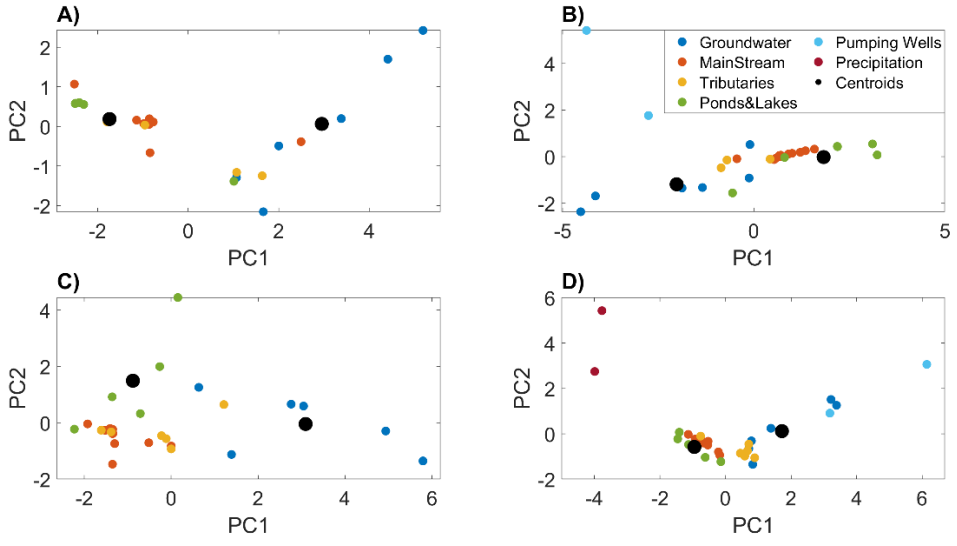

Figure 11: Principal component plots for water samples, separated by field campaign: (A) July 2022, (B) November 2022, (C) May 2023, (D) July 2023

By solving the mixing equation, the proportion of end member contributions to each stream sample were computed. The proportion of groundwater (versus wetland water) of stream samples ranged widely. At the downstream gauging station, groundwater was found to contribute between 19 to 35% of flow (Table 3), while wetlands makeup the remainder. The proportion of groundwater contribution to streamflow is markedly lower in the July 2022 and July 2023 samples compared to November 2022 and May 2023

Table 3: Proportional groundwater contribution to stream flow across sampling periods, including antecedent precipitation and associated uncertainty

Sample Period	7-day antecedent precipitation (mm)	Precipitation during sampling (mm)	GW Composition (%) at Downstream Station	Uncertainty (1σ)
July 2022 (moderate flow)	3.1	23	25.8	13.8
November 2022 (low flow)	0	2	31.4	17.2
May 2023 (high flow with snowmelt runoff)	0.7	1	*33.5	*15.4
July 2023 (high flow)	11.4	9	23.7	12.8

*Unreliable results due to possible unaccounted for end member

When examining the spatial distribution of groundwater contributions to main stream samples (Figure 11), two patterns emerge. First, spring and tributary samples generally have significantly higher groundwater composition than the main river. This

difference is especially notable in small streams draining steep, incised gullies, where groundwater contributions exceed the main river by more than 15%. Second, samples higher in the watershed have lower groundwater composition and greater wetland contributions. In contrast, samples taken further downstream in the watershed show an increase in groundwater composition.

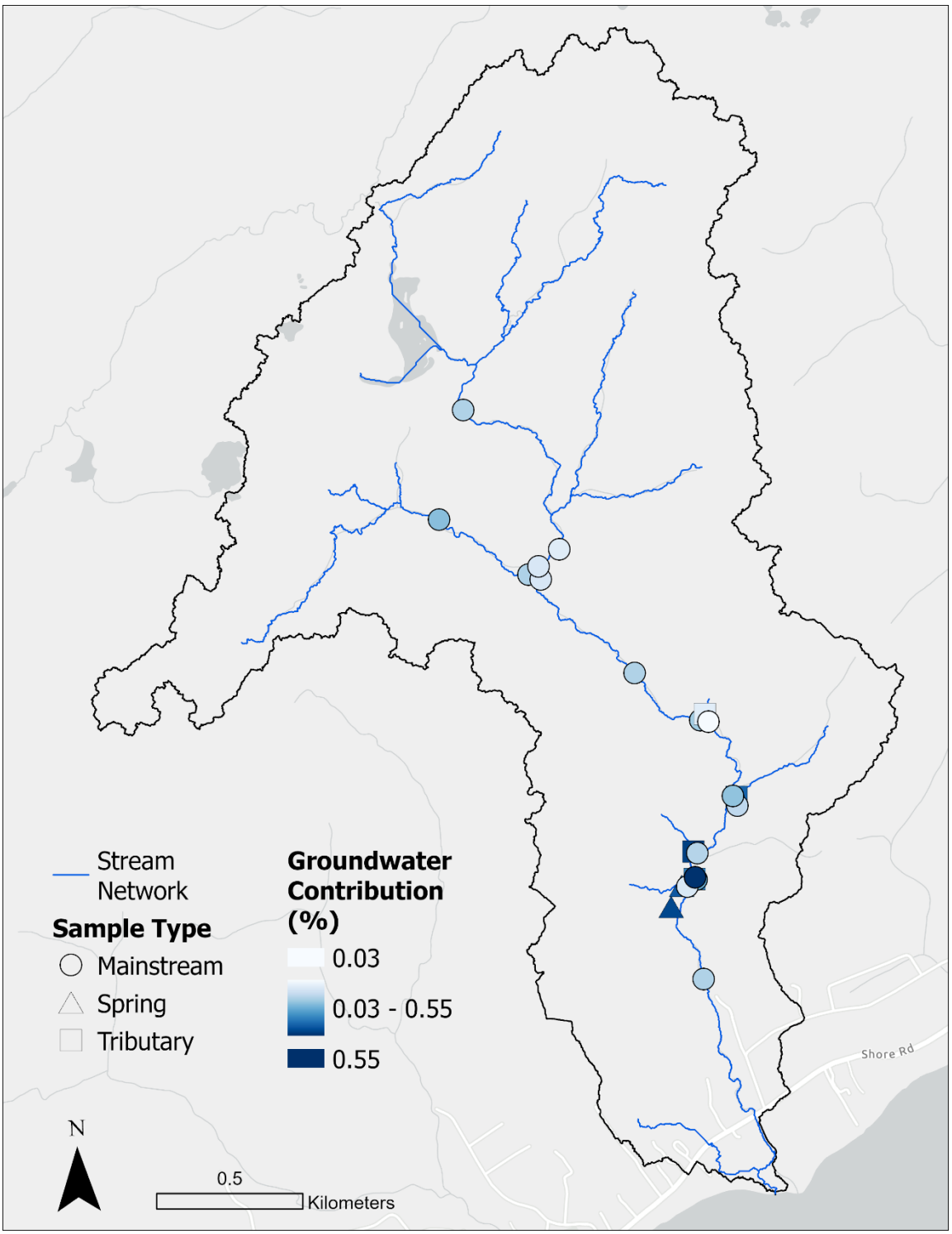

Figure 12: Spatial distribution of groundwater contribution to stream flow within the watershed, based on stream water samples averaged across the July 2022, November 2022, and July 2023 sampling campaigns.

Monte Carlo error propagation for each of the sampling periods (iterations = 1000) was used to investigate the impact of uncertainty in the measurements on end-member mixing results. Increasing the number of iterations past 1000 did not provide any discernable change in uncertainty. The uncertainty metric (1 standard deviation or the 68% confidence bounds) for each sampling period is provided in Table 3.

3.4 Baseflow Separation

The seven baseflow separation methods were applied to daily discharge data from July 2022 to July 2023 at the lowland station in the Christmas Brook watershed, yielding a range of Baseflow Index (BFI) values. Among the methods, Hydsep-LM produced the highest BFI (0.788), while Hydrun showed the lowest (0.531). The digital filtering methods (DF-F1 to DF-F5) exhibited varying BFIs, with results summarized in Table X. The Flow Duration Curve (FDC) for the lowland gauging station showed a steep slope, indicative of the stream's high responsiveness to runoff events. Consistent with this observation, the BFI estimated from Q90 was 0.48.

Table 4: Baseflow Index (BFI) values derived from seven separation methods applied to daily discharge data at the lowland station in the Christmas Brook watershed (July 2022–July 2023)

Method	BFI
Hydrun	0.531
Hydsep-LM	0.788
Lyne-Hollick filter method (DF-F1)	0.439
Chapman filtering method (DF-F2)	0.585
Chapman and Maxwell filtering method (DF-F3)	0.421
Boughton-Chapman filtering method (DF-F4)	0.602
Eckhardt filtering method (DF-F5)	0.686
Q90/Q50	0.48

DF-F3 (Chapman and Maxwell method) was chosen as the most representative method following comparison of BFIs, visual inspection and sensitivity analysis. The moderate filtering approach of DF-F3 effectively excludes high-frequency noise from small rainfall events, making it less sensitive to minor fluctuations and ideal for basins with pronounced seasonal variation. Mao et al. (2024) determined that the mechanism of action inherent to the method was more significant than the specific parameter values, further supporting the robustness of DF-F3 in this context.

For DF-F3, a coefficient (k) range of 0.90–0.925 is generally suitable for snow-influenced, mountainous basins with high seasonal variability, characterized by "flashy" rivers and lower groundwater contributions (Mao et al., 2024). We used a coefficient of 0.925. Figure 12 illustrates the baseflow separation results using the DF-F3 filter.

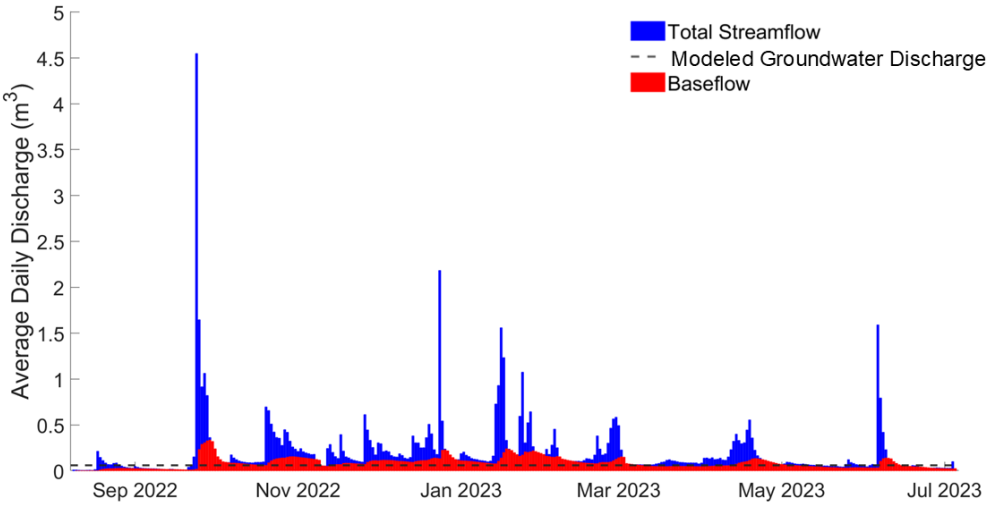

Figure 13: Streamflow and baseflow at the lower gauging station using the Chapman and Maxwell filtering method (DF-F3). Dashed lined represents simulated groundwater discharge to Christmas Brook from the hydrogeologic model.

3.5 Groundwater Modeling

3.5.1 Model Calibration and Evaluation

The observed groundwater levels were used to calibrate the MODFLOW6 groundwater flow model. The primary calibration parameters (parameters that were further examined with PEST and/or sensitivity analysis) were recharge rate, and hydraulic conductivity of the various geologic units. Lake and streambed hydraulic conductivity were manually calibrated. The initial hydraulic conductivities (i.e., a starting point for PEST calibration) for the hydrologic units within zones 1 and 3 were estimated from Freeze & Cherry (1979) and aligned with provincial surficial geologic mapping by Barr & White (2017). Model input and calibration parameter values are provided in Table 3.

Table 5: Calibrated parameters for the groundwater flow model. L1, L2, and L3 refer to the top middle and bottom layers, respectively. HU1, HU2, and HU3 refer to the three zones shown in Figure 2.

Model Parameter	Value	Source
Recharge Rate	280 mm/yr	Kennedy et al., 2010
Pumping Rate	-0.0017 m^3/s (x2)*	Polatbekov, 2020
K for Streambed	K_x * 10	Manual calibration
K for Lake Bottom	K_x * 10	Manual calibration
K for L1 HU1	2.00E-05 m/s	PEST
K for L1 HU 2	9.79E-09 m/s	PEST
K for L1 HU 3	9.97E-11 m/s	PEST
K for L2 HU 1	5.89E-05 m/s	PEST
K for L2 HU 2	2.00E-06 m/s	PEST
K for L2 HU 3	9.98E-10 m/s	PEST
K for L3 HU 1	1.89E-04 m/s	PEST
K for L3 HU 2	1.11E-07 m/s	PEST
K for L3 HU 3	1.00E-09 m/s	PEST

* A pumping rate of 0.0017 m^3/s was applied to both Arena Road Pumping Well 1 and Arena Road Pumping Well 2. While Polatbekov (2020) reported a 20-year safe yield (Q_{20year}) rate of 0.0066 m^3/s for Arena Road Pumping Well 2, current pumping rates could not be obtained from the community. Additionally, convergence issues were encountered when using the MAW package. To address this, the pumping rate for both wells was set at 0.0017 m^3/s, matching the rate reported for Arena Road Pumping Well 1 (Nolan, Davis & Associates Limited, 1984).

The recharge rate of the calibrated model was 280 mm/yr. The regional groundwater budget map developed by Kennedy et al. (2010), shows Cape Breton Regional Municipality having a recharge range of 260-300 mm/yr and an assigned recharge ratio of 0.17 (recharge/precipitation). The calibrated hydraulic conductivities for the fault and damage zone align with pumping test results in Appendix 2., from Polatbekov (2020).

The simulated hydraulic heads compare well with the average observed hydraulic heads (Figure 13; Table 6). The simulations achieve moderate goodness-of-fit metrics, as the RMSE is greater than half of the standard deviation but remains within the full standard deviation (RMSE = 3.97; Table 5). According to the guidelines by Moriasi et al. (2007), this indicates that the model provides a reasonable approximation of observed conditions. The modelled head in the highland observation wells are in closest agreement with the observations (absolute differences of 2.40, 2.49, 0.27, 1.44, 2.11 meters for MW1, MW2, MW3, PNA, and PNC, respectively). The observation well adjacent to the pumping well field shows the largest deviation (absolute difference of 4.46 meters). The input minus output for the calibrated model only varied by 5.6E-8 L^3/s. The inclusion of the single lowland observation well introduces significant skew to both the RMSE and PBIAS metrics because of the large disparity in hydraulic head between the highland and lowland wells. This discrepancy disproportionately affects the calculated goodness-of-fit metrics, as the lowland well's extreme value has an outsized influence on the overall error statistics. Since this lowland well represents a single observation and does not provide a sufficient basis for generalizing model performance across the domain, excluding it ensures the performance metrics reflect the majority of the dataset more accurately.

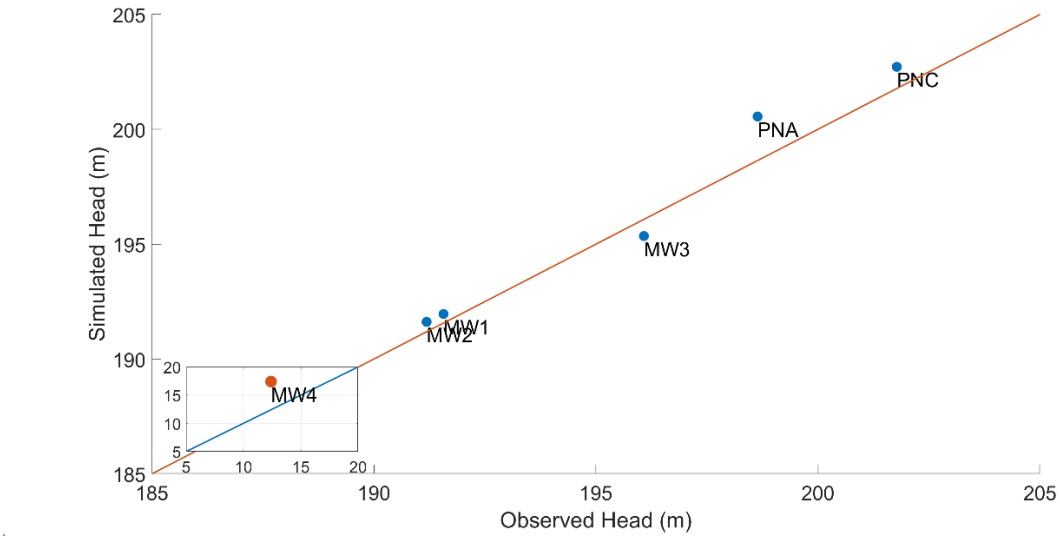

Figure 14: Observed vs. simulated hydraulic head values for the groundwater flow model. The inset shows monitoring well 4 which is at a lower elevation.

Table 6: Groundwater flow model performance metrics

Calibrated Model	**RMSE (m)**	**PBIAS (%)**
All Observation Points	2.53	- 11
Performance Targets (Moriasi et al., 2007)	1.98 (excluding MW4) (<0.5 * Observed SD)	+/- 25

Sensitivity analysis indicated that the model was most sensitive to hydraulic conductivity, followed by recharge rate. Hydraulic conductivity was varied across all layers simultaneously; however, model convergence issues arose when the difference in hydraulic conductivity between units (particularly HU5) was reduced to one order of magnitude, requiring adjustments for convergence. Recharge values were adjusted by +100 mm and -60 mm in accordance with recharge ranges from Kennedy et al. (2010), while hydraulic conductivity was varied by one order of magnitude in either direction

(Table 6). These scenarios were tested individually, and edge cases were assessed by combining increased recharge with increased hydraulic conductivity, and vice versa. Reducing K showed the largest influence on simulated head, substantially increasing head at the observation points. It is worth noting that in a steady-state model, the hydraulic heads are primarily influenced by the ratio of R to K rather than their absolute values, though the sensitivity of heads to these parameters can vary depending on the downgradient boundary conditions. Additionally, recharge is currently applied uniformly across all hydrogeological units (HUs). Allowing recharge to vary spatially between HUs could better reflect local hydrogeological conditions and may improve the overall model fit.

Table 7: Reported head values from calibrated model sensitivity analysis

Observed Head (m)		Simulated Head (m)				
Observation ID	Observed Values	Calibrated Model	Reduced Recharge	Increased Recharge	Reduced K	Increased K
MW1	191.57	189.17	189.03	189.39	196.33	188.60
MW2	191.19	193.68	193.31	194.24	208.70	191.81
MW3	196.08	196.35	195.76	197.26	226.54	193.07
MW4	12.40	16.86	16.76	17.03	18.48	16.91
PNC	199.25	201.36	200.41	203.44	267.25	197.12
PNA	201.07	199.62	198.78	201.27	252.44	195.57

3.5.2 Groundwater Flow Pathways and Particle Tracking

The simulated hydraulic heads in the model are highest in the highland plateau and decline towards the stream valley and lowlands (Figure 14A). Hydraulic gradients are steepest in Layer 1, particularly along the stream valley and the upper fault boundary. Flow is largely channeled through the surficial and fractured bedrock layers towards the stream network.

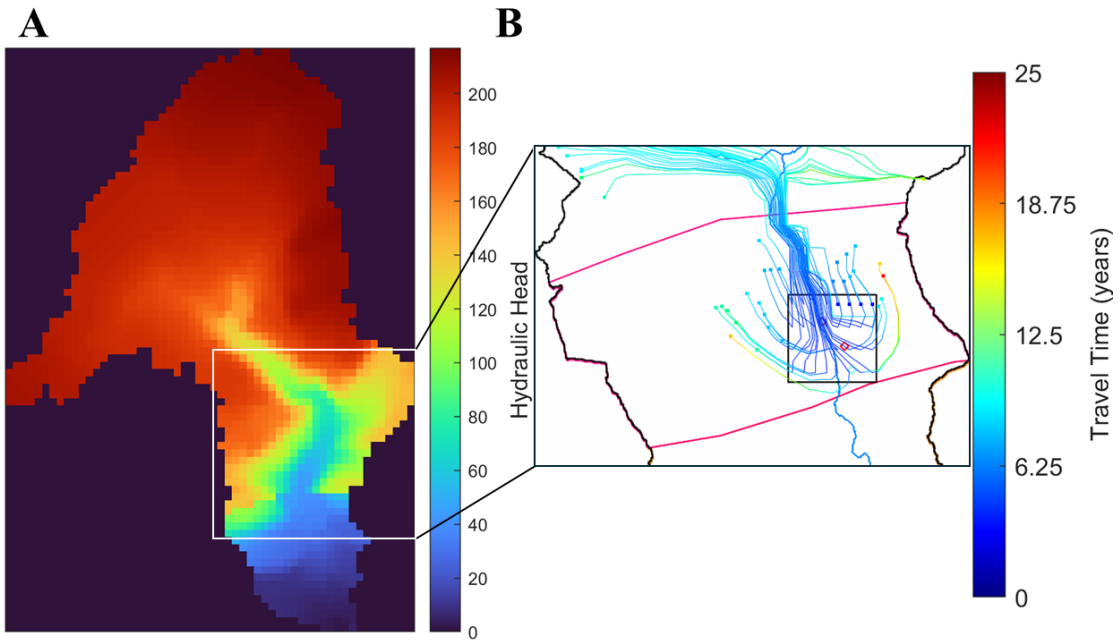

Figure 15: (A) Heat map of hydraulic head distribution across layer 1 of the model domain (B) reverse particle tracking from a square around the pumping wells (black square), over a 25-year period. Blue indicates shorter transit times; red indicates longer transit times. The pink lines are the fault zone boundaries.

Reverse particle tracking from the area around the pumping wells indicates two primary water sources for the pumping wells and the fault aquifer: (1) streamflow which infiltrates into the fault aquifer, representing 60% of the particle sources, and (2) localized capture zone (i.e., precipitation recharged near the pumping wells), which accounts for the remaining 40% (Figure 14B). While these percentages reflect the proportional contribution of particles, it is important to note that particles originating from local precipitation recharge have somewhat longer transit times (3-5 years from the stream and 1-2 years from the surrounding ground surface), suggesting that the faster travel of stream water particles to the wells increases the effective contribution of stream-derived recharge to the pumping wells over time. This implies that, despite representing only 60% of the particle sources, the influence of stream water on the total recharge volume reaching the wells could be considerably greater.

Occasionally, particles in Layer 2 (fractured bedrock) would exhibit looping paths before reaching a termination point, indicating vertical mixing between shallow and deep flow systems. The particle tracking results support the concept of enhanced groundwater-

surface water interactions within the fault zone, facilitated by fractures and permeable zones that channel flow efficiently. Furthermore, the reverse particle tracks from the well area suggest that the pumping wells create a substantial (~300-400m radius) capture zone around the pumping wells, redirecting local flow patterns.

Forward particle tracking showed that particles released in both the highland plateau wetlands and the forested gorge flowed towards the river network (Figure 15). Flow was much faster in the top model layer given the higher hydraulic conductivity with particles generally reaching the stream within 6-25 years. Mean particle transit times are provided in Table 4. Flow in the fractured rock layer was much slower, particularly in the plateau area which has a low hydraulic gradient. Particles released in the fractured rock beneath the wetland plateau moved only tens of meters over the 100-year simulation (Figure 15b).

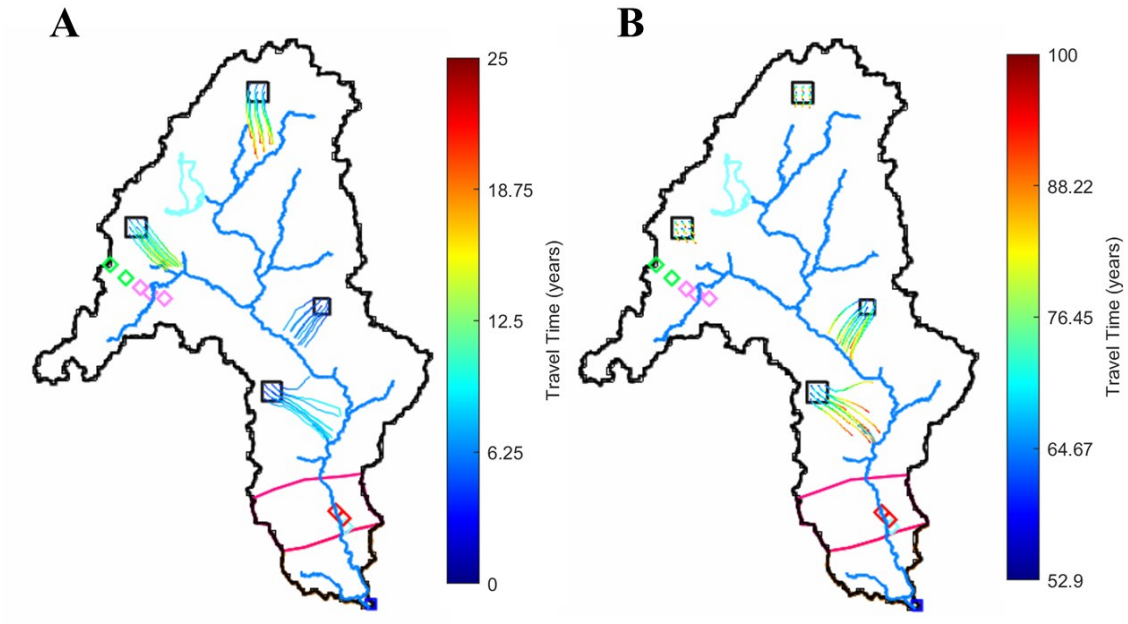

Figure 16: Forward particle tracking from four square areas within the model domain (2 in the wetland, 2 in the forested gorge). (A) Each square released nine particles from the model top. Particles were tracked over a period of 25 years. (B) Each square released nime particles from the top of layer 2 minus 1 meter. Particles were tracked over a period of 100 years.

Table 8: Forward particle tracking results

Particle Starting Position	Particle Summary			
	Released	Remain Active	Terminated at Weak Sink Cell	Average Transit Time of Particles that Reached Termination (Years)
Model Top	18	3	15	17.7
	18	-	18	4.6
Layer 2	18	18	-	-
	18	8	10	75.2

CHAPTER 4 – DISCUSSION

4.1 VARIABILITY AND CONTROLS ON TRACER CONCENTRATIONS

4.1.1 Charge Balance Error

Major ions were a key tool in understanding hydrologic dynamics at our study site. However, the average CBEs for each sapling campaign were all positive and were near or exceeded 5% (+19.7%, +7.1%, +23.4%, and +5.2%), for July, November 2022, May and July 2023, respectively), a data quality threshold proposed by Fetter (2001). According to Fritz (1994), positive CBE is often associated with alkalinity measurements in the lab. If the water is supersaturated with respect to calcite and/or dolomite, and alkalinity is measured in the lab, minerals may precipitate out of solution. When acidified, these minerals do not precipitate, but the alkalinity may be underreported, leading to a positive CBE. Furthermore, Fritz (1994) found that the quality of the CBE is influenced by ionic strength. A subset of their data with ionic strength below 0.001 showed CBEs over 10% higher than the complete data set, despite a smaller mean difference between cations and anions (cations-anions, in mEq/L). In the Christmas Brook samples, the ionic strengths for the field campaigns were relatively weak: 0.00088, 0.00122, 0.00102, and 0.00105 for July 2022, November 2022, May 2023, and July 2023, respectively, which may help to explain the relatively high CBEs. Meanwhile, the cation-anion differences were relatively large 5.98, 3.69, 8.78, and 2.77 mEq/L.

Additionally, positive CBEs might indicate the omission of some negatively charged ions, such as organic acids from wetlands. Given that the wetlands at our study site were a substantial source of streamflow, this may have also contributed to our CBE. Generally, the groundwater samples were found to have lower CBE while the wetland samples had higher CBE (November and May showed minor variations) which supports the idea that organic acids were a missing ionic component and contributed to CBE. Finally, analytical errors can contribute to CBE, but this source of error is expected to be minor since laboratory equipment is regularly tested using standard solutions. Given that

mixing analysis relies on the relative concentrations of ions rather than absolute concentrations, the CBE is not expected to negatively impact the accuracy of the mixing analysis.

4.1.2 Ionic Ratios and Geologic Influence

The hydrochemical analysis, incorporating ionic ratios based on Blumstock et al. (2014) and Langmuir (1971), provides insight into the influence of geology on watershed flow dynamics. The Ca^{2+}/Cl^{-} ratio, consistently below 1 and dropping below 0.5 in November, suggests that chloride is influenced by sources other than precipitation, such as ocean spray, road salt, or evaporite dissolution from the lowland Windsor group. The lower ratio during November indicates that chloride inputs may spike due to stored Cl^{-} being flushed by precipitation or reduced ion exchange affecting Ca^{2+} and Mg^{2+}.

The Ca^{2+}/Mg^{2+} ratio, ranging from 4.2 to 5.0, indicates the dominance of weathering processes involving calcium-rich minerals, such as feldspar, and the absence of significant magnesium-rich minerals like dolomite. This ratio is consistent with the geochemical interactions documented by Geofirma Engineering Ltd. (2012), where granodiorite bedrock's mineral composition, including feldspar and biotite, shaped water chemistry in similar ways.

The Na^{+}/Cl^{-} ratio, close to or exceeding 1 in most months but dropping to 0.42 in November, implies a shift in chloride dynamics, possibly from increased road salt input or flushing during precipitation events. Similar seasonal shifts in sodium and chloride dynamics have been reported by Geofirma Engineering Ltd. (2012), particularly in areas influenced by anthropogenic inputs. The Na^{+}/Ca^{2+} ratio (0.97-1.94) points to notable sodium contributions, likely from sodium-rich bedrock or ion exchange where sodium displaces calcium, reinforcing the influence of local geological features.

PH measurements between 5.5 and 7.0 suggest acidic conditions compared to typical groundwater (pH 7.0–8.5). This is consistent with the findings of Geofirma

Engineering Ltd. (2012), where acidic pH values were attributed to limited carbonate buffering in granodiorite bedrock systems. In this study, the acidic pH likely stems from weak acids such as organic acids or dissolved CO_2, potentially originating from wetland areas.

The absence of strong acids, such as sulfuric or nitric acid, is supported by the results in Appendix 3., which indicate no detectable CO_3 in any sample, ruling out pH variations due to strong acid-base neutralization. Additionally, the detection of minimal HCO_3^- (average concentration of 6.15 mg/L), suggests a minor buffering effect, likely sourced from the limited weathering of trace carbonate minerals rather than extensive carbonate buffering.

Collectively, these hydrochemical ratios and pH findings illustrate that the groundwater chemistry is tied to the regional geology, with limited carbonate influence and significant contributions from granodiorite minerals. The ionic ratios also indicate dynamic flow processes within the watershed, where interactions between surface water, wetlands, and underlying geological formations shape the chemical profile, particularly during periods of varying precipitation.

4.1.3 Isotopes

Isotopic signatures, like ion concentrations, exhibited variation with seasonality and discharge. Precipitation and surface water samples were generally more depleted in winter and spring and more enriched in summer and fall. At the stream gauging stations, the isotopic signatures were relatively homogeneous, except in November, when both $\delta^{18}O$ and $\delta^{2}H$ were somewhat more depleted. This period at the beginning of winter likely had isotopically depleted precipitation and low evaporitic enrichment in the watershed, which explains the depleted isotope signatures in the stream.

The average isotopic signatures at the lowland stream gauging station were -47.5 and -7.4, while at the upstream station, they were -44.1 and -6.8 (δ^2H and $\delta^{18}O$, respectively). Typically, waters at higher elevations tend to be more isotopically depleted since heavier isotopes preferentially precipitate at lower elevations. However, the opposite phenomenon was observed in this study, albeit over a limited elevation range. The more enriched isotope signature at the highland station is likely due to the influence of evaporative processes within the wetlands in the highland plateau. The wetlands store large amounts of water near the ground surface and in shallow ponds. They are also exposed to more solar radiation and wind which increase evaporation and lead to enriched isotopic signatures.

The isotopic composition of groundwater samples in this study showed a closer resemblance to winter precipitation compared to summer precipitation, suggesting that recharge is predominantly driven by winter precipitation including snowmelt. However, these results must be interpreted with caution, as we only have one true winter precipitation isotope sample. Despite this limitation, a similar isotopic signature was observed in spring surface water samples, which closely align with the winter isotope signature and can be inferred to be heavily influenced by snowmelt. This finding is consistent with studies from other regions where isotopic analysis revealed that winter precipitation often dominates recharge due to greater volume and effective infiltration (e.g., Valdivielso et al., 2024; Yapiyev et al., 2023). The extended presence of snow and delayed melt contribute to higher recharge rates during these transitional seasons. In the Christmas Brook watershed, the predominance of winter-driven recharge and extended snowmelt periods indicate that water table dynamics may be sensitive to shifts in winter and spring precipitation patterns which could be caused by climate change (Mao et al., 2021; Yapiyev et al., 2023).

4.2 Mixing Analysis indicates Wetland Water Dominates Streamflow

The results from the End-Member Mixing Analysis (EMMA) indicate that wetland ponds and peat porewater are dominant contributors to streamflow in Christmas Brook. Despite wetlands covering only 11% of the watershed, they account for an average of 73% of streamflow at the lower gauging station, underscoring their disproportionately important role in sustaining streamflow. Although the 11% spatial coverage based on the Nova Scotia Forest Inventory layer may underestimate the prevalence of treed wetlands. This finding aligns with studies in some other low mountain environments, which also highlight wetlands as critical contributors to streamflow (e.g. Liu et al., 2004; Soulsby et al., 2000). The outsized role of wetlands in maintaining hydrological stability is especially noteworthy in a region prone to seasonal variability.

These findings are consistent with other research emphasizing the significance of wetlands in hydrological processes. For example, research by Spence (2010), Liu et al. (2004), and St. Amour et al. (2005) have documented similar patterns where wetlands substantially contribute to streamflow, even in relatively small proportions of watershed area. The outsized influence of wetlands on streamflow dynamics is crucial for understanding water resource management, particularly in mountain watersheds that face pressures from climate variability and human development.

Groundwater contribution, by contrast, showed a marked increase during low-flow conditions (35%) compared to high-flow periods (19%), illustrating its importance for sustaining baseflow during drier periods. Similar trends have been observed in other studies, where groundwater was found to contribute around 20% of streamflow during both wet and dry seasons in certain regions of the Hudson Bay lowlands, Canada (Orlova & Branfireun, 2018), and up to 21% in fractured bedrock catchments of the Canadian Rockies (Paznekas & Hayashi, 2015). The Monte Carlo error propagation analysis reinforced the reliability of the EMMA results, showing generally non-overlapping end-member signatures. The calculated uncertainty, averaging ~15% at the outflow, was about half of the typical groundwater contribution (~27%).

However, the EMMA analysis for May 2023 is likely unreliable, as over half of the surface water samples were not bounded by the groundwater and wetland centroids (Figure 10). This anomaly suggests that an additional end-member, likely snowmelt, influenced the stream samples at that time. Other studies have demonstrated that snowmelt recharge plays a crucial role in controlling groundwater discharge to hillslope faces, while seasonal freezing and thawing of the subsurface can drive groundwater discharge to streams by acting as a piston, forcing groundwater to the surface (e.g., Evans et al., 2018). Similarly, Frisbee et al. (2009) found that groundwater can account for a smaller proportion of streamflow during the spring (14–44%) but tends to increase throughout the rest of the year, ranging from 19–78%. Therefore, in addition to missing an end-member, it is likely that the groundwater contribution is also underestimated in May 2023. Consequently, the mixing model does not accurately represent this period, and the reported error does not fully capture the poor fit of the data due to the method used for calculating the proportional contribution (normalized distance from centroids). Despite the uncertainty, the finding that wetlands contribute strongly to streamflow is robust and was consistent through all sampling campaigns.

The pumping wells were only able to be sampled twice during the study, and therefore our ability to use hydrochemistry to interpret the water origins is limited. Ionically, the pumping wells cluster with the stream water, which agrees with the groundwater modelling finding that Christmas Brook infiltration contributes substantially to the pumping wells. Isotopically, the pumping wells cluster centrally but are somewhat depleted, potentially indicating the importance of winter precipitation for recharge. In PC space, the pumping wells are somewhat distinct from other samples. This may reflect the similar ion chemistry to the surface water samples but a time-lag in the isotopes due to their slower flow compared to surface waters. Further sampling and analysis would be necessary to better understand the chemical origins of the pumped groundwater.

Overall, while the seasonal variability in streamflow sources highlights the complex interplay between wetland and groundwater sources, the reliability of the EMMA results and the strong contribution of wetlands indicate their critical role in the hydrology of Christmas Brook. Future work could further refine these findings by

integrating additional seasonal data and evaluating the influence of runoff, snowmelt and other transient sources on streamflow composition.

4.3 BASEFLOW

The DF-F3 baseflow separation method (Chapman and Maxwell) was selected for baseflow separation and yielded a BFI of 0.421. This method was particularly effective in balancing the exclusion of high-frequency noise from rainfall with the retention of gradual baseflow variations. This approach aligned with the watershed's characteristics—snow-influenced, with marked seasonal variability and lower sustained groundwater input. The use of multiple baseflow separation techniques emphasized the importance of comparing their results to understand how seasonal and event-driven variability affects baseflow estimation. By evaluating the strengths and limitations of each method, we were able to select the most appropriate one for the Christmas Brook watershed. Additionally, the findings of Li et al. (2023), demonstrated that topography influences baseflow and streamflow accumulation, a pattern also observed in Christmas Brook, where downstream flow characteristics are shaped by terrain. Both factors support the choice of the DF-F3 method for detailed analysis

The separated baseflow for Christmas Brook showed pronounced variability between wet and dry periods, with baseflow as a relative portion of streamflow aligning with seasonal flow dynamics observed in similar studies. For example, Bosch et al. (2017) found that baseflow in the South Georgia, U.S., watershed was highest during the dry season when overall streamflow was low, and lowest during the wet season, reflecting precipitation and evapotranspiration cycles. A similar trend emerged in Christmas Brook: from November to March, event flow dominated, coinciding with higher precipitation and potential snowmelt, while baseflow became a more significant portion of streamflow during the late spring and summer months (May to September), except during a notable precipitation event in July that temporarily altered the hydrograph.

4.4 Groundwater Flow Patterns in a Low Mountain Catchment

4.4.1 Observed Head and Vertical Hydraulic Gradients

Groundwater levels across the monitoring wells were relatively shallow and responded rapidly to precipitation events. This suggests that recharge to the fractured rock aquifer occurs quickly following rainfall. Rathay, Allen, and Kirste (2018) noted that in fractured bedrock aquifers, groundwater level rise (recharge) generally correlates more strongly with cumulative rainfall over multiple events rather than single heavy rainfall events. Our data, on the other hand, show rapid response to precipitation events, although some smaller precipitation events did not illicit a groundwater level response. This difference may be due to the degree of fracturing at our study site and/or the shallow groundwater table location.

Two of the highland bedrock monitoring wells (MW2 and MW3) exhibited weak upward hydraulic gradients according to spot measurements while MW1 indicated a stronger downward hydraulic gradient according to continuous level measurements in both shallow and deep wells. MW1 is located closer to the river gorge, and the average groundwater levels are deeper than the other two highland bedrock wells. Therefore, this well is likely in a groundwater recharge area with flow downwards and towards the river valley. Meanwhile, MW2 and MW3 are located further into the plateau, close to wetlands. Furthermore, MW2 is located at the bottom of a small slope where wetland water may be discharging. When a wetland is underlain by a shallow, less permeable layer (in this case peat overlying bedrock), water tends to exit the wetland's low point as overland flow, channel flow, or interflow. Therefore, MW2 and MW3 are likely in areas of weak local groundwater discharge.

4.4.2 Groundwater Flow Paths and Fault Aquifer Recharge Sources

The groundwater flow model indicated that groundwater flow in the highland plateau was generally shallow and slow whereas rapid shallow flow occurs in proximity to the steep river gorge where hydraulic gradients are steepest. Similarly, a study conducted in the crystalline rock highlands and peneplains of the Czech Republic found that in down-slope transition zones, shallow rapid flow is often the preferential groundwater flow pathway (Doležal, Kvítek, Soukup, Kulhavý, & Tippl, 2004).

Particle tracking simulations provided insights into flow paths and recharge sources within the fault aquifer. Forward tracking revealed that particles released at the wetland plateau predominantly followed shallow pathways, with all particles discharging to streams within approximately 12-25 years. The particles released in the gorge moved more rapidly to the stream with transit times of 1-10 years. When particles were introduced at the stream feature in the fractured zone (L2 Z2), a marked losing stream condition was observed, where streamflow infiltrated to recharge the fault aquifer. The observed infiltration of streamflow into the aquifer along the toe of the slope is similar to surface mountain front recharge (surface MFR) but on a small scale. Surface MFR is a well-documented source of recharge to lowland aquifers near high mountains, particularly in arid or semi-arid regions (Bouimouass et al., 2019; Carling et al., 2012; Burness, Chermak, & Brookshire, 2004) but has not been well documented in low mountains, particularly in humid climates like Nova Scotia.

Reverse particle tracking analysis highlighted a well capture zone near the pumping well (approximately 300 m wide). Approximately 40% of the pumping well supply was attributed to local precipitation recharge within the well capture zone which directly recharged the fractured fault aquifer. Despite the considerable hydraulic gradient exerted by the highland topography, there was little subsurface flow from the lower-permeability rock of HU1 to the area around the pumping wells. In other words, there appears to be very little mountain block recharge (MBR) in the Christmas Brook watershed, i.e., subsurface flow from the highlands to the lowlands. However, the

equivalent porous medium approach to simulating groundwater flow in bedrock may not accurately capture concentrated flow that can occur in fractures. Instead, there is considerable surface MFR wherein stream water enters the subsurface at the transition zone between the upland and the adjacent lowland. The reverse particle tracking from the pumping wells to the upper extent of the fault boundary suggested a travel time of approximately 2-5 years from when stream water infiltrates to when it was pumped from the well.

Several limitations are associated with the particle tracking. First, the steady-state model was converted to transient to quantify transit times (Figure 15; Table 7). However, the model continued to simulate average conditions (i.e., it was quasi steady-state), which means that pulse or event-driven flow which may decrease transit times cannot be simulated. Second, factors like the initial layer for particle release, the direction of particle tracking (forward or backward), and whether particles bypass or terminate at weak sinks significantly influenced particle pathways. A single simulation cannot fully capture the complexity of flow processes, given these limitations. Thus, multiple model outputs were be interpreted collectively to provide a comprehensive understanding of recharge dynamics. This collective approach helps to account for interactions not well-represented in a single model run, supporting more robust conclusions about the dominant recharge mechanisms and their spatial variability.

Isotope tracer analysis and ion concentration data agree with the particle tracking results that the wetland contributes substantially to the recharge observed in the fault zone via stream water infiltration. This is inferred from the chemical signatures indicating that the source of water in the pumping well aligns more closely with water samples from the wetlands and stream water, rather than bedrock monitoring well samples. This also suggest relatively rapid recharge since the stream/wetlands chemical signatures are not being altered by geologic contact or long transit times.

4.4.3 Groundwater Model Evaluation and Uncertainty

The steady-state groundwater model achieved strong performance metrics and reasonably recreated the observed average hydraulic heads. The model's streamflow routing package simulated an outflow of 0.06 m^3/s (from groundwater discharge only, i.e., no runoff). For comparison, the BFI from the DF-F3 baseflow separation (0.421) can be multiplied by the average streamflow (0.185 m^3/s) to get 0.078 m^3/s which is close to the simulated groundwater discharge. This baseflow estimate supports the model's outputs, reinforcing the interpretation that groundwater is a substantial but perhaps not dominant, component of streamflow, with higher contributions during drier periods.

The sensitivity analysis revealed that the simulated hydraulic heads were highly sensitive to decreasing K, and only somewhat sensitive to increasing K or changing the recharge rate (R). However, hydraulic head in steady-state models depends primarily on the R/K ratio, rather than the absolute values of R or K. While both R and K were varied within acceptable ranges, K inherently has greater uncertainty due to its high spatial variability and the difficulty of direct measurement, compared to R, which can often be better constrained through hydrological studies. Certain sensitivity runs resulted in model convergence errors or high water-balance errors when parameters became unrealistic. For example, in the scenario of reduced hydraulic conductivity, K in the faulted unit (L2 Z2) could only be reduced by 0.5 orders of magnitude before the model failed to converge. This limitation likely reflects the fact that reduced K creates disproportionate increases in simulated heads, disrupting the balance with recharge and exceeding the tolerances of the numerical solution. While this allowed the model to converge, the Multi-Aquifer Well package (MAW) had a +26% discrepancy in water budget and the porewater wells in the wetlands reported heads above ground surface. Similarly, in the edge case of decreased precipitation and decreased hydraulic conductivity, HU 5 could only be reduced by 0.5 orders of magnitude, and the error for the MAW package was positive 56%. However, the reported porewater values were reasonable (Table 6). Therefore, for some of the extreme sensitivity cases, the sensitivity may not be well captured due to water balance errors.

An additional model characteristic that was considered during this research was the fault aquifer shape and extent. Upon consultation with a local expert and through inspecting various geospatial datasets, three different fault shapes were proposed (Figure 16): (1) the fault (HU2) is represented by the East Bay fault, coinciding with a band of granodiorite material from the Geologic Map of the Province of Nova Scotia (Nova Scotia Department of Natural Resources, 2017); (2) the fault is represented by the East Bay fault and the fault swarm to the north (3) the fault is represented by the East Bay fault, the fault swarm, and the river gorge also follows a fault. In all cases, the lower fault boundary is abutted by the same third hydrogeologic unit (HU3), which represents the Bras D'Or Lowlands, Horton Group geology (sedimentary evaporites, clastic, and organics).

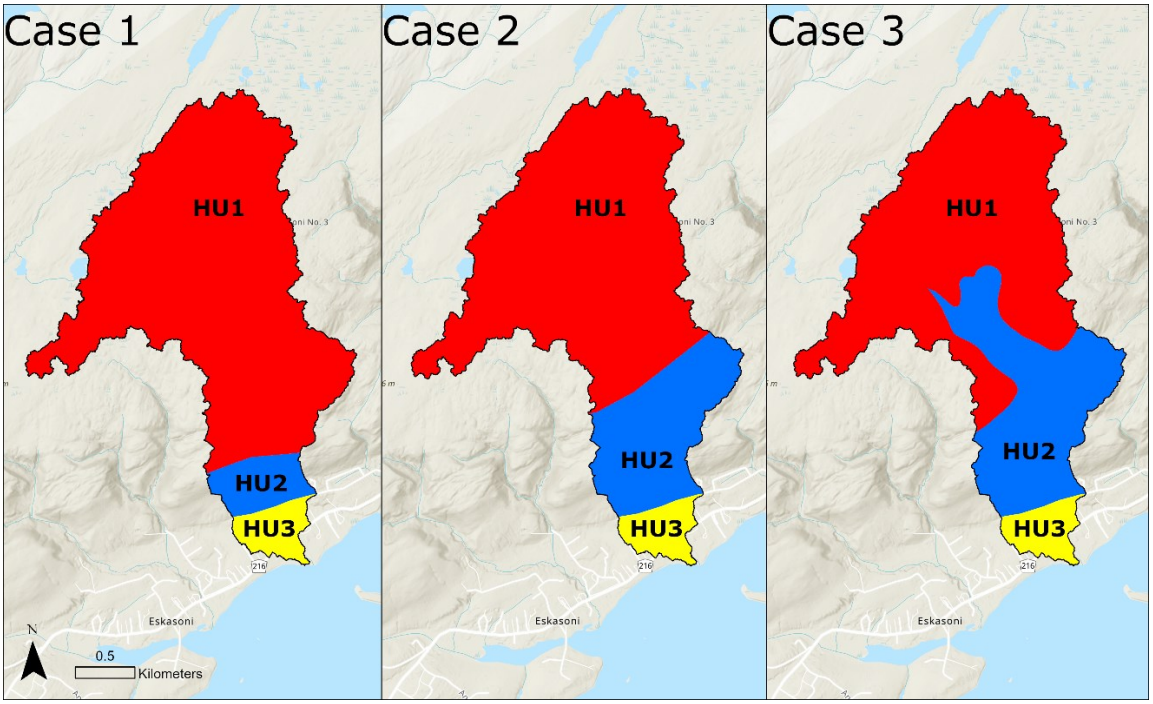

Figure 17: Different fault shapes considered for modelling. (A) East Bay fault (B) A + Fault Swarm (C) B + faulted gorge. HU1- intact crystalline bedrock, HU2- fault and damage zone, HU3- intact sedimentary evaporites.

Given the lack of knowledge of the fault extent, the modelling for this research was based on case 1 above. Future modeling using alternative fault scenarios could

provide new insights into watershed flow dynamics. Additional borehole analysis, LiDAR analysis (lineaments), and thermal imaging of springs could be useful tools to assess the fault extent. A larger fault aquifer extent could significantly impact groundwater dynamics by increasing local recharge potential, as it would allow precipitation to infiltrate rapidly over a broader area. This could create a more extensive zone of losing stream along Christmas Brook, thereby enhancing the amount of streamflow that could recharge the fault aquifer. Additionally, an expanded fault zone may facilitate increased groundwater flow beneath the river channel, contributing to more substantial hyporheic exchange flows. Such changes could alter the local water table, potentially impacting nearby ecosystems and influencing water availability downstream.

As a potential next step, employing a Discrete Fracture Network (DFN) numerical model of groundwater flow could offer valuable insights into how the fractured rock mass influences flow patterns, especially in the context of fault aquifers. Costanzo, Vidal, & Marshall (2021) used a DFN model to simulate groundwater flow in fractured rock aquifers, providing a detailed analysis of how the fracture network structure influences flow behavior. The study demonstrated the challenges of characterizing fracture properties and emphasized the importance of using site-specific fracture data to improve the accuracy of groundwater flow models. Many DFN models exist that could be applied here; however, it is important to note that parameterizing these models may require additional data on fracture networks and their properties, which may not be readily available.

4.5 Complementary Insights of Tracer and Modeling Methods

The tracer mixing analysis and groundwater flow modelling provided complementary information about the hydrologic dynamics in the study watershed. While many tracer studies have been conducted in mountain settings (Gibson et al., 2005; Vystavna et al., 2020; Liu & Yamanaka, 2012), relatively few hydrogeologic modeling studies have been conducted in mountains and it is even less common to apply both methodologies. We found that the tracer study was most useful in quantifying streamflow

sources and characterizing seasonality of flow dynamics. The tracers were less useful in understanding groundwater recharge sources given that groundwater flow influences chemical composition. However, the isotopic and ionic measurements did provide a link between the pumping wells and stream flow and also suggested the importance of winter precipitation in groundwater recharge. Meanwhile, the groundwater modelling provided insights into subsurface flow paths and aquifer recharge sources.

The combined methods agreed on the spatial patterns in groundwater discharge, with both models showing that, further downstream, groundwater flow paths contributed more significantly to streamflow. Both the mixing model and the groundwater flow model indicated that the fractured zone played a critical role in allowing streamflow to infiltrate into the fault aquifer. The consistency between methods also highlighted how groundwater discharge varied with changes in local streambed topography, with higher groundwater contributions in areas with steep valley streams. Furthermore, both models showed a similar temporal variation, with greater groundwater influence during low-flow conditions compared to periods of high rainfall, emphasizing the importance of subsurface flow in maintaining streamflow during dry periods.

Tracer-enabled modeling studies provide additional opportunities to constrain numerical groundwater flow models with field data beyond hydraulic head and streamflow. For instance, isotopic tracers such as tritium/helium-3 and noble gases have been used to distinguish multiple recharge components that were not identifiable using hydraulic head data alone. Holmes et al. (2023) conclude that flow data should remain the primary focus of hydrogeologic modeling, but adding isotopic tracer data—alongside streamflow—produced better flow simulation ensembles and improved model validation performance. Similarly, studies like that of Doyle et al. (2015) demonstrate how isotopic tracers can enhance the conceptual understanding of groundwater flow by revealing different recharge components, such as modern water with warm recharge temperatures and premodern water with colder temperatures and highlighting the limitations of hydraulic head data in capturing complex recharge processes like mountain block recharge.

4.6 Recommendations for Source Water Protection

To ensure a sustainable and high-quality water supply, protecting key areas that contribute to both groundwater recharge and streamflow is recommended. First, the immediate surroundings of the pumping wells, which are drilled into the fault aquifer, require careful management. The fault zone is highly permeable, facilitating quick infiltration of water. Pumping the well draws water from all directions surrounding the well but particularly from the upgradient direction. Any disturbances in this recharge zone—whether through land development or contamination—could alter the sustainability of the water supply. Christmas Brook watershed represents only a portion of the larger fault aquifer that is used for water supply in Eskasoni. The interconnected nature of the fault aquifer across the three well fields in the region underlines the need for a multi-watershed study to better understand the hydrological relationships between the wells, surface water, and recharge zones.

Second, our findings highlight the importance of safeguarding the wetlands at the headwaters of Christmas Brook, as they are the primary source of stream flow which later infiltrates into the fault aquifer which feeds the community's pumping wells. Wetlands act as natural hydrologic buffers, filtering water and maintaining streamflow in dry periods, which is directly linked to the health of the community's drinking water supply (Worrall et al., 2003).

Third, the steep gorge banks show relatively rapid groundwater flow towards Christmas Brook and also require considered management. Although outside the scope of the current study, these slopes are also likely important for rapid runoff responses which can cause flooding. These areas can quickly channel water into the stream, carrying sediment and contaminants that may degrade water quality and affect both surface and groundwater. Protection of these areas ensures that water quality remains adequate by preventing excessive runoff, especially during storm events, which could otherwise pollute the aquifers feeding into the wells.

Additionally, a comprehensive water quantity study should complement the focus on source water quality protection. Better understanding the volume and flow of water within these systems will help ensure that the community's water needs are met without depleting the resources. Upgrading and maintaining water infrastructure to eliminate pumping losses, minimize drinking water contamination, and reduce transmission losses are key to improving the efficiency and reliability of the water supply. By enhancing these systems, the community can better manage its water resources, reduce operational costs, and protect both water quality and availability in the long term.

4.7 Limitations and Future Research

The primary limitation of the hydrochemical mixing analysis is the synoptic nature of the four sampling campaigns. With only four datasets, it is difficult to accurately capture seasonal variation or account for measurement uncertainty and outliers. A multi-year dataset would reduce uncertainty by providing more data points that better represent the true water types. Over time, this would allow for tighter clustering of values, diminishing the influence of seasonal outliers and leading to more reliable estimates of water chemistry. In addition, a broader sampling effort during the winter months (December-March), would help to assess the influence of meltwater on streamflow. The end-member mixing model assumes that tracers remain stable over space and time, but the hydrochemical system is dynamics, with constant ion exchange and chemical interactions. To mitigate this uncertainty, multiple datasets were analyzed, both individually and as an ensemble.

The hydrologic model also has limitations and uncertainties that influence the results. One of the biggest challenges in groundwater research, particularly in montane environments, is obtaining and accessing hydrogeologic data. Of the nine hydrogeologic units parameterized in the model, only four had drill log information, and even that data was limited. As is common in groundwater modeling, hydraulic parameters often carry the most uncertainty (Andserson, Hunt, & Woessner, 2015). Uncertainties remained

regarding hydraulic conductivities, the depth of geologic layers, and the size and shape of the fault. Additionally, the steady-state nature of the model is inherently limiting. By relying on steady-state assumptions, extreme values are not represented, and the input data, being annual averages, does not capture the influence of seasonality. As noted by Alley, Reilly, & Franke (1999), using average conditions can underestimate the importance of precipitation events and droughts.

Another constraint in the modeling process was the limited data from the lowland area. Only one lowland monitoring well was equipped with a logger (August-March 2023) to calibrate the lower half of the model domain. During uncertainty analysis, this monitoring well showed the largest variation between observed and simulated head, possibly due to the minimal data available and/or its proximity to the pumping wells where hydraulic gradients are steep and pumping rates are temporally variable.

CHAPTER 5 – CONCLUSION

This study enhances our understanding of groundwater-surface water interactions and aquifer recharge processes within small, low-mountain watersheds with complex geology. The study had three primary objectives: (1) to quantify the sources and contributions of streamflow and fault groundwater within the watershed using End-Member Mixing Analysis (EMMA), (2) to develop a numerical groundwater flow model to analyze flow paths to the fault aquifer used for drinking water, and (3) to compare the results from these two approaches to gain a comprehensive understanding of hydrological dynamics within the watershed.

The hydrochemical analysis revealed that streamflow within the Christmas Brook watershed is primarily composed of groundwater and wetland water. Groundwater contributes 27 ± 15% of the streamflow at the downstream gaging station, with the remaining 73 ± 15% sourced from wetlands. The contribution of groundwater increases downstream and is notably higher during spring and fall.

A hydrogeologic model was developed and calibrated using MODFLOW 6, ModelMuse, PEST, and MODPATH. The model calibration achieved an acceptable fit to observed data, with an RMSE of 2.53 m (~1.3% of average head) and a PBIAS of -0.55%. Local flow paths were assessed using MODPATH, revealing that all of particles released in the highland plateau exhibited shallow, slow flows. Reverse particle tracking from the wells identified two predominant flow paths. Forty percent of the particles followed semi-direct paths, likely indicating that they were primarily influenced by localized recharge, with groundwater movement exhibiting radial flow towards the pumping well. In contrast, 60% of the particles terminated near the upper fault boundary, where surface water infiltrates into the aquifer.

Various baseflow separation methods were evaluated, with the Chapman and Maxwell filtering method (DF-F3) identified as the most representative, yielding a Baseflow Index (BFI) of 0.421. The model's average outflow (0.06 m^3/s) accurately

captured the hydrograph's baseflow troughs and agreed with groundwater discharge simulated by the steady state model.

This research highlights the importance of wellhead protection but also protecting the wetlands and river valley upstream given the tight stream-aquifer connection. It also demonstrates that surface mountain front recharge can be an important water resource in low mountains in a humid environment. Future research should focus on long-term data collection and analysis, particularly isotopic studies, to facilitate advanced analyses such as young water fraction estimation and tracer-based model calibration. The current steady-state model should be further developed into a transient model to better represent seasonal and event-based variations in hydrometric and groundwater levels. Additionally, probing wetland peat could improve quantification of highland near-surface storage. A more extensive field sampling campaign during the winter months (December-March) could also help quantify the impact of meltwaters on streamflow.

BIBLIOGRAPHY

Acreman, M., & Holden, J. (2013). How Wetlands Affect Floods. *23*, 773–786. doi:https://doi.org/10.1007/s13157-013-0473-2

Agriculture Canada. (1981). Soil Survey of Cape Breton Island Nova Scotia.

Alberta Forest Products Association. (2024). *Boreal Forest*. Retrieved from Alberta Forest Products Association.

Allen, D. M., & Nott, A. H. (2021). How Important Are Those Fracture Zones? Scale Dependent Characteristics Revealed Through Field Studies and an Integrated Hydrological Model of a Mountain Headwater Catchment. *Frontiers in Water*. doi:http://dx.doi.org/10.3389/frwa.2021.767399

Alley, W. M., Reilly, T. E., & Franke, O. L. (1999). Sustainability of Gorundwater Resources. Denver, Colorado.

Andermann, C., Longuevergne, L., Bonnet, S., Crave, A., Davy, P., & Gloaguen, R. (2012). Impact of transient groundwater storage on the discharge of Himalayan rivers. *Nature Geoscience*, 127-32.

Andserson, M. P., Hunt, R. J., & Woessner, W. W. (2015). Applied Groundwater Modeling, Simulation of Flow and Advection Transport, Second Edition. doi:https://doi.org/10.1016/C2009-0-21563-7

Aquilina, L., Stumpp, C., Tonina, D., & Buffington, J. M. (2023). Hydrodynamics and geomorphology of groundwater environments. In 2 (Ed.), *Groundwater Ecology and Evolution* (pp. 3-37). doi:https://doi.org/10.1016/B978-0-12-819119-4.00014-7

Assembly of First Nations. (2021). *Marine Indigenous Protected and Conserved Areas.* Ottawa.

Baechler, F. (2009). Targeting fault aquifers on Cape Breton Island. *GeoHalifax Annual conference*, (p. 7).

Baechler, F. (2015). The Geology and Hydrogeology of Faults on Cape Breton Isalnd, Nova Scotia, Canada: and Overview. *Atlantic Geology*, 51, 242-268.

Baechler, F. E., Cross, H. J., & Baechler, L. (2019). The Geology and Hydrogeology of Springs on Cape Breton Island, Nova Scotia, Canada: an Overview. *Atlantic Geoscience*, 55, 137-151.

Ball, L. B., Ge, S., Caine, J. S., Revil, A., & Jardani, A. (2010). Constraining fault-zone hydrogeology through integrated hydrological and geoelectrical analysis. *Hydrogeology Journal*, 1057-1067. doi:DOI 10.1007/s10040-010-0587-z

Barnett, T. P., Adam, J. C., & Lettenmaier, D. P. (2005). Potential impacts of a warming climate on water availability in snow-dominated regions. *Nature*, 303-309. doi:https://doi.org/10.1038/nature04141

Barr, S., & White, C. (2017). Bedrock Geology Map of the Grand Narrows Area, NTS 11F/15, Cape Breton, Inverness, Richmond and Victoria Counties, Nova Scotia.

Benischke, R. (2021). Review: Advances in the methodology and application of tracing in karst aquifers. *Hydrogeology Journal, 29*(5). doi:http://dx.doi.org/10.1007/s10040-020-02278-9

Bense, V. F., Gleeson, T., Loveless, S. E., Bour, O., & Scibek, J. (2013). Fault zone hydrogeology. *Earth-Science Reviews*, 171-192. doi:https://doi.org/10.1016/j.earscirev.2013.09.008

Blackstock, M. (2001). Water: A First Nations' spiritual and ecological perspective. *Journal of Ecosystems and Management, 1*(1).

Blumstock, M., Tetzlaff, D., Malcolm, I. A., Nuetzmann, G., & Soulsby, C. (2014). Baseflow dynamics: Multi-tracer surveys to assess variable groundwater contributions to montane streams under low flows. *Journal of Hydrology*, 121-133. doi:http://dx.doi.org/10.1016/j.jhydrol.2015.05.019

Boehner, R. C., Adams, G. C., & Giles, P. S. (2003). *Mineral Resources Branch, Report of Activities 2002.* Nova Scotia Department of Natural Resources.

Boehner, R., & Giles, P. (2008). Geology of the Sydney Basin, Cape Breton and Victoria Counties, Cape Breton Island, Nova Scotia.

Bosch, D. D., Arnold, J. G., Allen, P. G., Lim, K.-J., & Park, Y. S. (2017). Temporal variations in baseflow for the Little River experimental watershed in South Georgia, USA. *Journal of Hydrology: Regional Studies, 10*, 110-121. doi:https://pdf.sciencedirectassets.com/287972/1-s2.0-S2214581817X00025/1-s2.0-S2214581816301501/dx.doi.org/10.1016/j.ejrh.2017.02.002

Bouimouass, H., Fakir, Y., Leblanc, M., & Tweed, S. (2019). Investigation of groundwater recharge under a semiarid irrigated mountain-front area (Haouz-Tensift basin, Morocco). *46th Annual Congress of the International Association of Hydrogeologists.*

Boulton, A. J., Datry, T., Kasahara, T., Mutz, M., & Stanford, J. A. (2010). Ecology and management of the hyporheic zone: stream–groundwater interactions of running waters and their floodplains. *Freshwater Science, 29*(1).

Brown, K., Naylor, L. A., & Quinn, T. (2017). Making Space for Proactive Adaptation of Rapidly Changing Coasts: A Windows of Opportunity Approach. *Sustainability*. doi:https://doi.org/10.3390/su9081408

Brunner, P., Therrien, R., Renard, P., Simmons, C. T., & Franssen, H.-J. H. (2017). Advances in understanding river-groundwater interactions. *Reviews of Geophysics'*. doi:https://doi.org/10.1002/2017RG000556

Burkey, J. (2024). Hydrograph Separation using HYDSEP. MATLAB Central File Exchange. Retrieved 2024, from https://www.mathworks.com/matlabcentral/fileexchange/36387-hydrograph-separation-using-hydsep

Burness, S., Chermak, J., & Brookshire, D. (2004). Water management in a mountain front recharge aquifer. *Water Resource Research*. doi:https://doi.org/10.1029/2003WR002160

Burns, D. A., McDonnell, J. J., Hooper, R. P., Peters, N. E., Freer, J. E., Kendall, C., & Beven, K. (2001). Quantifying contributions to storm runoff through end-member mixing analysis and hydrologic measurements at the Panola Mountain Research Watershed (Georgia, USA). *Hydrological Processes, 15*, 1903-1924. doi:10.1002/hyp.246

Burt, T. P., & Ferranti, E. J. (2012). Changing patterns of heavy rainfall in upland areas: a case. *International Journal of Climatology*, 518-532. doi:10.1002/joc.2287

Caine, J. S., Evans, J. P., & Forster, C. P. (1996). Fault zone architecture and permeability structure. *Geology*, 1025-1028. doi:http://dx.doi.org/10.1130/0091-7613(1996)024%3C1025:FZAAPS%3E2.3.CO;2

Cao, V., Schaffer, M., Taherdangkoo, R., & Licha, T. (2020). Solute Reactive Tracers for Hydrogeological Applications: A Short Review and Future Prospects. *Water, 12*(3). doi:https://doi.org/10.3390/w12030653

Carling, G. T., Mayo, A. L., Tingey, D., & Bruthans, J. (2012). Mechanisms, timing, and rates of arid region mountain front recharge. *Journal of Hydrology, 428-429*, 15-31. doi:https://doi.org/10.1016/j.jhydrol.2011.12.043

Carrera, J., Vazquez-Sune, E., Castillo, O., & Sanchez-Vila, X. (2004). A methodology to compute mixing ratios with uncertain end-members. *Water Resource Research*. doi:https://doi.org/10.1029/2003WR002263

Chapman, T. (1999). A comparison of algorithms for stream flow recession and baseflow separation. *Hydrological Processes*. doi:https://doi.org/10.1002/(SICI)1099-1085(19990415)13:5%3C701::AID-HYP774%3E3.0.CO;2-2

Christophersen, N., & Hooper, R. P. (1992). Multivariate analysis of stream water chemical data: The use of principal components analysis for the end-member mixing problem. *Water Resource Research*. doi:https://doi.org/10.1029/91WR02518

Cochand, F., Therrien, R., & Lemieux, J.-M. (2018). Integrated Hydrological Modeling of Climate Change Impacts in a Snow-Influenced Catchment. *Groundwater*. doi:https://doi.org/10.1111/gwat.12848

Cook, P. (2020). *Introduction to Isotopes and Environmental Tracers as Indicators of Groundwater Flow.* Guelph: Groundwater Project. doi:https://doi.org/10.21083/978-1-7770541-8-2

Costall, A. R., Harris, B. D., Teo, B., Schaa, R., Wagner, F. M., & Pigois, J. P. (2020). Groundwater Throughflow and Seawater Intrusion in High Quality Coastal Aquifers. *Scientific Reports, 10*(9866). doi:https://doi.org/10.1038/s41598-020-66516-6

Costanzo, C. P., Vidal, A. C., & Marshall, B. (2021). Integration of discrete fracture networks and flow simulator for quantification of hydrogeological uncertainty. *Águas Subterrâneas, 35*(2). doi:http://dx.doi.org/10.14295/ras.v35i2.30024

Cowie, R. M., Knowles, J. F., Dailey, K. R., Williams, M. W., Mills, T. J., & Molotch, N. P. (2017). Sources of streamflow along a headwater catchment elevational gradient. *Journal of Hydrology, 549*, 163-178. doi:https://doi.org/10.1016/j.jhydrol.2017.03.044

de Graaf, I. E., Gleeson, T., van Beek, L. P., Sutanudjaja, E. H., & Bierkens, M. F. (2019). Environmental flow limits to global groundwater pumping. *Nature*, 90-94. doi:https://doi.org/10.1038/s41586-019-1594-4

Doherty, J. (2018). *Calibration and uncertainty analysis for complex environmental models.* doi:ISBN: 978-0-9943786-0-6

Doležal, F., Kulhavý, Z., Kvítek, T., Soukup, M., & Tippl, M. (2003). METHODS OF RUNOFF SEPARATION APPLIED TO SMALL STREAM AND TILE DRAINAGE RUNOFF. *9 th Conference of the European Network of Experimental and Representative Basins (ERB)* (pp. 131-136). Demänovská dolina : International Hydrological Programme (IHP).

Doležal, F., Kvítek, T., Soukup, M., Kulhavý, Z., & Tippl, M. (2004). Czech highlands and peneplains and their hydrological role, with special regard to the Bohemo-Moravian Highland. In G. I. Committee, *Studies in Mountain Hydrology* (pp. 41-56).

Dubois, E., Larocque, M., Gagne, S., & Braun, M. (2022). Climate Change Impacts on Groundwater Recharge in Cold and Humid Climates: Controlling Processes and Thresholds. *Climate*. doi:https://doi.org/10.3390/cli10010006

Dunn, S. M., Langan, S. J., & Colohan, R. J. (2001). The impact of variable snow pack accumulation on a major Scottish water resource. *Science of TheTotal Environment, 265*(1-3), 181-194. doi:https://doi.org/10.1016/S0048-9697(00)00658-6

Eckhardt, K. (2004). How to construct recursive digital filters for baseflow separation. *Hydrological Processes*. doi:https://doi.org/10.1002/hyp.5675

Eckhardt, K. (2008). A comparison of baseflow indices, which were calculated with seven different baseflow separation methods. *Journal of Hydrology, 352*(1-2), 168-173. doi:https://doi.org/10.1016/j.jhydrol.2008.01.005

Evans, S. G., Ge, S., Voss, C. I., & Molotch, N. P. (2018). The Role of Frozen Soil in Groundwater Discharge Predictions for Warming Alpine Watersheds. *Water Resource Research, 54*(3). doi:https://doi.org/10.1002/2017WR022098

Evaristo, J., & McDonnell, J. (2017). Prevalence and magnitude of groundwater use by vegetation: a global stable isotope meta-analysis. *Scientific Reports, 7*. doi:https://doi.org/10.1038/srep44110

Fernandez, R., & Zegre, N. (2019, May). Seasonal Changes in Water and Energy Balances over the Appalachian Region and Beyond throughout the Twenty-First Century . *Journal of Applied Meteorology and Climatology, 58*(5), 1079-1102. doi:https://doi.org/10.1175/JAMC-D-18-0093.1

Fetter, C. (2001). Applied Hydrogeology Fourth Edition. New Jersey: Prentice-Hall Inc. .

Fetter, C. W. (2001). *Applied Hydrogeology* (Fourth ed.). Prentice Hall.

Findlay, C. S., & Kadykola, A. N. (2016). The flow regulation services of wetlands. *Ecosystem Services, 20*, 91-103. doi:https://doi.org/10.1016/j.ecoser.2016.06.005

First Nations Information Governance Centre. (2023). *The First Nations Principals of OCAP*. Retrieved from First Nations Information Governance Centre: https://fnigc.ca/ocap-training/

Fisher, B. E., & Poole, J. C. (2006). DP ME 43, Version 2, 2006. Digital Version of Nova Scotia Department of Natural Resources Map ME 2000-1, Geological Map of the Province of Nova Scotia, Scale 1:500 000, Compiled by J. D. Keppie, 2000. (V. 2, Ed.) Halifax: Nova Scotia Department of Natural Resources, Mineral Resources Branch.

Freeze, A., & Cherry, J. (1979). *Groundwater.*

Frisbee, M. D., Phillips, F. M., Campbell, A. R., Hendrickx, J. M., & Engle, E. M. (2009). Modified passive capillary samplers for collecting samples of snowmelt infiltration for stable isotope analysis in remote, seasonally inaccessible watersheds 2: field evaluation. *Hydrologic Processes, 24*(7). doi:https://doi.org/10.1002/hyp.7524

Fritz, S. J. (1994). A Survey of Charge-Balance Errors on Published Analyses of Potable Ground and Surface Waters. *Groundwater*. doi:https://doi.org/10.1111/j.1745-6584.1994.tb00888.x

Fronzi, D., Mirabella, F., Cardellini, C., Caliro, S., Palpacelli, S., Cambi, C., . . . Tazioli, A. (2021). The Role of Faults in Groundwater Circulation before and after Seismic Events: Insights from Tracers, Water Isotopes and Geochemistry. *Water*(Applying artificial and environmental tracing techniques in hydrogeology). doi:https://doi.org/10.3390/w13111499

Galleani, L., Vigna, B., Banzato, C., & Lo Russo, S. (2011). Validation of a Vulnerability Estimator for Spring Protection Areas: The VESPA index. *Journal of Hydrology*, 233-245.

Geofirma Engineering Ltd. (2012). *Draft comments on groundwater quality, Eskasoni, Nova Scotia.*

Gibson, J. J., Holmes, T., Stadnyk, T. A., Birks, S. J., Eby, P., & Pietroniro, A. (2020). 18O and 2H in streamflow across Canada. *Journal of Hydrology: Regional Studies*. doi:https://doi.org/10.1016/j.ejrh.2020.100754

Gleeson, T., Befus, K. M., Jasechko, S., Luijendijk, E., & Bayani Cardenas, M. (2016). The global volume and distribution of modern groundwater. *9*, 161-167. doi:https://doi.org/10.1038/ngeo2590

Goulden, M. L., & Bales, R. C. (2014). Mountain runoff vulnerability to increased evapotranspiration with vegetation expansion. (S. C. Wofsy, Ed.) *Environmental Science, 111*(39). doi:Mountain runoff vulnerability to increased evapotranspiration with vegetation expansion

Goverment of Canada. (2024). *Lone Shieling*. Retrieved from Parks Canada.

Governemnt of Canada. (2021). *Census of Population*. Retrieved from Statistics Canada.

Government of Canada. (2017). *Groundwater Contamination*. Retrieved from Government of Canada: https://www.canada.ca/en/environment-climate-change/services/water-overview/pollution-causes-effects/groundwater-contamination.html

Government of Canada. (2022). *Acadian Forest*. Retrieved from Parks Canada.

Government of Canada. (2022). *The Climate of Northern Cape Breton*. Retrieved from Parks Canada.

Government of Canada. (2024). *Boreal Forest*. Retrieved from Parks Canada.

Government of Canada. (2024). *Census of Environment: A snapshot of Canada's growing coastal communities and their natural environment*. Retrieved from Statisitcs Canada: https://www150.statcan.gc.ca/n1/daily-quotidien/240126/dq240126b-eng.htm

Government of Canada. (2024, 10 1). *Environment and Climate Change Canada*. Retrieved from Daily data report for ESKASONI FIRST NATION AUTOMATIC WEATHER STATION: https://climate.weather.gc.ca/climate_data/daily_data_e.html?hlyRange=2011-12-01%7C2025-01-05&dlyRange=2011-12-01%7C2025-01-05&mlyRange=%7C&StationID=49748&Prov=NS&urlExtension=_e.html&searchType=stnProv&optLimit=yearRange&StartYear=1840&EndYear=2025&selR

Government of Nova Scotia. (2020). GeoNova, DataLocator - Elevation Explorer.

Government of Nova Scotia. (2021). *Forest Inventory - Geographic Information Systems*. Retrieved from Nova Scotia Canada: https://novascotia.ca/natr/forestry/gis/forest-inventory.asp

Government of Nova Scotia. (2021). *Groundwater Quality*. Retrieved from Nova Scotia Canada: https://novascotia.ca/natr/meb/water-resources/groundwater-quality.asp

Government of Nova Scotia. (2023). *Environement and Climate Change*. Retrieved from Nova Scotia Canada: https://www.novascotia.ca/nse/groundwater/

Green, T. R., Taniguchi, M., Kooi, H., Gurdak, J. J., Allen, D. M., Hiscock, K. M., . . . Aureli, A. (2011). Beneath the surface of global change: Impacts of climate change on groundwater. *Journal of Hydrology*, 532-560. doi:https://doi.org/10.1016/j.jhydrol.2011.05.002

Gremaud, V., Goldscheider, N., Savoy, L., Faver, G., & Masson, H. (2009). Geological structure, recharge processes and underground drainage of a glacierised karst aquifer system, Tsanfleuron-Sanetsch, Swiss Alps. *Hydrogeology Journal*, 1833-1848. doi:http://dx.doi.org/10.1007/s10040-009-0485-4

Griebler, C., & Maria, A. (2015, March). Groundwater ecosystem services: a review. *Freshwater Science, 34*(1), 355-367.

Hauer, M. E., Hardy, D., Kulp, S. A., Mueller, V., Wrathall, D. J., & Clark, P. U. (2021). Assessing population exposure to coastal flooding due to sea level rise. *Nature Communications, 12*(6900). doi:https://doi.org/10.1038/s41467-021-27260-1

Hayashi, M. (2019). Alpine Hydrogeology: The Critical Role of Groundwater in Sourcing the Headwaters of the World. *Groundwater*. doi:https://doi.org/10.1111/gwat.12965

Health Canada. (2023). *Guidelines for Canadian Drinking Water Quality - Summary Tables.* Health Canada.

Healy, R. W. (2010). *Estimating Groundwater Recharge .* Cambridge: Cambridge University Press.

Helbig, M., Waddington, J. M., Alekseychik, P., & et al. (2020). Increasing contribution of peatlands to boreal evapotranspiration in a warming climate. *Nature Climate Change, 10*, 555-560. doi:https://doi.org/10.1038/s41558-020-0763-7

Helsel, D. R. (2005). More Than Obvious: Better Methods for Interpreting Nondetect Data. *Environmental Science and Technology, 39*(20), 415A-8112. doi:https://doi.org/10.1021/es053368a

Hester, E. T., & Fox, G. A. (2020). Preferential Flow in Riparian Groundwater: Gateways for Watershed Solute Transport and Implications for Water Quality Management. *Water Resource Research*. doi:https://doi.org/10.1029/2020WR028186

Hester, E. T., McEwan, A. M., Kim, B.-J., & Rost, E. A. (2020). Abundance, distribution, and geometry of naturally occurring streambank soil pipes. *Freshwater Science, 39*(4). doi:https://doi.org/10.1086/711655

Hock, R., Rasul, G., Adler, C., Caceres, B., Gruber, S., Hirabayashi, Y., . . . Stelzer, H. (2019). High Mountain Areas. In: IPCC Special Report on the Ocean and.

Holmes, T. L., Stadnyk, T. A., Asadzadeh, M., & Gibson, J. J. (2023). Guidance on large scale hydrologic model calibration with isotope tracers. *Journal of Hydrology, 621*. doi:https://doi.org/10.1016/j.jhydrol.2023.129604

Hood, J. L., & Hayashi, M. (2015). Characterization of snowmelt flux and groundwater storage in an alpine headwater basin. *Journal of Hydrology, 521*, 482-497. doi:https://doi.org/10.1016/j.jhydrol.2014.12.041

Hooper, R. P. (2003). Diagnostic tools for mixing models of stream water chemistry. *Water Resource Research*. doi:https://doi.org/10.1029/2002WR001528

IAEA. (2011). Technical procedure for sampling. *Programme on isotopic composition of precipitation: global network of isotopes in precipitation (GNIP)*. IAEA-WMO.

Jasechko, S., Berks, S. J., Gleeson, T., Wada, Y., Fawcett, P. J., Sharp, Z. D., . . . Jeffery, W. M. (2014). The pronounced seasonality of global groundwater recharge. *Water Resource Reseach*. doi:https://doi.org/10.1002/2014WR015809

Jasechko, S., Perrone, D., Befus, K. M., Cardenas, M. B., Ferguson, G., Gleeson, T., . . . Kirchner, J. W. (2017). Global aquifers dominated by fossil groundwaters but wells vulnerable to modern contamination. *Nature Geoscience*, 425-429. doi:https://doi.org/10.1038/ngeo2943

Jenicek, M., & Ledvinka, O. (2020). Importance of snowmelt contribution to seasonal runoff and summer low flows in Czechia. *Hydrology and Earth System Sciences, 24*(7). doi:https://doi.org/10.5194/hess-24-3475-2020

Jia, X., Hou, D., Wang, L., O'Connor, D., & Luo, J. (2020). The development of groundwater research in the past 40 years: A burgeoning trend in groundwater depletion and sustainable management. *Journal of Hydrology*. doi:https://doi.org/10.1016/j.jhydrol.2020.125006

Karasaki, K., Ito, K., Wu, Y.-S., Shimo, M., Sawada, A., Maekawa, K., & Hatanaka, K. (2011). Uncertainty reduction of hydrologic models using data. *Journal of Hydrology*. doi:http://dx.doi.org/10.1016/j.jhydrol.2011.03.039

Karthikyan, B., & Lakshmanan, E. (2011). Fluoride in Groundwater: Causes, Implications and Mitigation Measures. In *Fluoride Properties, Applications and Environmental Management* (1 ed.). Nova.

Kennedy, G. W., Garroway, K. G., & Finlayson-Bourque, D. .. (2010). ESTIMATION OF REGIONAL GROUNDWATER BUDGETS IN NOVA SCOTIA. Nova Scotia Department of Natural Resources.

Kimmel, K., Kull, A., & Mander, U. (2008). The status, conservation and sustainable use of Estonian wetlands. *Wetlands Ecology and Management, 18*, 375-395. doi:https://doi.org/10.1007/s11273-008-9129-z

Kirchner, J. W. (2023). Mixing Models With Multiple, Overlapping, or Incomplete End-Members, Quantified Using Time Series of a Single Tracer. *Geophysical Research Letters*. doi:https://doi.org/10.1029/2023GL104147

Klove, B., Ala-Aho, P., Bertrand, G., Gurdak, J. J., Kupfersberger, H., Kvae, J., . . . Pulido-Velazquez, M. (2014). Climate change impacts on groundwater and dependent ecosystems. *Journal of Hydrology*, 250-266. doi:https://doi.org/10.1016/j.jhydrol.2013.06.037

Kurwadkar, S., Kanel, S. R., & Nakarmi, A. (2020). Water Environmental Research. *Groundwater pollution: Occurrence, detection, and remediation of organic and inorganic pollutants, 92(10), 1659-1668*.

Kurylyk, B. L., MacQuarrie, K. T., & Voss, C. I. (2014). Climate change impacts on the temperature and magnitude of groundwater discharge from shallow, unconfined aquifers. *Water Resource Research*. doi:https://doi.org/10.1002/2013WR014588

Langevin, C., Hughes, J., Banta, E., Niswonger, R., Provost, A., & Panday, S. (2017). Documentation for the MODFLOW 6 Groundwater Flow Model: U.S. Geological Survey Techniques and Methods.

Langevin, C., Hughes, J., Banta, E., Provost, A., Niswonger, R., & Panday, S. (2017). *MODFLOW 6 Modular Hydrologic Model: U.S. Geological Survey Software*.

Langmuir, D. (1971). The geochemistry of some carbonate ground waters in central Pennsylvania. *Geochemica et Cosmochimica Acta, 35*(10). doi:https://doi.org/10.1016/0016-7037(71)90019-6

Larkin, R. G., & Sharp, Jr., J. M. (1992). On the relationship between river-basin geomorphology, aquifer hydraulics, and ground-water flow direction in alluvial aquifers. Texas: Department of Geological Sciences, University of Texas at Austin.

Lasagna, M., De Luca, D. A., & Franchino, E. (2016). The role of physical and biological processes in aquifers and their importance on groundwater vulnerability to nitrate pollution. *Environmental Earth Science, 75*. doi:10.1007/s12665-016-5768-1

Leray, S., de Dreuzy, J. -R., Bour, O., & Bresciani, E. (2013). Numerical modeling of the productivity of vertical to shallowly dipping fractured zones in crystalline rocks. *Journal of Hydrology*, 64-75. doi:https://doi.org/10.1016/j.jhydrol.2012.12.014

Li, H., Wang, W., Fu, J., & Wei, J. (2023). Spatiotemporal heterogeneity and attributions of streamflow and baseflow changes across the headstreams of the Tarim River Basin, Northwest China. *Science of The Total Environment, 836*. doi:https://doi.org/10.1016/j.scitotenv.2022.159230

Li, H., Wang, W., Fu, J., Chen, Z., Ning, Z., & Liu, Y. (2021). Quantifying the relative contribution of climate variability and human activities impacts on baseflow dynamics in the Tarim River Basin, Northwest China. *Journal of Hydrology: Regional Studies, 36*. doi:https://doi.org/10.1016/j.ejrh.2021.100853

Li, S., Liu, M., Adam, J. C., Pi, H., Su, F., Li, D., . . . Yao, Z. (2021). Contribution of Snow-Melt Water to the Streamflow over the Three-River Headwater Region, China. *Remote Sensing, 13*(8). doi:https://doi.org/10.3390/rs13081585

Li, W., Liu, Z., Guo, H., Li, N., & Kang, W. (2011). Simulation of a groundwater fall caused by geological discontinuities. *Hydrogeology Journal, 19*(6). doi:DOI:10.1007/s10040-011-0747-9

Lintern, A., Webb, J. A., Ryu, D., Liu, S., Bende-Michl, U., Waters, D., . . . Western, A. W. (2017). Key factors influencing differences in stream water quality across space. *WIREs Water*. doi:https://doi.org/10.1002/wat2.1260

Liu, F., Bales, R. C., Conklin, M. H., & Conrad, M. E. (2008). Streamflow generation from snowmelt in semi-arid, seasonally snow-covered, forested catchments, Valles Caldera, New Mexico. *Water Resource Research*. doi:https://doi.org/10.1029/2007WR006728

Liu, F., Williams, M. W., & Caine, N. (2004). Source waters and flow paths in an alpine catchment, Colorado Front Range, United States. *Water Resources Research*, 1-16. doi:https://doi.org/10.1029/2004WR003076

Mackay, J. D., Barrand, N. E., Hannah, D. M., Krause, S., Jackson, C. R., Everest, J., . . . Dochartaigh, B. E. (2020). Proglacial groundwater storage dynamics under climate change and glacier retreat. *Hydrological Processes*. doi:https://doi.org/10.1002/hyp.13961

Malekinezhad, H., & Banadkooki, F. B. (2018). Modeling impacts of climate change and human activities on groundwater resources using MODFLOW. *Journal of Water and Climate Change, 9*(1), 156-177. doi:https://doi.org/10.2166/wcc.2017.147

Mao, B., Wang, X., Jia, S., & Liu, Z. (2024). Multi-methods to investigate the baseflow: Insight from watershed scale spatiotemporal variety perspective. *128*. doi:https://doi.org/10.1016/j.ecolind.2024.111573

Markovich, K. H., Manning, A. H., Condon, L. E., & McIntosh, J. C. (2019). Mountain-Block Recharge: A Review of Current Understanding. *Water Resource Research*. doi:https://doi.org/10.1029/2019WR025676

Maule, C. P., & Stein, J. (1990). Hydrologic Flow Path Definition and Partitioning of Spring Meltwater. *Water Resource Research*. doi:https://doi.org/10.1029/WR026i012p02959

McGranahan, G., Balk, D., & Anderson, B. (2007). The rising tide: assessing the risks of climate change and human settlements in low elevation coastal zones. *Environment and Urbanization, 19*(1). doi:https://doi.org/10.1177/0956247807076960

Mcmohan, T., & Nathan, R. (2021). Baseflow and transmission loss: A review. *Wiley Interdiciplinary Reviews Water, 8*(1). doi:http://dx.doi.org/10.1002/wat2.1527

Michael, H. A., Post, V. E., Wilson, A. M., & Werner, A. D. (2017). Science, society, and the coastal groundwater squeeze. *Water Resource Research*. doi:https://doi.org/10.1002/2017WR020851

Millennium Ecosystem Assessment. Condition and Trends Working Group. (2005). The Millennium Ecosystem Assessment series. In *Ecosystems and human well-being, vol. 1: Current state and trends;findings of the Condition and Trends Working Group of the Millennium Ecosystem Assessment* (pp. 167-201).

Miller, S. A., Lyon, S. W., & Miller, S. N. (2020). Quantifying contributions of snowmelt water to streamflow using graphical and chemical hydrograph separation. *Hydrological Processes*. doi:https://doi.org/10.1002/hyp.13981

Minder, J. R., Durran, D. R., Roe, G. H., & Anders, A. M. (2008). The climatology of small-scale orographic precipitation over. *QUARTERLY JOURNAL OF THE ROYAL METEOROLOGICAL SOCIETY*. doi:10.1002/qj.258

Moore, J. P., & Walsh, J. J. (2021). Quantitative analysis of Cenozoic faults and fractures and their impact on groundwater flow in the bedrock aquifers of Ireland. *Hydrogeology Journal*. doi:https://doi.org/10.1007/s10040-021-02395-z

Moriasi, D., Arnold, J., Van Liew, M. W., Bingner, R., Harmel, R. D., & Veith, T. L. (2007). Model Evaluation Guidelines for Systematic Quantification of Accuracy in Watershed Simulations. *Transactions of the ASABE, 50*(3). doi:http://dx.doi.org/10.13031/2013.23153

Mountain Research Initiative EDW Working Group. (2015). Elevation-dependent warming in mountain regions of the world. *Nature Climate Change, 5*, 424-430. doi:https://doi.org/10.1038/nclimate2563

Nash, T. (2021, April 12). *Emerging Indigenous Protected and Conserved Areas: The Unama'ki Mi'kmaw IPCA Project*. Retrieved from Conservation through Reconciliation and Partnership: https://conservation-reconciliation.ca/blog/emerging-indigenous-protected-and-conserved-areas-the-unamaki-mikmaw-ipca-project

Nathan, R. J., & McMahon, T. A. (1990). Evaluation of automated techniques for base flow and recession analyses. *Water Resouce Reserach*. doi:https://doi.org/10.1029/WR026i007p01465

Natural Resources Canada. (2020). *The Forest of Canada*. Retrieved from Canadian Forest Services.

Naumann, B., Vafeidis, A. T., Zimmermann, J., & Nicholls, R. J. (2015). Future Coastal Population Growth and Exposure to Sea-Level Rise and Coastal Flooding - A Global Assessment. *PLOS ONE*. doi:https://doi.org/10.1371/journal.pone.0118571

Nolan, Davis & Associates Limitted. (1984). *Eskasoni Groundwater Study Phase 2.*

Nova Scotia Department of Natural Resources. (2017). *Ecological Land Classification for Nova Scotia.*

Nova Scotia Museum. (2017). Natural History of Nova Scotia. Retrieved from https://novascotia.ca/nse/surface.water/docs/NSMuseum_FreshwaterEnvironments.pdf

Ntona, M. M., Busico, G., Mastrocicco, M., & Kazakis, N. (2022). Modeling groundwater and surface water interaction: An overview of current status and future challenges. *Science of The Total Environment, 846*. doi:https://doi.org/10.1016/j.scitotenv.2022.157355

Nygren, M., Giese, M., Klove, B., Haaf, E., Rossi, P. M., & Barthel, R. (2020). Changes in seasonality of groundwater level fluctuations in a temperate-cold climate transition zone. *Journal of Hydrology X*. doi:https://doi.org/10.1016/j.hydroa.2020.100062

Orlova, J., & Branfireun, B. A. (2018). Surface Water and Groundwater Contributions to Streamflow in the James Bay Lowland, Canada. *Arctic, Antarctic, and Alpine Research*. doi:https://doi.org/10.1657/1938-4246-46.1.236

Pardo, L. H., Green, M. B., Bailey, S. W., McGuire, K. J., & McDowell, W. H. (2022). Identifying Controls on Nitrate Sources and Flowpaths in a Forested Catchment Using a Hydropedological Framework. *Journal of Geophysical Research: Biogeosciences, 127*(2). doi:http://dx.doi.org/10.1029/2020JG006140

Paznekas, A., & Hayashi, M. (2015). Groundwater contribution to winter streamflow in the Canadian Rockies. *Canadian Water Resource Journal*. doi:https://doi.org/10.1080/07011784.2015.1060870

Peacock, D., Sanderson, D. J., & Rotevatn, A. (2017). Relationships between fractures. *Journal of Structural Geology*. doi:http://dx.doi.org/10.1016/j.jsg.2017.11.010

Pepin, N. C., Arnone, E., Gobiet, A., Haslinger, K., Kotlarski, S., Notarnicola, C., . . . Adler, C. (2022). Climate Changes and Their Elevational Patterns in the Mountains of the World. *Reviews of Geophysics'*. doi:https://doi.org/10.1029/2020RG000730

Petrie, B., & Bugden, G. (2002). The Physical Oceanography. *Nova Scotia Institute of Science*, (pp. 42, 1, 9-36).

Podgorski, J., & Berg, M. (2020). Global threat of arsenic in groundwater. *Science, 368*. doi:https://doi.org/10.1126/science.aba1510

Polatbekov, A. (2020). *Eskasoni Arena Road Well Field.* Final Report, EXP Services.

Raeside, R. P., & Barr, S. M. (1990). Geology and tectonic development of the Bras d'Or suspect terrane, Cape Breton Island, Nova Scotia.

Raposo, V. d., Costa, V. A., & Rodrigues, A. f. (2023). A review of recent developments on drought characterization, propagation, and influential factors. *Science of The Total Environment, 898*. doi:https://doi.org/10.1016/j.scitotenv.2023.165550

Rathay, S. Y., Allen, D. M., & Kirste, D. (2018). Response of a fractured bedrock aquifer to recharge from heavy rainfall events. *Journal of Hydrology, 561*. doi:https://doi.org/10.1016/j.jhydrol.2017.07.042

Reimann, C., Finne, T. E., Nordgulen, O., Saether, O. M., Arnoldussen, A., & Banks, D. (2019). The influence of geology and land-use on inorganic stream water quality in the Oslo region, Norway. *Applied Geochmistry, 24*(10), 1862-1874. doi:https://doi.org/10.1016/j.apgeochem.2009.06.007

Roques, C., Bour, O., Aquilina, L., Dewandel, B., Leray, S., Schrotter, J. M., . . . Mougin, B. (2014). Hydrological behavior of a deep sub-vertical fault in crystalline basement and relationships with surrounding reservoirs. *Journal of Hydrology*. doi:https://doi.org/10.1016/j.jhydrol.2013.11.023

Rozanski, K., Araguas-Araguas, L., & Gonfiantini, R. (1992). Isotopic patterns in Global Precipitation. *Journal of Geophysical Research Atmospheres*. doi:http://dx.doi.org/10.1029/GM078p0001

Samways, J., Salehi, S., McKenzie, J. M., & Somers, L. D. (2024, September). Long-term trends in mountain groundwater levels across Canada and the United States. *Hydrological Processes*. doi:https://doi.org/10.1002/hyp.15280

Schilling, O. S., Halloran, L. J., Delottier, H., Sano, Y., & Therrien, R. (2023). Editorial: Advances and emerging methods in tracer hydrogeology. *Frontiers in Water, 5*. doi:https://doi.org/10.3389/frwa.2023.1243114

Schnorbus, M., Werner, A., & Bennett, K. (2012). Impacts of climate change in three hydrologic regimes in British Columbia, Canada. *Hydrological Processes*. doi:https://doi.org/10.1002/hyp.9661

Scibek, J., Gleeson, T., & McKenzie, J. M. (2016). The biases and trends in fault zone hydrogeology conceptual models: global compilation and categorical data analysis. *Geofluids*. doi:https://doi.org/10.1111/gfl.12188

Shaw, J., Taylor, R., Patton, E., Potter, P., Parkes, G. S., & Hayward, S. (2006). *SENSITIVITY OF THE COASTS OF THE BRAS D'OR LAKES TO SEA-LEVEL RISE.* Geologic Survey of Canada (Atlantic).

Smith, R. B., & Barstad, I. (2003). A Linear Theory of Orographic Precipitation. Connecticut: Department of Geology and Geophysics, Yale University.

Soil Landscapes of Canada Working Group. (2010). Soil Landscapes of Canada version 3.2. Agriculture and Agri-Food Canada. (digital map and database at 1:1 million scale).

Somers, L. D., & McKenzie, J. M. (2020). A review of groundwater in high mountain environments. *WIREs Water*. doi:https://doi.org/10.1002/wat2.1475

Somers, L. D., McKenzie, J. M., Mark, B. G., Lagos, P., Ng, G.-H. C., Wickert, A. D., . . . Silva, Y. (2019). Groundwater Buffers Decreasing Glacier Melt in an Andean Watershed—But Not Forever. *Geophysical Research Letters*. doi:https://doi.org/10.1029/2019GL084730

Soulsby, C., Malcolm, R., & Malcolm, I. (2000). Groundwater in headwaters: hydrological and ecological significance. *Geological Society, 182*, 19-34. doi:https://doi.org/10.1144/GSL.SP.2000.182.01.03

Spence, C. (2010). A Paradigm Shift in Hydrology: Storage Thresholds Across Scales Influence Catchment Runoff Generation. *Geography Compass, 4*(7). doi:https://doi.org/10.1111/j.1749-8198.2010.00341.x

St. Amour, N. A., Gibson, J. J., Edwards, T. W., Prowse, T. D., & Pietroniro, A. (2005). Isotopic time-series partitioning of streamflow components in wetland-dominated catchments, lower Liard River basin, Northwest Territories, Canada. *Hydrologic Processes*. doi:https://doi.org/10.1002/hyp.5975

Steiness, M., Jessen, S., Spitilli, M., van't Veen, S. G., Hojberg, A. L., & Engesgaard, P. (2019). The Role of Management of Stream–Riparian Zones on Subsurface–Surface Flow Components. *Water, 11*(9). doi:https://doi.org/10.3390/w11091905

Stewart, I. T., Cayan, D. R., & Dettinger, M. D. (2005). Changes toward Earlier Streamflow Timing across Western North America. *American Meteorological Society*, 1136-1155. doi:https://doi.org/10.1175/JCLI3321.1

Stigter, T. Y., Miller, J., Chen, J., & Re, V. (2022). Groundwater and climate change: threats and opportunities. *Hydrogeology Journal*, 7-10.

Stocker, T. F., Plattner, G.-K., Tignor, M., & Dahe, Q. (2015). *IPCC Workshop on Regional Climate Projections and their Use in Impacts and Risk Analysis Studies.* IPPC. IPPC Working Group.

Tang, W., & Carey, S. K. (2017). HydRun: A MATLAB toolbox for rainfall–runoff analysis. *Hydrological Processes*. doi:https://doi.org/10.1002/hyp.11185

Tetzlaff, D., Buttle, J., Carey, S. K., McGuire, K., Laudon, H., & Soulsby, C. (2014). Tracer-based assessment of flow paths, storage and runoff generation in northern catchments: a review. *Hydrological Processes*. doi:https://doi.org/10.1002/hyp.10412

The Indigenous Circle of Experts. (2018). *We Rise Together.*

Tromp-Van Merveld, H. J., Peters, N. E., & McDonnell, J. J. (2007). Effect of bedrock permeability on subsurface stormflow and the water balance of a trenched hillslope at the Panola Mountain Research Watershed, Georgia, USA. *Hydrological Processes, 21*(6). doi:https://doi.org/10.1002/hyp.6265

U.S. Geological Survey. (1999). Ground water. Reston, Virginia.

United Nations. (2022). *GROUNDWATER Making the invisible visible.* Paris, France: United Nations Educational, Scientific and Cultural Organization.

United Nations. (2024). *The United Nations World Water Development Report 2024: water for prosperity and peace.* Paris: UNESCO.

Valdivielso, S., Murray, J., Custodio, E., Hassanzadeh, A., Martínez, D. E., & Vázquez-Suñé, E. (2024). Seasonal and isotopic precipitation patterns in the semi-arid and high mountain areas. *Science of the Total Environment, 925*. doi:https://doi.org/10.1016/j.scitotenv.2024.171750

Viviroli, D., Archer, D. R., Buytaert, W., Fowler, H. J., Greenwood, G. B., Hamlet, A. F., . . . Woods, R. (2011). Climate change and mountain water resources: overview and recommendations for research, management and policy. *Hydrology and Earth System Sciences, 15*(2). doi:https://doi.org/10.5194/hess-15-471-2011

Viviroli, D., Durr, H. H., Messerli, B., Meybeck, M., & Weingartner, R. (2007). Mountains of the world, water towers for humanity: Typology, mapping, and global significance. *Water Resource Research*. doi:https://doi.org/10.1029/2006WR005653

Viviroli, D., Kummu, M., Meybeck, M., Kallio, M., & Wada, Y. (2020). Increasing dependence of lowland populations on mountain water resources. *Nature Sustainability*, 917-928.

White, B. A., & Burbey, T. J. (2007). Evidence for structurally controlled recharge in the Blue Ridge Province, Virginia, USA. *Hydrogeology Journal*, 929-943. doi:http://dx.doi.org/10.1007/s10040-006-0150-0

Winston, R. (2024, August). ModelMuse version 5.3: U.S. Geological Survey Software Release. *2024*.

Winston, R. B. (2024, April 3). Model Convergence.

Woessner, W. W. (2000). Stream and Fluvial Plain Ground Water Interactions: Rescaling Hydrogeologic Thought. *Groundwater, 38*(3), 423-429. doi:http://dx.doi.org/10.1111/j.1745-6584.2000.tb00228.x

Woessner, W. W., & Poeter, E. P. (2020). *Hydrogeologic Properties of Earth Materials and Principles of Groundwater Flow.* Guelph: The Groundwater Project.

Xiao, X., Zhang, X., Shi, X., Yu, Z., Liu, K., & Liu, Z. (2023). Identifying river water sources using end-member mixing analysis in a subtropical monsoon basin China. *Hydrological Processes*. doi:https://doi.org/10.1002/hyp.14824

Yapiyev, V., Rossi, P. M., Ala-Aho, P., & Marttila, H. (2023). Stable Water Isotopes as an Indicator of Surface Water Intrusion in Shallow Aquifer Wells: A Cold Climate Perspective. *Water Resource Research, 59*(2). doi:https://doi.org/10.1029/2022WR033056

Zarate, E., Hobley, D., MacDonald, A. M., Swift, R. T., Chambers, J., Kashaigili, J. J., . . . Cuthbert, M. O. (2021). The role of superficial geology in controlling groundwater recharge in the weathered crystalline basement of semi-arid Tanzania. *Journal of Hydrology: Regional Studies, 36*. doi:https://doi.org/10.1016/j.ejrh.2021.100833

Zhang, H., Zhang, X., Liu, W., Yeh, P. J.-F., Ye, P., & He, X. (2022). Impacts of active tectonics on geogenic arsenic enrichment in groundwater in the Hetao Plain, Inner Mongolia. *Quaternary Science Reviews, 278*. doi:https://doi.org/10.1016/j.quascirev.2021.107343

APPENDICES

1. SCATTER PLOTS FOR ALL FIELD CAMPAIGNS

July 2022 Scatter Plots

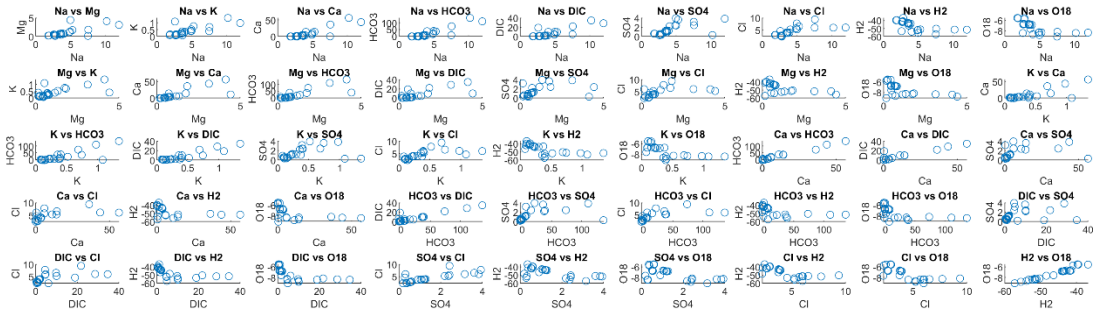

November 2022 Scatter Plots

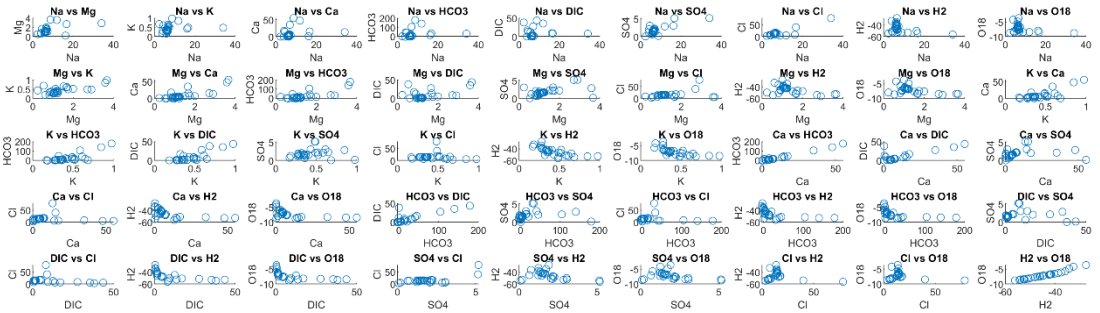

May 2023 Scatter Plots

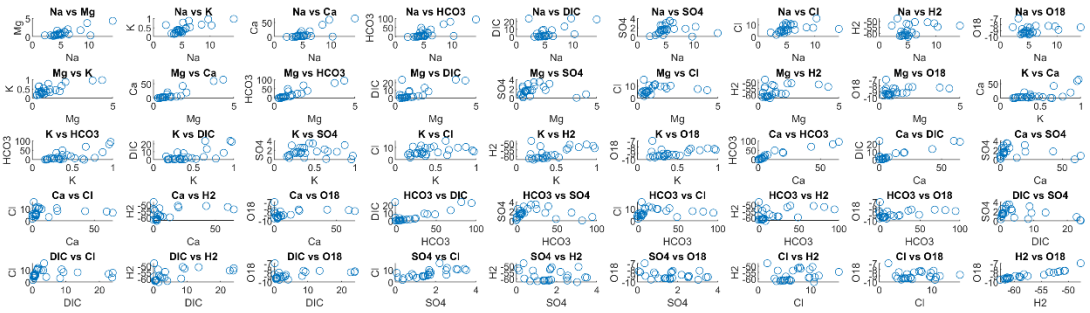

July 2023 Scatter Plots

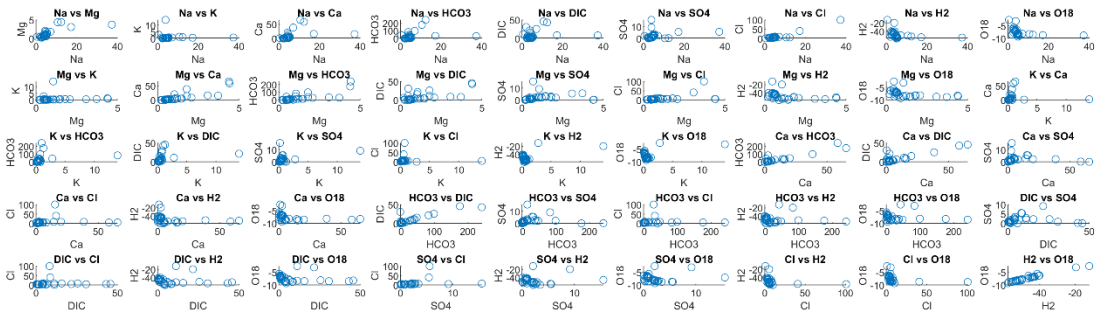

2. PUMP TEST RESULTS (POLATBEKOV, 2020)

AQTESOLV for Windows — 72 Hour Pump Test PW-2

Aquifer Model: Fractured
Solution Method: Moench w/slab blocks

VISUAL ESTIMATION RESULTS

Estimated Parameters

Parameter	Estimate	
K	0.0007137	m/min
Ss	0.001667	m^{-1}
K'	1.	m/min
Ss'	0.03902	m^{-1}
Sw	0.	
Sf	0.	
r(w)	0.2	m
r(c)	0.2	m

K = 0.00119 cm/sec
T = K*b = 0.04282 m²/min (7.137 sq. cm/sec)

3. SAMPLE DATA

July 2022

								Field							Lab				
Sample ID	Date	Time	Comments	LAT	LONG	Elevation	Temperature (C)	DO(%)	DO(mg/L)	Specific Conductivity	Conductivity	Salinity	pH	Bicarbonate (ppm HCO3)	DIC (mg/L)	pH	Conductivity (uS/cm)	Temperature (C)	Detection Limit
CB1	2022-07-05	14:16:00	Swapped labs	45.95	-60.62	49.94	15.00	106.70	10.76	38.10	30.90	0.02	6.70	5.92	1.84	6.93	22.65	20.58	
CB2	2022-07-05	14:06:00		45.95	-60.62	47.66	12.30	102.40	11.51	0.50	0.40	0.00	7.60	38.76	10.09	8.29	74.72	20.38	
CB3	2022-07-05	13:56:00	See comment	45.95	-60.62	40.60	15.20	105.60	10.60	38.00	30.90	0.02	6.80	5.96	2.11	6.92	23.07	20.24	
CB4	2022-07-05	14:32:00		45.95	-60.62	58.28	14.41	103.70	10.61	39.00	30.90	0.02	7.00	15.41	4.62	7.20	42.45	20.09	
CB5	2022-07-05	14:40:00		45.95	-60.62	55.55	15.10	106.70	10.75	37.40	30.40	0.02	6.60	5.93	1.81	6.95	22.23	20.72	
CB6	2022-07-05	14:58:00		45.95	-60.62	67.62	15.10	106.90	10.76	36.60	29.60	0.02	6.60	5.11	1.62	6.95	20.96	20.04	
CB7	2022-07-05	15:08:00		45.95	-60.62	68.27	15.30	106.60	10.68	30.60	25.00	0.01	6.60	5.83	1.65	6.81	20.88	20.53	
CB8	2022-07-05	15:19:00		45.95	-60.62	72.22	13.70	105.30	10.95	40.10	31.20	0.02	7.00	21.45	4.56	7.34	45.31	19.67	
CB9	2022-07-07	15:08:00		45.96	-60.64	187.60	13.80	80.80	8.33	26.60	20.70	0.01	5.20	1.23	1.62	5.70	16.58	20.56	
CB10	2022-07-07	15:16:00		45.96	-60.63	202.09	17.90	102.20	9.69	21.30	18.80	0.01	4.60	-0.99	0.85	5.10	15.40	21.14	
CB11	2022-07-07	15:24:00		45.96	-60.63	195.09	17.80	101.50	9.64	27.10	23.60	0.01	4.60	0.05	1.13	5.20	14.81	20.62	
MW1A	2022-07-06	13:00:00		45.96	-60.63	7.78	7.60	90.70	10.84	0.20	0.10	0.00	5.50	6.84	4.83	6.12	28.29	20.36	
MW1B	2022-07-06	13:00:00		45.96	-60.63	7.78	7.30	25.90	3.11	0.20	0.10	0.00	6.50	35.60	9.82	7.32	76.23	21.19	
MW2A	2022-07-06	12:30:00		45.96	-60.64	12.21	11.20	44.80	4.91	0.20	0.10	0.00	6.50	37.24	10.06	6.85	70.67	20.50	
MW2B	2022-07-06	12:30:00		45.96	-60.64	12.21	11.40	90.00	9.83	0.20	0.10	0.00	7.70	110.95	28.57	7.69	188.21	20.67	
MW3A	2022-07-06	12:00:00		45.96	-60.64	12.08	10.20	31.10	3.49	0.20	0.10	0.00	7.40	73.70	21.81	7.43	145.91	20.45	
MW3B	2022-07-06	12:00:00		45.96	-60.64	12.08	11.30	92.20	10.03	0.20	0.20	0.00	8.10	136.67	34.58	7.64	215.17	20.35	
Pond 1	2022-07-07	11:39:00		45.96	-60.64	207.49	18.90	102.20	9.50	25.70	22.90	0.01	4.30	-2.88	0.58	4.59	13.72	20.82	
Lake 1	2022-07-07	11:32:00		45.96	-60.64	203.69	19.20	100.50	9.30	25.70	22.80	0.01	4.30	-2.17	0.60	4.69	14.05	20.41	
Lake 2	2022-07-07	11:59:00	Only time adj	45.96	-60.64	209.67	19.60	102.40	9.38	25.40	22.80	0.01	4.30	-2.17	0.43	4.70	13.38	21.40	
Lake 3	2022-07-07	12:14:00	Only time adj	45.96	-60.64	214.60	19.60	100.80	9.24	25.40	22.60	0.01	4.40	-1.91	0.54	4.73	12.87	21.35	
PNA	2022-07-07	13:00:00		45.96	-60.64	14.00	12.80	60.00	6.34	27.80	21.20	0.01	4.50	-2.91	6.19	4.56	17.93	20.93	
PNC	2022-07-07	12:30:00	PNC was inst	45.96	-60.64	206.33	9.60	61.00	6.97	48.00	33.60	0.02	4.50	-0.95	18.92	4.83	29.30	21.22	
CB Dam	2022-07-05	10:45:00		45.95	-60.62	12.81	14.20	104.40	10.70	37.80	30.10		6.30	7.50	2.17	6.97	23.91	21.26	
CB Upstream Station	2022-07-05	15:30:00	sample durin	45.96	-60.63	14.45	22.80			26.50	25.50		4.30	-0.03	1.14	5.18	13.04	20.87	
Inside of upstream station	2022-07-07	16:19:00	Sampled during the second sample collection day											-0.40	0.94	5.05	15.15	20.25	
Qamsipuk	2022-07-08	10:50:00	Not included	45.96	-60.63	15.15	14.00	109.30	11.26	29.30	23.20	0.01	6.50						
Qamsipuk		new coords:	See above	45.95	-60.60														
				(manually placed)															
																LS Field Blank 2 June26/22 Opened @ CB Dam July 5/22 11:00th			
																	LS Fiels Blank 1 July26/22		

what to do with double samples?
I included both in the mixing analysis for MS
CB9 was manually placed on ArcGIS because of waypoint issues
Qamsipuk was manually placed to the new coordinates because of waypoint issues

7Li (KED)	23Na (KED)	24Mg (KED)	27Al (KED)	31P (KED)	39K (KED)	44Ca (KED)	49Ti (KED)	51V (KED)	52Cr (KED)	55Mn (KED)	56Fe (KED)	59Co (KED)	60Ni (KED)	65Cu (KED)	66Zn (KED)	75As (KED)	78Se (KED)	107Ag (KED)	111Cd (KED)	121Sb (KED)	135Ba (KED)	140Ce (KED)	208Pb (KED)	238U (KED)	Fluoride	Chloride	Nitrite	Bromide	Nitrate	Phosphate	Sulfate			
ppb	ppm	ppm	ppb	ppb	ppm	ppm	ppb	ppb	ppb	ppb	ppb	ppb	ppb	ppb	ppb	ppb	ppb	ppb	ppb	ppb	ppb	ppb	ppb	ppb	ppm	ppb	ppm	ppb	ppb	ppb	ppm			
0.4	0.3	0.3	4	0.3 ppb	0.3	10 ppb	0.5	0.4	0.4	0.8	7	0.4	0.4	0.7	0.6	0.4	1	0.4	0.4	2	0.5	0.4	0.4	0.4	9	0.3	9	9	0.2	10	0.2	62H, in ‰	δ18O, in ‰	Date analyzed
0.48	3.45	0.72	199.16	150.00	0.15	3.63	1.64	0.20	0.20	4.48	259.69	0.20	0.20	0.35	2.41	0.20	5.00	0.20	0.20	1.00	2.31	0.20	0.20	0.20	16.55	3.94	4.50	14.04	2.46	5.00	1.21	-43.70	-6.85	14/11/2022
0.20	4.99	4.43	17.94	150.00	0.41	11.21	0.25	0.20	0.20	0.40	7.89	0.20	0.20	0.35	0.30	0.20	0.50	0.20	0.20	1.00	12.23	0.20	0.20	0.20	53.47	5.28	4.50	13.57	6.68	10.04	2.38	-55.50	-8.80	14/11/2022
0.48	3.91	0.79	215.78	150.00	0.15	3.87	1.75	0.20	0.20	6.05	278.45	0.20	0.20	0.35	3.55	0.20	1.27	0.20	0.20	1.00	2.81	0.20	0.20	0.20	13.00	3.97	4.50	12.57	7.18	5.00	1.23	-43.90	-6.85	14/11/2022
0.20	4.86	1.16	42.93	150.00	0.40	6.05	0.25	0.20	0.20	0.40	13.90	0.20	0.20	0.35	1.09	0.20	0.50	0.20	0.20	1.00	3.93	0.20	0.20	0.20	21.96	5.72	10.79	15.68	6.93	5.00	2.43	-52.30	-8.36	14/11/2022
0.44	3.60	0.72	208.36	150.00	0.15	3.62	1.72	0.20	0.20	5.04	281.12	0.20	0.20	0.35	1.68	0.20	0.50	0.20	0.20	1.00	2.29	0.20	0.20	0.20	19.80	3.93	4.50	14.54	5.29	5.00	1.19	-43.50	-6.82	14/11/2022
0.20	3.63	0.71	219.62	150.00	0.37	3.61	2.02	0.20	0.20	5.51	290.99	0.20	0.20	0.84	10.33	0.20	1.06	0.20	0.20	1.00	2.37	0.20	0.20	0.20	16.19	3.84	4.50	13.69	11.36	5.00	1.09	-43.30	-6.76	14/11/2022
0.20	3.48	0.66	217.42	150.00	0.15	3.42	1.79	0.20	0.20	5.13	294.72	0.20	0.20	0.35	2.41	0.20	0.50	0.20	0.20	1.00	2.25	0.20	0.20	0.20	17.73	3.83	4.50	13.86	2.98	5.00	1.05	-42.80	-6.69	14/11/2022
0.20	4.95	1.33	29.42	150.00	0.52	5.97	0.25	0.20	0.20	0.40	3.50	0.20	0.20	1.05	5.97	0.20	0.50	0.20	0.20	1.00	2.66	0.20	0.20	0.20	21.18	7.74	4.50	32.51	5.72	5.00	3.93	-51.70	-8.26	14/11/2022
0.57	3.67	0.47	506.82	150.00	0.15	1.72	2.37	0.20	0.20	72.00	311.25	0.20	0.20	0.35	5.04	0.20	0.50	0.20	0.20	1.00	5.35	0.82	0.20	0.20	11.32	3.79	4.50	15.31	4.01	5.00	0.91	-46.40	-7.58	14/11/2022
0.50	2.66	0.45	379.18	150.00	0.15	1.49	3.51	0.57	0.20	99.12	551.86	0.20	0.20	0.35	8.46	0.20	0.50	0.20	0.20	1.00	3.80	0.51	0.68	0.20	12.12	2.72	4.50	4.50	19.65	5.00	0.53	-41.80	-6.76	14/11/2022
0.61	2.73	0.48	394.35	150.00	0.15	1.54	3.93	0.63	0.20	103.57	566.26	0.20	0.20	0.35	6.28	0.20	0.50	0.20	0.20	1.00	3.06	0.56	0.72	0.20	11.83	2.75	4.50	4.50	4.88	5.00	0.56	-41.90	-6.76	14/11/2022
0.64	7.51	0.15	35.55	150.00	0.39	0.45	0.25	0.20	0.20	19.12	3.50	0.20	0.20	0.35	4.22	0.20	0.50	0.20	0.20	1.00	0.99	0.20	0.20	0.20	26.95	6.02	23.55	10.49	22.51	89.52	3.16	-57.20	-9.08	14/11/2022
1.69	5.29	1.74	18.92	150.00	0.74	14.48	0.25	0.20	0.20	107.71	27.20	0.20	0.20	1.26	4.41	0.20	0.50	0.20	0.20	1.00	4.78	0.20	0.20	0.20	73.46	6.55	16.97	15.56	9.80	5.00	3.61	-51.10	-8.30	14/11/2022
0.94	4.04	0.72	4.25	150.00	0.36	14.18	0.25	0.20	0.20	3.33	3.50	0.20	0.20	1.32	7.33	0.20	0.50	0.20	0.20	1.00	6.90	0.20	0.20	0.20	30.06	5.26	12.72	17.72	0.81	5.00	2.20	-53.90	-8.85	14/11/2022
8.58	11.96	3.13	17.26	150.00	0.98	43.75	0.25	0.20	0.20	9.30	12.20	0.20	0.54	3.89	18.79	12.56	0.50	0.20	0.20	1.00	69.81	0.20	0.20	0.67	109.29	6.06	9.68	17.07	6.30	10.99	3.83	-51.50	-8.33	14/11/2022
1.52	7.56	1.83	5.01	150.00	0.69	36.31	0.25	0.76	0.20	28.66	634.12	0.20	0.20	2.24	5.34	0.95	1.07	0.20	0.20	1.00	4.75	0.20	0.20	0.20	96.55	9.38	18.61	20.16	12.65	15.43	2.43	-50.30	-8.17	14/11/2022
7.56	10.19	4.13	10.75	150.00	1.35	56.50	0.25	0.20	0.20	422.47	13.96	0.20	0.96	9.02	18.70	0.55	0.50	0.20	0.20	1.00	6.52	0.20	0.20	0.43	48.40	5.99	13.14	14.88	2.74	5.00	0.32	-51.40	-8.41	14/11/2022
1.87	2.81	0.15	24.72	150.00	0.15	0.12	0.25	0.20	0.20	2.03	26.43	0.20	0.20	1.05	11.58	0.20	0.50	0.20	0.20	1.00	2.24	0.20	0.57	0.20	4.50	2.35	4.50	4.50	3.61	5.00	0.38	-41.00	-5.75	14/11/2022
0.20	1.91	0.15	20.16	150.00	0.15	0.19	0.25	0.20	0.20	2.90	49.70	0.20	0.20	0.35	13.83	0.20	0.50	0.20	0.20	1.00	1.84	0.20	0.20	0.20	4.50	3.02	4.50	4.50	37.27	5.00	0.60	-38.50	-5.59	14/11/2022
0.50	1.83	0.15	16.99	150.00	0.15	0.18	0.25	0.20	0.20	2.59	46.43	0.20	0.20	0.35	7.41	0.20	0.50	0.20	0.20	1.00	1.67	0.20	0.20	0.20	4.50	2.97	4.50	4.50	7.43	5.00	0.61	-39.70	-5.54	14/11/2022
0.20	1.87	0.15	19.32	150.00	0.15	0.17	0.25	0.20	0.20	2.65	47.77	0.20	0.20	0.35	5.54	0.20	0.50	0.20	0.20	1.00	1.25	0.20	0.20	0.20	4.50	2.98	4.50	4.50	18.36	5.00	0.59	-39.70	-5.53	17/11/2022
																									4.50	2.31	4.50	4.50	13.78	28.81	0.20	-48.40	-7.67	17/11/2022
0.58	2.60	0.54	15.60	150.00	1.08	0.55	0.25	0.20	0.41	5.88	103.40	0.20	1.19	2.16	41.30	0.20	0.50	0.20	0.20	1.00	2.04	0.20	0.20	0.20	15.32	4.61	4.50	77.15	20.25	49.88	0.29	-53.30	-8.41	17/11/2022
0.20	3.67	0.81	192.47	150.00	0.15	3.79	1.60	0.20	0.20	5.26	241.20	0.20	0.20	1.09	2.09	0.20	0.50	0.20	0.20	1.00	2.60	0.20	0.30	0.20	18.16	4.00	4.50	13.46	6.51	5.00	1.29	-44.10	-6.83	17/11/2022
0.54	2.84	0.44	394.16	150.00	0.15	1.38	3.97	0.62	0.20	72.54	794.45	0.20	0.20	0.94	11.90	0.20	1.23	0.20	0.20	1.00	6.24	0.44	0.83	0.20	4.50	2.53	4.50	4.50	18.80	19.88	0.36	-38.80	-5.58	17/11/2022
0.20	2.75	0.46	388.54	150.00	0.15	1.48	3.92	0.60	0.20	96.23	587.68	0.20	0.20	1.73	6.13	0.20	0.50	0.20	0.20	1.00	3.57	0.49	0.79	0.20	10.57	2.70	4.50	4.50	10.73	15.69	0.52	-41.50	-6.65	17/11/2022
0.20	0.15	0.15	2.00	150.00	0.15	0.04	0.25	0.20	0.20	0.40	3.50	0.20	0.20	0.35	1.76	0.20	0.50	0.20	0.20	1.00	0.25	0.20	0.20	0.20										
0.20	0.15	0.15	2.00	150.00	0.15	0.01	0.25	0.20	0.20	0.40	3.50	0.20	0.20	0.35	0.30	0.20	0.50	0.20	0.20	1.00	0.25	0.20	0.20	0.20										

November 2022

							Field Data							Lab Data					
Sample ID	Date	Time	Comments	Latitude	Longitude	Elevation	Temperature (C)	Conductivity (uS/cm)	DO(%)	DO(mg/L)	Specific conductivity	pH	Bicarbonate (ppm HCO3)	DIC (mg/L)	pH	Conductivity (uS/cm)	Temperature (C)	Detection Limit
CB1	2022-11-08	9:08:00 AM		5091144.24	684493.28	40.60	9.54	94.00	86.10	9.82	-44.93	6.04	13.70	5.23	6.85	86.78	17.65	
CB2	2022-11-08	9:08:00 AM		5091144.91	684493.10	47.66	9.18	57.00	103.10	11.87	-26.34	6.43	5.81	1.98	6.78	64.76	18.34	
CB3	2022-11-08	9:08:00 AM		5091151.15	684486.09	49.94	9.16	73.00	102.80	11.83	-33.67	6.55	5.89	2.05	6.75	66.69	18.08	
CB4	2022-11-08	9:40:00 AM		5091241.67	684486.49	58.28	9.62	55.00	100.80	11.48	-26.49	6.76	15.51	4.42	7.00	84.75	17.90	
CB5	2022-11-08	9:52:00 AM		5091234.79	684501.59	55.55	9.11	71.00	102.90	11.86	-32.60	6.74	20.70	1.90	6.74	65.98	18.12	
CB6	2022-11-08	10:20:00 AM		5091396.13	684631.34	67.62	8.96	70.00	103.20	11.94	-31.70	6.85	5.50	1.68	6.65	65.27	18.53	
CB7	2022-11-08	10:10:00 AM		5091429.03	684615.85	68.27	9.45	96.00	101.40	11.59	-45.50	6.83	14.42	4.41	6.84	91.45	18.66	
CB8	2022-11-08	10:28:00 AM		5091426.41	684628.42	72.22	8.92	69.00	102.20	11.84	-31.14	6.64	4.79	1.61	6.82	63.74	18.68	
CB13	2022-11-08	11:24:00 AM	Random main	5092374.61	683610.16	181.55	7.68	63.00	100.10	11.94	-25.57	6.41	3.69		6.61	57.04	17.90	
CB14	2022-11-08	11:50:00 AM		5092188.32	683945.55	142.82	8.39	63.00	101.60	11.91	-27.13	6.61	5.62	1.76	6.83	58.26	18.89	
CB15	2022-11-08	12:12:00 PM		5092199.60	683939.71	147.32	8.41	68.00	100.70	11.81	-29.34	6.32	3.73	1.17	6.55	61.61	17.91	
CB16	2022-11-08	12:03:00 PM		5092170.27	683955.47	144.08	8.42	67.00	101.30	11.87	-28.93	6.39	3.04		6.46	61.31	18.07	
CB17	2022-11-08	2:30:00 PM	random main	5091849.88	684279.38	104.95	8.36	53.00	98.70	11.63	-22.77	4.71	4.60	1.33	6.49	61.92	18.59	
MW1A	2022-11-07	2:16:00 PM		5092244.89	683327.84	7.78	9.95	58.00	93.30	10.53	-28.86	6.11	13.93	9.55	6.30	56.03	18.48	
MW1B	2022-11-07	2:10:00 PM		5092244.89	683327.84	7.78	8.04	110.00	59.60	6.85	-45.99	6.47	40.61	13.71	6.92	101.19	18.14	
MW2A	2022-11-07	1:31:00 PM		5092282.94	683230.77	12.21	12.08	105.00	50.00	5.16	-66.29	6.18	45.04	17.12	6.74	106.67	18.25	
MW2B	2022-11-07	1:44:00 PM		5092282.94	683230.77	12.21	11.78	295.00	47.40	4.96	-179.44	7.19	139.73	35.45	7.94	275.96	17.84	
MW3A	2022-11-07	2:00:00 PM		5092316.92	683165.79	12.08	11.45	224.00	48.70	5.23	-130.99	6.68	104.37	27.71	7.39	217.10	18.23	
MW3B	2022-11-07	2:46:00 PM		5092316.92	683165.79	12.08	13.56	334.00	58.10	5.94	-259.32	7.20	178.58	43.62	7.79	335.84	18.33	
Pond 1	2022-11-07	3:30:00 PM		5092466.43	682912.48	207.49	12.79	89.00	92.50	9.71	-61.72	3.95	0.00	0.70	4.15	79.47	18.57	
Lake 1	2022-11-07	3:24:00 PM		5092504.16	682928.81	203.69	12.18	36.00	103.20	11.06	-23.02	4.25	-3.74	0.62	4.55	42.73	17.67	
Lake 4	2022-11-08	1:12:00 PM	Only time this	5092984.32	683093.56	204.65	9.28	66.00	97.10	11.16	-30.78	4.19	-2.19	0.51	4.50	64.66	18.39	
Lake 5	2022-11-08	1:00:00 PM		5092861.24	683356.14	202.61	8.17	53.00	98.70	11.63	-22.40	4.71	0.58		5.48	53.59	17.67	
PNA	2022-11-07	3:05:00 PM		5092387.98	683060.84	14.00	12.56	89.00	38.10	4.04	-59.81	4.01	0.00	12.60	4.06	82.82	18.16	
PNC	2022-11-07	3:20:00 PM		5092482.74	682952.63	206.33	12.59	42.00	66.20	7.01	-28.34	4.40	0.68	38.13	5.00	31.27	17.88	
CB Dam	2022-11-08	10:30:00 AM		5090803.98	684515.78	12.81	9.00	41.60	99.90	11.55	-18.91	7.00	6.20	2.00	6.84	66.48	17.70	
CB Upstream Station	2022-11-07	12:06:00 PM		5092748.92	683692.79	14.45	13.55	67.00	88.00	9.15	-51.94	4.45	-1.06	1.44	4.97	62.53	17.94	
River	2022-09-08	2:40:00 PM																	
Pumphouse	2022-09-08	2:55:00 PM																	
Rain Gage Sample	2022-08-22	2:00:00 PM																	
Rain Collector	2022-09-08	2:40:00 PM																	
CB Pumping Well 1	2022-11-08	10:45:00 AM					8.10	0.10	90.10	10.57	-0.04	7.40	30.42	8.18	7.03	280.02	17.98		
CB Pumping Well 2	2022-11-08	10:47:00 AM					8.10	0.10	89.30	10.37	-0.04	7.30	33.40	8.90	7.06	196.80	18.74		

NO CHANGES TO SAMPLE ID'S FROM THIS FIELD CAMPAIGN
Times weren't clear in pictures of samples

7Li (KED)	23Na (KED)	24Mg (KED)	27Al (KED)	31P (KED)	39K (KED)	44Ca (KED)	49Ti (KED)	51V (KED)	52Cr (KED)	55Mn (KED)	56Fe (KED)	59Co (KED)	60Ni (KED)	65Cu (KED)	66Zn (KED)	75As (KED)	78Se (KED)	107Ag (KED)	111Cd (KED)	121Sb (KED)	135Ba (KED)	140Ce (KED)	208Pb (KED)	238U (KED)	Fluoride	Chloride	Nitrite	Bromide	Nitrate	Phosphate	Sulfate		
ppb	ppm	ppm	ppb	ppb	ppm	ppm	ppb	ppb	ppb	ppb	ppb	ppb	ppb	ppb	ppb	ppb	ppb	ppb	ppb	ppb	ppb	ppb	ppb	ppb	ppb	ppm	ppb	ppb	ppb	ppb	ppm		
0.4	0.3	0.3	4	0.3 ppm	0.3	10 ppb	0.5	0.4	0.4	0.8	7	0.4	0.4	0.7	0.6	0.4	1	0.4	0.4	2	0.5	0.4	0.4	0.4	9	0.3	9	9	0.2	10	0.2	δ2H, in ‰	δ18O, in ‰
0.20	6.70	2.00	13.52	150.00	0.52	7.07	0.25	0.20	0.20	0.40	3.50	0.20	0.20	0.35	4.24	0.20	0.50	0.20	0.20	1.00	4.37	0.20	0.20	0.20	26.97	17.46	79.70	28.16	62.45	5.00	2.21	-47.20	-7.58
0.67	6.27	1.22	111.28	150.00	0.35	5.18	1.29	0.20	0.20	3.47	148.66	0.20	0.20	0.35	1.97	0.20	0.50	0.20	0.20	1.00	3.33	0.20	0.20	0.20	20.29	14.84	36.35	23.12	124.97	5.00	1.65	-42.50	-6.91
0.64	6.41	1.20	107.88	150.00	0.37	4.99	1.23	0.20	0.20	3.49	142.35	0.20	0.20	0.35	5.53	0.20	0.50	0.20	0.20	1.00	3.42	0.20	0.20	0.20	18.89	14.98	47.19	23.45	106.51	5.00	1.68	-42.30	-6.87
0.79	6.79	1.53	22.82	150.00	0.65	7.52	0.25	0.20	0.20	0.85	3.50	0.20	0.20	0.35	3.66	0.20	0.50	0.20	0.20	1.00	5.02	0.20	0.20	0.20	27.28	15.85	47.30	28.30	73.70	5.00	2.28	-48.10	-7.71
0.89	6.72	1.16	116.28	150.00	0.41	4.85	1.82	0.20	0.20	4.26	153.73	0.20	0.20	0.83	5.14	0.20	0.50	0.20	0.20	1.00	3.13	0.20	0.20	0.20	19.58	14.46	66.93	21.54	224.50	5.00	1.57	-41.90	-6.77
0.59	6.34	1.12	115.61	150.00	0.34	4.81	1.41	0.20	0.20	3.21	155.75	0.20	0.20	0.35	1.49	0.20	0.50	0.20	0.20	1.00	3.03	0.20	0.20	0.20	20.09	14.82	46.29	23.64	114.08	5.00	1.57	-41.70	-6.72
0.41	6.67	1.75	17.69	150.00	0.49	7.94	0.25	0.20	0.20	1.15	3.50	0.20	0.20	0.35	0.69	0.20	0.50	0.20	0.20	1.00	3.53	0.20	0.20	0.20	23.45	17.89	49.79	35.88	76.19	5.00	2.18	-46.40	-7.42
2.08	7.41	1.13	144.22	150.00	0.52	4.80	3.37	0.20	0.20	8.90	198.80	0.20	0.67	2.12	11.33	0.20	0.50	0.20	0.42	1.00	4.18	0.20	0.46	0.20	19.87	14.75	42.26	22.35	173.40	5.00	1.54	-41.80	-6.69
0.96	6.32	0.92	155.65	150.00	0.37	4.01	1.67	0.20	0.20	65.80	217.91	0.20	0.20	0.35	5.24	0.20	0.50	0.20	0.20	1.00	3.32	0.20	0.20	0.20	20.19	13.33	39.84	25.49	183.34	5.00	1.25	-45.00	-7.30
0.69	5.88	0.92	89.40	150.00	0.35	4.13	1.27	0.20	0.20	3.56	95.99	0.20	0.20	0.35	1.53	0.20	0.50	0.20	0.20	1.00	3.12	0.20	0.20	0.20	20.32	12.86	25.77	25.33	143.18	5.00	1.46	-46.00	-7.42
0.80	6.38	1.06	193.15	150.00	0.15	4.36	2.56	0.20	0.20	62.75	320.07	0.20	0.20	0.73	4.22	0.20	0.50	0.20	0.20	1.00	3.72	0.20	0.20	0.20	18.75	15.01	58.83	18.72	113.61	5.00	1.36	-38.90	-6.34
0.60	6.19	1.02	169.60	150.00	0.15	4.32	2.06	0.20	0.20	45.33	267.50	0.20	0.20	0.35	3.08	0.20	0.50	0.20	0.20	1.00	3.34	0.20	0.20	0.20	17.80	14.57	49.09	20.92	139.37	5.00	1.39	-40.40	-6.57
0.62	6.20	1.07	140.25	150.00	0.31	4.41	1.71	0.20	0.20	8.68	190.52	0.20	0.20	0.35	2.59	0.20	0.50	0.20	0.20	1.00	3.41	0.20	0.20	0.20	23.49	14.72	37.54	22.69	104.13	5.00	1.48	-41.70	-6.74
4.23	16.27	0.15	349.70	150.00	0.43	1.45	5.42	0.20	3.07	22.02	180.01	0.20	3.20	1.29	14.55	0.41	0.50	0.20	0.20	1.00	5.45	2.05	1.21	0.20	20.20	8.42	31.91	22.50	1971.30	156.87	3.06	-49.80	-7.95
1.38	4.54	1.69	7.08	150.00	0.61	14.69	0.25	0.20	0.20	7.88	3.50	0.20	0.20	0.35	2.21	0.20	0.50	0.20	0.20	1.00	2.25	0.20	0.20	0.20	58.27	6.58	39.51	14.64	188.83	5.00	3.08	-52.30	-8.46
1.09	4.19	0.83	142.48	150.00	0.32	17.50	0.93	0.20	0.20	11.71	19.81	0.20	0.20	1.42	3.81	0.20	0.50	0.20	0.20	1.00	21.45	0.20	0.20	0.20	16.46	6.63	24.77	22.75	81.65	5.00	2.07	-50.70	-8.17
7.62	11.97	3.59	2.00	150.00	0.85	47.80	0.25	0.20	0.20	465.11	3.50	0.20	0.20	1.73	7.02	28.50	0.50	0.20	0.20	1.00	87.38	0.20	0.20	0.82	67.20	5.70	18.17	4.50	139.22	21.59	2.87	-52.70	-8.39
1.69	7.07	1.66	9.40	150.00	0.59	35.15	0.51	0.87	0.20	218.63	1437.89	0.20	0.20	0.73	4.67	1.68	0.50	0.20	0.20	1.00	18.67	0.20	0.20	0.20	83.70	8.55	21.17	20.21	193.51	5.00	2.16	-51.30	-8.25
6.85	8.83	3.67	2.00	150.00	0.98	55.18	0.25	0.20	0.20	715.26	383.37	0.20	0.20	1.69	4.65	0.20	0.50	0.20	0.20	1.00	12.44	0.20	0.20	0.20	32.72	5.76	24.74	4.50	12.11	24.64	0.20	-52.50	-8.42
0.53	6.29	1.24	24.16	150.00	0.15	0.51	0.65	0.20	0.20	6.69	41.07	0.20	0.20	0.35	11.09	0.20	0.50	0.20	0.20	1.00	1.26	0.20	0.59	0.20	4.50	14.43	33.44	24.44	83.57	5.00	1.75	-34.50	-4.84
0.47	3.98	0.62	18.62	150.00	0.15	0.35	0.25	0.20	0.20	5.01	45.41	0.20	0.20	0.35	6.18	0.20	0.50	0.20	0.20	1.00	1.08	0.20	0.20	0.20	4.50	7.81	18.34	13.65	83.54	5.00	1.26	-32.80	-4.20
0.48	6.60	1.01	17.39	150.00	0.15	0.44	0.25	0.20	0.20	6.65	18.29	0.20	0.20	0.35	6.82	0.20	0.50	0.20	0.20	1.00	1.33	0.20	0.53	0.20	4.50	13.74	35.83	25.81	138.80	5.00	1.92	-27.80	-3.65
0.82	5.99	0.83	135.36	150.00	0.15	2.97	1.51	0.20	0.20	80.96	399.73	0.20	0.20	0.35	3.92	0.47	0.50	0.20	0.20	1.00	1.76	0.20	0.41	0.20	4.50	13.74	56.66	4.50	74.05	5.00	0.78	-36.10	-5.72
0.43	5.76	0.91	19.27	150.00	0.36	0.61	0.78	0.20	0.20	7.01	234.75	0.20	0.57	0.94	18.37	0.20	0.50	0.20	0.20	1.00	1.32	0.20	0.59	0.20	12.91	13.16	34.65	4.50	94.95	5.00	0.67	-44.70	-7.12
0.20	2.45	0.55	13.05	150.00	0.68	0.47	0.25	0.20	0.20	5.79	146.68	0.20	0.44	3.21	12.58	0.20	0.50	0.20	0.20	1.00	2.41	0.20	0.20	0.20	4.50	3.49	10.79	69.32	221.80	5.00	0.10	-54.30	-8.63
0.60	6.41	1.26	103.63	150.00	0.38	5.42	1.20	0.20	0.20	8.28	129.18	0.20	0.20	0.35	2.87	0.20	0.50	0.20	0.20	1.00	3.65	0.20	0.20	0.20	18.75	15.17	70.81	24.23	123.73	5.00	1.69	-42.20	-6.77
0.66	6.43	1.05	256.45	150.00	0.15	2.72	3.48	0.41	0.20	125.09	493.92	0.20	0.20	0.35	7.01	0.20	0.50	0.20	0.20	1.00	4.02	0.20	0.55	0.20	16.11	14.66	40.35	14.34	97.27	5.00	1.26	-37.70	-6.13
																																-40.40	-6.18
																																-55.50	-8.69
																																-41.40	-6.77
																																-30.50	-5.14
1.39	34.07	2.91	1.72	150.00	0.48	13.60	0.25	1.41	0.20	0.40	3.50	0.20	0.20	3.47	14.50	0.20	0.50	0.20	0.20	1.00	2.84	0.20	0.20	0.57	64.27	78.34	77.55	41.50	393.90	5.00	5.19	-56.10	-8.78
1.98	16.78	2.72	2.28	150.00	0.49	15.62	0.25	1.61	0.20	0.40	3.50	0.20	0.20	3.12	17.03	0.20	0.50	0.20	0.20	1.00	1.25	0.20	0.20	1.34	65.39	40.02	37.49	38.47	299.30	5.00	5.16	-53.90	-8.47

May 2023

							Field Data						Lab Data					
Sample ID	Date	Time	Commen	Lattitude	Longitude	Elevation	Temperature (C)	Conductivity (µS/cm)	DO(%)	DO(mg/L)	Specific conductivity	pH	Bicarbonate (ppm HCO3)	DIC (mg/L)	pH	Conductivity (uS/cm)	Temperature (C)	Detection Limit
CB 4	04-May-23	10:41:00					4.60		97.70		73.10	6.96	17.10	2.06	7.40		18.57	
CB 5	04-May-23	10:46:00					4.70		98.80		44.50	6.72	3.29	0.51	6.73		16.32	
CB 9	04-May-23	11:14:00	Formerly CB10				4.30		97.60		50.90	6.88	7.83	1.55	6.95		15.71	
CB 10	04-May-23	11:25:00	Formerly CB11				4.70		98.70		41.60	6.57	3.56	0.60	6.78		17.69	
CB 11	04-May-23	11:20:00	Formerly CB12				4.70		98.60		41.40	6.64	3.39	0.60	6.72		18.53	
CB 14	04-May-23	10:02:00					4.50		97.70		42.90	6.62	2.38	0.61	6.38		13.83	
CB 15	04-May-23	12:35:00					4.90		97.60		37.30	6.52	3.50	0.50	6.52		14.41	
CB 16	04-May-23	12:34:00					4.80		97.80		38.90	6.50	4.45	0.74	6.44		14.05	
CB 20	04-May-23	10:11:00	Formerly CB3-1				4.90		96.50		72.30	7.13	23.07	2.66	7.20		16.61	
CB 21	04-May-23	10:22:00	Formerly CB2-1				4.60		98.60		45.30	6.79	5.25	0.81	6.93		15.77	
Spring 1	04-May-23	09:56:00	Spring 1 and 2 likely have the same source				5.00		97.90		61.40	6.86	13.05	1.70	7.00		13.06	
Spring 2	04-May-23	10:01:00	Spring 1 and 2 likely have the same source				4.90		98.80		83.20	7.19	24.29	3.29	8.27		13.30	
Spring 5	04-May-23	11:52:00					4.80		97.10		66.20	6.90	8.75	1.43	6.92		15.37	
Spring 6	04-May-23	10:29:00	Formerly spring3				4.70		98.70		45.70	6.74	5.09	0.87	6.84		14.65	
MW1A	03-May-23	12:18:00					4.70		88.60		69.00	5.47	3.94	3.53	5.76		13.53	
MW1B	03-May-23	12:18:00					5.80		51.50		138.40	6.49	39.01	8.74	6.89		13.89	
MW2A	03-May-23	12:30:00					3.60		39.90		136.50	6.36	35.17	9.31	6.88		16.15	
MW2B	03-May-23	13:00:00					4.70		20.00		394.30	7.38	94.50	22.75	7.43		18.64	
MW3A	04-May-23	13:09:00					5.70		25.00		270.60	7.22	68.28	13.51	7.23		16.12	
MW3B	03-May-23	13:38:00					4.30		37.00		375.90	7.20	81.63	23.95	6.70		14.44	
Pond 1	04-May-23	13:23:00					6.80		95.30		41.10	4.61	-0.79	0.23	4.29		14.94	
Lake 1	04-May-23	13:29:00					7.30		95.10		47.10	4.52	-0.49	0.23	4.97		13.27	
Lake 5	04-May-23	13:47:00					8.40		83.30		118.00	6.61	48.64	8.31	7.08		14.54	
PNA	03-May-23	14:11:00					4.60		54.90		49.50	4.49	-1.01	4.17	4.30		14.21	
PNC	03-May-23	14:35:00					5.10		83.80		0.70	4.56	-1.54	23.81	4.68		15.12	
CB Dam	04-May-23	09:43:00					4.60		98.40		46.30	6.73	6.30	0.94	6.90		15.38	
CB upstream	03-May-23	10:50:00					4.80		87.40		34.60	6.46	0.51	0.66	5.55		15.70	
Christmas Brook	25-Nov-22																	
Christmas Brook (Downstream)	16-Dec-22																	
Christmas Brook	28-Feb-23																	
Christmas Brook (River)	28-Apr-23																	
Precipitation Collector	25-Nov-22																	
Rain Collector	28-Apr-23																	
Precipitation Collector																		
Snow Collector	25-Nov-22																	
Pumphouse																		

7Li (KED)	23Na (KED)	24Mg (KED)	27Al (KED)	31P (KED)	39K (KED)	44Ca (KED)	49Ti (KED)	51V (KED)	52Cr (KED)	55Mn (KED)	56Fe (KED)	59Co (KED)	60Ni (KED)	65Cu (KED)	66Zn (KED)	75As (KED)	78Se (KED)	107Ag (KED)	111Cd (KED)	121Sb (KED)	135Ba (KED)	140Ce (KED)	208Pb (KED)	238U (KED)	Fluoride	Chloride	Nitrite	Bromide	Nitrate	Phosphate	Sulfate		
ppb	ppm	ppm	ppb	ppb	ppm	ppm	ppb	ppb	ppb	ppb	ppb	ppb	ppb	ppb	ppb	ppb	ppb	ppb	ppb	ppb	ppb	ppb	ppb	ppb	ppb	ppm	ppb	ppb	ppb	ppb	ppm		
0.4	0.3	0.3	4	0.3 ppm	0.3	10 ppb	0.5	0.4	0.4	0.8	7	0.4	0.4	0.7	0.6	0.4	1	0.4	0.4	2	0.5	0.4	0.4	0.4	9	0.3	9	9	0.2	10	0.2	δ2H, in ‰	δ18O, in ‰
0.48	5.77	1.10	46.99	150.00	0.48	5.81	0.25	0.20	0.20	0.40	3.50	0.20	0.20	0.35	0.66	0.20	0.50	0.20	0.20	1.00	3.89	0.20	0.20	0.20	36.13	10.81	12.52	12.48	297.00	5.00	3.43	-58.80	-9.23
0.85	4.32	0.57	187.56	150.00	0.39	3.04	2.41	0.20	0.20	4.20	167.52	0.20	0.20	0.74	5.04	0.20	0.50	0.20	0.20	1.00	1.98	0.20	0.20	0.20	11.01	4.43	4.50	4.50	283.80	5.00	1.40	-61.20	-9.39
0.52	5.07	0.74	163.58	150.00	0.15	2.74	0.60	0.20	0.20	0.40	28.55	0.20	0.20	0.35	0.94	0.20	0.50	0.20	0.20	1.00	2.72	0.20	0.20	0.20	51.53	10.64	10.70	24.76	137.46	26.84	3.03	-62.60	-9.63
0.85	4.61	0.56	225.85	150.00	0.33	2.94	3.37	0.20	0.20	6.17	200.90	0.20	0.20	0.77	6.74	0.20	0.50	0.20	0.20	1.00	2.15	0.20	0.43	0.20	20.76	5.05	4.50	4.50	85.78	5.00	1.42	-61.30	-9.38
0.69	4.54	0.55	221.58	150.00	0.15	2.91	2.42	0.20	0.20	5.90	198.16	0.20	0.20	0.35	3.25	0.20	0.50	0.20	0.20	1.00	1.90	0.20	0.20	0.20	20.85	4.89	4.50	4.50	133.21	5.00	1.35	-61.20	-9.39
0.95	5.22	0.56	228.51	150.00	0.34	2.63	2.43	0.20	0.20	5.55	206.95	0.20	0.20	1.09	8.59	0.20	0.50	0.20	0.20	1.00	2.81	0.20	0.71	0.20	33.68	6.25	4.50	4.50	111.48	5.00	1.63	-61.40	-9.54
0.62	3.92	0.47	251.29	150.00	0.15	2.59	3.30	0.20	0.20	16.66	238.31	0.20	0.20	0.35	1.66	0.20	0.50	0.20	0.20	1.00	7.29	0.20	0.40	0.20	20.52	3.50	4.50	4.50	120.95	30.12	1.06	-61.80	-9.40
0.91	5.20	0.54	245.71	150.00	0.33	2.72	3.02	0.40	0.20	13.79	225.63	0.20	0.46	2.50	9.67	0.20	0.50	0.20	0.20	1.00	2.11	0.20	0.61	0.20	17.52	4.69	4.50	4.50	176.13	5.00	1.36	-61.50	-9.38
0.20	5.71	1.44	29.82	150.00	0.44	5.36	0.25	0.20	0.20	0.40	3.50	0.20	0.20	0.35	0.76	0.20	0.50	0.20	0.20	1.00	2.57	0.20	0.20	0.20	32.34	9.83	9.98	12.57	201.00	10.80	3.51	-59.00	-9.19
0.76	4.87	0.64	187.26	150.00	0.15	3.16	2.40	0.20	0.20	3.18	169.22	0.20	0.20	0.35	3.33	0.20	0.50	0.20	0.20	1.00	2.01	0.20	1.03	0.20	26.12	5.48	4.50	4.50	149.52	5.00	1.61	-61.00	-9.39
0.49	4.88	1.11	41.26	150.00	0.32	4.01	0.57	0.20	0.20	0.40	10.28	0.20	0.20	0.35	0.54	0.20	0.50	0.20	0.20	1.00	6.60	0.20	0.20	0.20	20.31	11.56	10.14	4.50	212.10	14.74	2.57	-57.50	-9.03
0.68	4.41	1.71	117.82	150.00	0.38	7.55	3.55	0.42	0.20	1.79	64.59	0.20	0.20	0.35	0.87	0.20	0.50	0.20	0.20	1.00	3.10	0.20	0.20	0.20	38.06	9.66	9.57	14.22	195.70	5.00	2.52	-59.10	-9.09
0.46	5.26	0.99	22.27	150.00	0.78	4.98	0.25	0.20	0.20	0.40	9.65	0.20	0.20	0.35	0.49	0.20	0.50	0.20	0.20	1.00	3.94	0.20	0.20	0.20	38.85	9.85	4.50	12.80	118.57	5.00	1.68	-52.70	-8.49
0.54	4.13	0.59	183.20	150.00	0.15	3.14	2.07	0.20	0.20	2.83	162.10	0.20	0.20	0.35	1.57	0.20	0.50	0.20	0.20	1.00	2.04	0.20	0.20	0.20	19.96	5.10	4.50	4.50	99.96	5.00	1.50	-61.20	-9.42
0.83	10.29	0.41	61.52	150.00	0.63	1.25	1.60	0.20	0.20	57.63	63.78	0.20	0.20	1.10	10.57	0.20	0.50	0.20	0.20	1.00	3.68	0.20	0.20	0.20	32.98	15.38	4.50	19.47	326.70	19.00	2.20	-54.50	-8.84
1.85	6.28	2.07	16.93	150.00	0.87	19.81	0.25	0.20	0.20	9.69	62.10	0.20	0.20	0.83	5.23	0.20	0.50	0.20	0.20	1.00	2.66	0.20	0.20	0.20	71.43	10.37	4.50	20.34	290.30	5.00	3.10	-50.60	-8.19
0.85	4.82	0.88	7.72	150.00	0.30	20.26	0.25	0.20	0.20	13.74	7.72	0.20	0.20	0.35	3.29	0.20	0.50	0.20	0.20	1.00	22.97	0.20	0.20	0.20	24.37	8.11	4.50	18.94	127.24	5.00	1.70	-51.90	-8.38
8.77	14.20	4.34	2.00	150.00	0.97	64.78	0.25	0.20	0.20	499.68	3.50	0.20	0.20	0.35	3.83	26.63	0.50	0.20	0.20	1.00	114.52	0.20	0.20	1.14	53.71	6.64	4.50	32.44	199.74	5.00	0.83	-53.50	-8.44
2.04	8.51	1.82	11.98	150.00	0.67	42.61	0.53	0.87	0.20	271.26	1073.33	0.20	0.20	0.99	4.63	1.07	0.50	0.20	0.20	1.00	20.05	0.20	0.20	0.42	72.14	7.95	4.50	19.13	78.26	5.00	1.76	-50.80	-8.21
6.80	9.70	3.75	2.00	150.00	0.96	59.94	0.25	0.20	0.20	1001.69	1577.22	0.20	0.20	0.35	2.33	0.20	0.50	0.20	0.20	1.00	28.35	0.20	0.20	0.20	43.17	7.61	4.50	31.66	163.98	5.00	0.10	-51.60	-8.28
0.75	3.88	0.31	21.91	150.00	0.15	0.19	0.64	0.20	0.20	3.99	24.85	0.20	0.20	0.85	11.26	0.20	0.50	0.20	0.20	1.00	0.25	0.20	0.74	0.20	4.50	5.30	4.50	4.50	149.30	5.00	0.90	-58.20	-8.73
0.88	3.22	0.43	17.58	150.00	0.15	0.28	0.25	0.20	0.20	3.69	43.11	0.20	0.20	0.35	3.72	0.20	0.50	0.20	0.20	1.00	0.70	0.20	0.20	0.20	4.50	1.76	4.50	4.50	157.28	12.22	0.37	-47.70	-7.00
1.30	4.59	0.85	130.55	150.00	0.38	13.37	1.65	0.20	0.20	74.05	323.31	0.20	0.20	1.16	8.46	0.64	0.50	0.20	0.20	1.00	2.99	0.20	1.05	0.20	14.45	3.15	4.50	4.50	80.45	5.00	0.40	-59.80	-9.02
1.21	3.66	0.15	16.08	150.00	0.15	0.18	1.15	0.20	0.20	3.00	127.99	0.20	0.46	1.12	9.86	0.20	0.50	0.20	0.20	1.00	0.25	0.20	0.56	0.20	4.50	4.22	4.50	4.50	62.07	12.88	0.69	-61.70	-9.60
0.43	2.23	0.43	15.19	150.00	0.64	0.33	0.64	0.20	0.20	4.24	98.47	0.20	0.46	0.98	14.09	0.20	0.50	0.20	0.20	1.00	0.85	0.20	0.20	0.20	9.90	3.75	4.50	66.41	318.90	31.55	0.10	-53.50	-8.42
0.78	6.49	0.71	214.14	150.00	0.53	3.33	3.66	0.41	0.20	6.03	179.11	0.20	0.45	1.91	13.41	0.20	0.50	0.20	0.20	1.00	2.31	0.20	0.47	0.20	22.11	5.98	4.50	4.50	130.94	5.00	1.74	-60.80	-9.33
0.20	4.10	0.41	224.44	150.00	0.35	1.57	2.91	0.48	0.20	33.87	251.36	0.20	0.48	1.95	18.25	0.20	0.50	0.20	0.20	1.00	1.72	0.20	1.17	0.20	22.09	6.02	4.50	4.50	251.80	15.39	2.54	-61.30	-9.25
																																-39.10	-6.74
																																-48.80	-8.13
																																-58.20	-9.31
																																-60.90	-9.41
																																-30.70	-6.24
																																-57.00	-8.90
																																-55.30	-9.04
																																-24.60	-5.50
																																-53.40	-8.45

July 2023

								Field Data							Lab Data					
Sample ID	Date	Time	Comments	Lattitude	Longitude	Elevation	Temperature (C)	Conductivity (µS/cm)	DO(%)	DO(mg/L)	Specific conductivity	pH	Bicarbonate (ppm HCO3)	DIC (mg/L)	pH	Conductivity (uS/cm)	Temperature (C)	Detection Limit
CB1	2023-07-05	10:44:00 AM					14.00		92.80		72.10	7.13	13.89	4.15	7.04		21.08	
CB3	2023-07-05	10:53:00 AM					15.20		97.60		41.00	6.46	14.57	th sample to	6.86		20.45	
CB4	2023-07-05	11:20:00 AM					13.70		95.80		73.30	7.22	12.91	3.63	7.11		20.80	
CB5	2023-07-05	11:25:00 AM					15.40		98.00		39.40	6.33	3.38	0.92	6.39		20.40	
CB6	2023-07-05	11:51:00 AM					15.50		98.40		39.50	6.28	3.88	1.12	6.38		20.42	
CB7	2023-07-05	11:40:00 AM					15.50		98.30		38.30	6.36	2.89	0.81	6.28		20.48	
CB8	2023-07-05	11:45:00 AM					113.10		95.80		70.20	7.00	14.00	4.15	7.11		20.65	
CB9	2023-07-05	12:28:00 PM	Formerly CB10				15.80		98.40		37.30	6.09	2.80	3.55	6.13		19.25	
CB10	2023-07-05	12:13:00 PM	Formerly CB11				12.40		96.20		48.90	6.68	5.62	1.78	6.78		20.04	
CB11	2023-07-05	12:20:00 PM	Formerly CB12				15.70		98.30		37.50	6.12	3.24	0.86	6.26		20.13	
CB14	2023-07-05	1:21:00 AM					14.50		97.10		38.00	6.04	5.52	1.57	6.10		19.34	
CB15	2023-07-05	1:34:00 AM	Isotope sample bottle broke				17.00		97.60		35.00	5.64	2.22	0.90	6.01		20.68	
CB16	2023-07-05	1:28:00 AM					16.40		97.70		35.80	5.82	2.18	0.61	6.02		20.33	
CB17	2023-07-05	12:57:00 PM					11.50		96.10		41.40	6.52	2.95	1.07	6.50		20.22	
CB19	2023-07-05	2:21:00 AM					16.90		95.30		35.50	5.67	2.11	0.69	6.02		20.31	
CB21	2023-07-05	11:00:00 AM	Formerly CB2 (CB2-2)				15.30		97.60		40.20	6.33	4.55	1.22	6.37		20.53	
Spring 2	2023-07-05	10:36:00 AM					16.30		97.10		89.80	7.40	26.28	6.89	7.33		20.43	
Spring 6	2023-07-05	11:06:00 AM					13.10		94.40		76.40	6.88	13.80	4.50	6.92		20.51	
MW1A	2023-07-05	1:28:00 PM					11.30	41.70	90.70	9.95	56.20	5.50	1.99	4.59	5.37		20.30	
MW1B	2023-07-05	1:22:00 PM					10.10	80.00	32.00	3.64	111.40	6.50	36.64	11.25	6.77		20.01	
MW2A	2023-07-05	2:03:00 PM					11.70	102.80	16.10	1.74	137.60	6.00	47.29	15.74	6.75		20.26	
MW2B	2023-07-05	1:53:00 PM					11.60	264.80	7.00	0.74	352.60	7.60	241.47	43.00	7.73		19.18	
MW3A	2023-07-05	12:55:00 PM					12.90	175.70	15.00	1.56	227.80	7.50	98.73	25.64	7.42		19.78	
MW3B	2023-07-05	11:43:00 AM					14.00	296.60	12.10	1.22	372.20	7.30	176.07	45.71	7.41		19.85	
Pond 1	2023-07-05	3:00:00 PM					20.70	32.80	95.90	8.60	35.50	4.50	-1.81	0.32	4.54		19.61	
Lake 1	2023-07-05	3:10:00 PM					20.10	31.00	93.00	8.42	33.80	4.50	-1.67	0.54	4.49		19.84	
Lake 5	2023-07-06	3:08:00 AM					16.90		95.30		35.50	5.67	-1.00	1.66	4.87		20.87	
PNA	2023-07-05	2:26:00 PM					17.50	32.20	41.50	3.96	37.30	4.40	-0.69	5.93	4.30		19.27	
PNC	2023-07-05	2:49:00 PM					13.00	34.20	20.70	2.17	44.10	4.50	-1.93	30.78	4.66		19.32	
CB Dam	2023-07-04	3:15:00 PM					15.50		98.30		43.30	7.59	4.61	1.30	6.48		20.29	
CB Upper	2023-07-05	11:15:00 AM					17.70	25.70	65.20	6.21	29.90	5.00	-0.38	1.90	5.04		19.77	
Top Precipitation Collector	2023-07-04	2:03:00 PM											41.16	11.31	7.62		20.33	
Bottom Precipitation Collector	2023-07-04	2:13:00 PM											82.55	21.73	7.84		20.53	
Pumping Well 1	2023-07-06	2:19:00 PM					9.40	757.80	84.70		383.90	7.31	28.64	8.34	7.19		20.28	
Pumping Well 2	2023-07-06	2:26:00 PM					9.80	757.80	78.20		245.10	7.47	32.37	8.73	7.30		20.40	
CB Rain Collector	2023-06-22																	
Rain Water	2023-05-31																	
Xmas Brook	2023-05-31																	
CB River	2023-06-22																	
CB Pumphouse	2023-06-22																	

7Li (KED)	23Na (KED)	24Mg (KED)	27Al (KED)	31P (KED)	39K (KED)	44Ca (KED)	49Ti (KED)	51V (KED)	52Cr (KED)	55Mn (KED)	56Fe (KED)	59Co (KED)	60Ni (KED)	65Cu (KED)	66Zn (KED)	75As (KED)	78Se (KED)	107Ag (KE	111Cd (KE	121Sb (KE	135Ba (KE	140Ce (KE	208Pb (KE	238U (KED	Fluoride	Chloride	Nitrite	Bromide	Nitrate	Phosphate	Sulfate			
ppb	ppm	ppm	ppb	ppb	ppm	ppm	ppb	ppb	ppb	ppb	ppb	ppb	ppb	ppb	ppb	ppb	ppb	ppb	ppb	ppb	ppb	ppb	ppb	ppb	ppm	ppb	ppb	ppb	ppb	ppm			
0.4	0.3	0.3	4	0.3 ppm	0.3	10 ppb	0.5	0.4	0.4	0.8	7	0.4	0.4	0.7	0.6	0.4	1	0.4	0.4	2	0.5	0.4	0.4	0.4	9	0.3	9	9	0.2	10	0.2	δ2H, in ‰	δ18O, in ‰
0.47	5.50	1.49	51.97	150.00	0.82	5.13	0.63	0.20	0.20	1.81	15.23	0.20	0.73	2.99	6.81	0.20	0.50	0.20	0.20	1.00	2.94	0.20	0.20	0.20	42.50	5.81	4.50	12.20	143.88	5.00	2.75	-55.00	-8.49
0.64	3.93	0.69	371.00	150.00	0.22	3.30	4.03	0.49	0.20	9.49	368.42	0.20	0.20	0.72	5.03	0.20	0.50	0.20	0.20	1.00	2.97	0.55	0.20	0.20	14.22	7.98	11.06	150.50	325.40	670.00	15.54	-45.40	-7.08
0.56	5.03	1.08	84.90	150.00	0.47	5.86	0.58	0.20	0.20	0.40	17.40	0.20	0.20	0.35	3.06	0.20	0.50	0.20	0.20	1.00	4.15	0.20	0.20	0.51	25.71	6.84	4.50	13.59	82.66	5.00	2.59	-55.20	-8.81
0.69	3.64	0.63	370.01	150.00	0.21	3.05	4.03	0.49	0.20	10.40	371.21	0.20	0.20	0.72	2.65	0.20	0.50	0.20	0.20	1.00	2.91	0.55	0.20	0.20	27.06	3.88	4.50	4.50	111.53	5.00	0.98	-44.50	-6.97
0.94	3.89	0.65	381.14	150.00	0.29	3.18	4.05	0.48	0.20	11.88	371.15	0.20	0.44	1.12	3.77	0.20	0.50	0.20	0.20	1.00	3.13	0.56	0.20	0.20	14.43	3.90	4.50	4.50	66.49	5.00	0.96	-44.50	-7.04
0.62	3.74	0.63	394.43	150.00	0.19	3.04	3.92	0.49	0.20	12.43	380.29	0.20	0.20	0.35	2.81	0.20	0.50	0.20	0.20	1.00	2.99	0.58	0.50	0.20	19.90	3.86	4.50	4.50	53.44	5.00	0.92	-44.20	-6.98
0.20	4.87	1.21	71.30	150.00	0.39	5.32	0.25	0.20	0.20	1.39	28.14	0.20	0.20	0.35	0.35	0.20	0.50	0.20	0.20	1.00	2.59	0.20	0.20	0.20	39.77	5.64	4.50	19.49	118.63	5.00	2.10	-53.70	-8.34
0.82	3.80	0.59	390.56	150.00	0.31	2.82	4.08	0.50	0.20	16.33	383.91	0.20	0.20	1.00	6.49	0.20	0.50	0.20	0.20	1.00	3.01	0.57	0.48	0.20	13.21	3.71	4.50	4.50	103.72	5.00	0.88	-44.20	-6.99
0.64	4.68	0.75	238.04	150.00	0.25	2.56	1.21	0.20	0.20	2.00	48.75	0.20	0.20	0.35	2.01	0.20	0.50	0.20	0.20	1.00	3.12	0.43	0.20	0.20	34.57	4.97	4.50	15.58	118.88	5.00	1.92	-51.30	-7.95
0.53	2.94	0.45	290.92	150.00	0.17	2.13	2.64	0.20	0.20	11.71	286.05	0.20	0.20	0.35	3.18	0.20	0.50	0.20	0.20	1.00	2.17	0.42	0.20	0.20	15.12	3.77	4.50	4.50	268.70	5.00	0.91	-42.80	-6.71
0.83	3.96	0.62	417.65	150.00	0.47	2.75	4.36	0.43	0.20	15.44	431.36	0.20	0.51	1.62	9.82	0.20	0.50	0.20	0.20	1.00	3.98	0.56	0.20	0.20	21.27	3.97	4.50	4.50	97.05	5.00	0.82	-46.40	-7.38
0.82	4.21	0.59	420.52	150.00	0.30	2.62	5.46	0.65	0.20	43.91	441.61	0.20	1.04	2.22	10.42	0.20	0.50	0.20	0.20	1.00	2.99	0.63	0.57	0.20	23.05	3.31	4.50	4.50	75.05	5.00	0.77		
0.62	3.58	0.59	415.01	150.00	0.19	2.66	4.37	0.55	0.20	34.66	436.80	0.20	0.20	0.84	7.26	0.20	0.50	0.20	0.20	1.00	3.24	0.62	0.48	0.20	11.41	3.49	4.50	4.50	94.98	5.00	0.84	-43.60	-6.87
0.45	4.93	0.54	327.10	150.00	0.31	1.75	1.64	0.20	0.20	1.71	44.94	0.20	0.57	1.27	3.24	0.20	0.50	0.20	0.20	1.00	2.60	0.67	0.41	0.20	19.86	4.77	4.50	12.88	145.90	5.00	1.74	-50.10	-7.79
0.60	3.73	0.59	425.67	150.00	0.20	2.57	4.68	0.60	0.20	48.24	457.73	0.20	0.20	1.23	5.95	0.20	0.50	0.20	0.20	1.00	2.95	0.63	0.60	0.20	18.59	3.29	4.50	4.50	67.93	5.00	0.74	-43.00	-6.66
0.65	3.84	0.66	377.35	150.00	0.22	3.27	4.26	0.48	0.20	9.90	377.61	0.20	0.20	0.72	13.95	0.20	0.50	0.20	0.20	1.00	2.99	0.56	0.20	0.20	22.27	3.86	4.50	4.50	100.02	5.00	1.00	-44.40	-6.97
0.20	4.54	2.08	86.67	150.00	0.57	8.18	3.55	0.74	0.20	2.42	62.41	0.20	0.20	1.57	6.30	0.20	0.50	0.20	0.20	1.00	3.25	0.20	0.20	0.20	29.98	5.18	4.50	15.16	443.30	5.00	1.97	-52.80	-8.12
0.20	5.43	1.44	63.62	150.00	0.36	4.95	1.51	0.20	0.20	3.29	38.82	0.20	0.20	0.35	7.30	0.20	0.50	0.20	0.20	1.00	2.52	0.20	0.20	0.20	26.51	6.78	4.50	19.74	109.77	5.00	3.47	-57.40	-8.78
0.20	5.09	0.89	77.41	150.00	0.47	2.37	0.25	0.20	0.20	17.67	10.17	0.20	0.20	0.35	3.17	0.20	0.50	0.20	0.20	1.00	2.16	0.20	0.20	0.20	42.79	10.24	4.50	15.71	319.00	5.00	2.21	-58.00	-9.28
1.43	4.71	1.80	11.73	150.00	0.68	14.35	0.25	0.20	0.20	10.15	12.46	0.20	0.20	0.96	4.70	0.20	0.50	0.20	0.20	1.00	3.83	0.20	0.20	0.20	37.33	8.99	4.50	20.24	320.80	5.00	2.93	-51.10	-8.28
1.12	4.32	1.03	107.35	150.00	0.38	20.22	1.44	0.20	0.20	17.16	67.11	0.44	0.45	1.12	12.09	0.20	0.50	0.20	0.20	1.00	28.34	0.20	0.52	0.20	16.60	8.70	4.50	27.28	279.30	40.97	2.29	-52.50	-8.44
8.86	12.38	4.41	54.87	150.00	0.98	58.64	0.69	0.41	0.20	952.49	299.16	0.20	0.20	0.35	3.31	43.94	0.50	0.20	0.20	1.00	32.91	0.20	0.20	1.27	35.35	5.59	4.50	11.06	393.10	5.00	0.30	-53.20	-8.49
1.83	7.12	1.79	58.15	150.00	0.74	38.49	2.76	1.03	0.20	879.41	963.52	0.20	0.63	2.87	35.17	1.32	0.50	0.20	0.20	1.00	22.42	0.20	0.47	0.20	61.87	8.88	4.50	11.13	200.56	5.00	2.29	-50.10	-8.12
9.30	10.64	4.38	78.40	150.00	1.28	65.48	2.02	1.06	0.20	1230.84	10029.31	0.20	1.02	3.33	45.93	4.94	1.66	0.20	0.20	1.00	22.95	0.20	1.38	0.20	13.09	6.01	4.50	4.50	60.90	20.14	0.10	-51.10	-8.22
0.20	3.01	0.45	22.22	150.00	0.20	0.31	0.25	0.20	0.20	4.73	46.13	0.20	0.20	0.35	10.13	0.20	0.50	0.20	0.20	1.00	1.72	0.20	0.48	0.20	5.54	5.44	4.50	4.50	53.56	5.00	1.02	-41.40	-5.63
0.20	2.50	0.27	23.98	150.00	0.16	0.17	0.79	0.20	0.20	2.61	35.08	1.03	0.20	0.35	14.08	0.20	0.50	0.20	0.20	1.00	1.17	0.20	0.66	0.20	16.24	3.89	4.50	4.50	330.60	15.77	0.65	-46.30	-6.34
0.20	2.43	0.25	116.42	150.00	0.05	0.27	2.17	0.54	0.20	4.01	368.20	0.20	0.20	0.35	7.74	0.20	1.02	0.20	0.20	1.00	0.72	0.20	1.37	0.20	5.90	2.19	4.50	4.50	67.64	5.00	0.10	-40.10	-6.26
0.95	2.77	0.21	36.87	150.00	0.19	0.23	1.73	0.47	0.20	3.56	44.77	1.25	1.01	2.26	22.51	0.20	0.50	0.20	0.20	1.00	1.37	0.20	1.25	0.20	16.67	2.57	4.50	4.50	76.05	5.00	0.10	-49.90	-7.66
0.20	2.11	0.49	26.28	150.00	0.77	0.91	0.84	0.20	0.20	7.17	94.74	0.20	0.20	1.12	14.47	0.20	0.50	0.20	0.20	1.00	5.83	0.20	0.20	0.20	76.60	4.57	4.50	76.74	838.10	81.81	0.97	-53.70	-8.49
0.20	3.69	0.66	376.49	150.00	0.26	3.32	3.42	0.41	0.20	12.78	286.62	0.20	0.20	0.35	5.00	0.20	0.50	0.20	0.20	1.00	2.98	0.61	0.20	0.20	21.73	3.50	4.50	4.50	243.30	5.00	0.98	-42.70	-6.83
3.57	4.29	0.51	429.47	150.00	0.25	1.76	7.20	0.83	0.20	67.29	542.32	0.20	1.13	2.95	36.41	0.42	0.50	0.20	0.20	1.00	3.93	0.69	6.40	0.20	22.84	3.12	4.50	4.50	365.00	5.00	0.72	-40.50	-6.37
0.20	0.56	0.47	16.88	1051.47	2.80	1.24	0.57	0.20	0.20	22.12	15.00	0.20	0.20	3.36	45.06	0.20	0.50	0.20	0.20	1.00	1.50	0.20	0.20	0.20	9.63	0.99	21.45	4.50	629.00	2821.10	2.14	-12.00	-2.66
0.20	3.94	1.06	61.88	3793.06	13.94	2.74	1.66	0.57	0.20	10.72	51.66	1.74	0.92	18.16	98.79	0.60	0.50	0.20	0.43	1.00	2.97	0.20	0.48	0.20	9.92	5.61	199.92	14.33	1165.10	10158.70	9.18	-19.50	-3.15
1.60	37.24	3.72	2.00	150.00	0.74	15.33	0.25	1.51	0.20	0.40	3.19	0.20	0.20	2.37	15.30	0.20	0.50	0.20	0.20	1.00	3.47	0.20	0.20	0.59	71.63	100.67	76.60	49.41	416.90	5.00	5.60	-55.70	-8.80
1.41	17.22	3.08	5.03	150.00	0.58	16.17	0.59	1.82	0.20	0.40	4.68	0.20	0.20	3.66	21.67	0.20	0.50	0.20	0.20	1.00	1.04	0.20	0.20	1.17	127.61	40.91	25.57	44.02	393.10	5.00	5.46	-55.00	-8.68
																																-31.90	-3.58
																																-81.50	-11.03
																																-58.20	-8.60
																																-55.50	-8.25
																																-54.90	-8.58

Values less than detection limit have been changed to half
Concentrations below detection limit

	mg/L	Other Value (mg/L)
Al	2.9	
As	0.01	ALARA
Ba	2	
Ca	N/A	
Cl	N/A	
Cu	2	
F-	1.5	
Fe	N/A	
Pb	0.005	ALARA
Mg	N/A	
Mn	0.12	AO < 0.02
NO3-	45	0 as NO3- -N
Se	0.05	
SO4	N/A	
U	0.02	
Zn		AO < 5
Na		AO < 200
Cr	0.05	
Cd	0.007	
Sb	0.006	
NO2	3	1 as NO2- -N
pH		7 to 10

4. Charge Balance Error

July 2022

	mEq\L									
Sample ID	Ca 2+	Mg 2+	Na 1+	K 1+	HCO3 1-	CO3 2-	SO4 2-	Cl -	CBE	CBE ABS
CB1	0.193273	0.064843	0.170163	0.007647	0.097744	0	0.025609	0.11197924	0.298833085	0.298833
CB2	0.559359	0.364205	0.21701	0.01041	0.635235	0	0.049552	0.148929569	0.159856165	0.159856
CB3	0.180897	0.059329	0.150067	0.006164	0.09699	0	0.025193	0.111133049	0.259049035	0.259049
CB4	0.301961	0.095207	0.211355	0.010128	0.252603	0	0.050593	0.161340366	0.142278995	0.142279
CB5	0.180398	0.059247	0.156591	0.005627	0.097252	0	0.024776	0.110850986	0.266225172	0.266225
CB6	0.180199	0.058177	0.158114	0.009591	0.083747	0	0.022694	0.108312414	0.308176871	0.308177
CB7	0.170767	0.054392	0.151285	0.005473	0.095547	0	0.021861	0.10803035	0.257637944	0.257638
CB8	0.297769	0.109607	0.215487	0.0133	0.351493	0	0.081824	0.218317209	-0.012013556	0.012014
CB9	0.085783	0.03884	0.159767	0.002046	0.020208	0	0.018946	0.106902096	0.324582548	0.324583
CB10	0.074155	0.036783	0.115704	0.002532	-0.01623	0	0.011035	0.076721293	0.524244057	0.524244
CB11	0.0767	0.039498	0.118792	0.002404	0.000803	0	0.011659	0.077567484	0.450072296	0.450072
MW1A	0.022456	0.013907	0.326885	0.010052	0.112149	0	0.065792	0.169802273	0.035441737	0.035442
MW1B	0.718499	0.143345	0.229928	0.019029	0.583479	0	0.075161	0.184751643	0.136838894	0.136839
MW2A	0.70767	0.059247	0.17573	0.009105	0.610275	0	0.045805	0.148365442	0.083878962	0.083879
MW2B	2.183243	0.257231	0.520057	0.024963	1.818368	0	0.079742	0.170930528	0.181313131	0.181313
MW3A	1.811967	0.150257	0.328711	0.017622	1.207897	0	0.050593	0.264575635	0.205002311	0.205002
MW3B	2.819552	0.33993	0.443415	0.034426	2.239826	0	0.006663	0.168956083	0.201871026	0.201871
Pond 1	0.005889	0.014153	0.122054	0.003606	-0.04713	0	0.007912	0.066284941	0.686717173	0.686717
Lake 1	0.009731	0.020901	0.083167	0.004118	-0.03558	0	0.012492	0.0851832	0.310102609	0.310103
Lake 2	0.008733	0.019914	0.079601	0.002762	-0.03561	0	0.0127	0.083772882	0.291787076	0.291787
Lake 3	0.008583	0.020325	0.081515	0.002788	-0.03135	0	0.012284	0.084054946	0.27061956	0.27062
PNC-New	0.027546	0.044106	0.113311	0.027725	-0.01554	0	0.006038	0.130031309	0.276561645	0.276562
CB Dam	0.188882	0.066735	0.159723	0.006113	0.122983	0	0.026858	0.112825431	0.232103989	0.232104
CB Upstrea	0.068966	0.036042	0.123577	0.002711	-0.00054	0	0.007495	0.071362085	0.494098436	0.494098
Bridge at u	0.073906	0.037688	0.119705	0.004118	-0.00659	0	0.010827	0.076157166	0.490865935	0.490866
Sum (ions)	10.95688	2.203909	4.731713	0.244461	8.238026	0	0.764106	3.157137619	0.197308247	
Average	0.438275	0.088156	0.189269	0.009778	0.329521	0	0.030564	0.126285505	0.197308247	0.197308
Sum (catio	18.13697				12.15927					

November 2022

	mEq/L									
Sample ID	Ca 2+	Mg 2+	Na 1+	K 1+	HCO3 1-	CO3 2-	SO4 2-	Cl -	CBE	CBE ABS
CB1	0.352662	0.164904	0.291521	0.013249	0.224591	0	0.04607537	0.492483	0.037330721	0.037330721
CB2	0.258346	0.100638	0.272861	0.008875	0.0952	0	0.034374349	0.418526	0.077908551	0.077908551
CB3	0.249014	0.098498	0.27895	0.00954	0.096598	0	0.03506142	0.422559	0.068713288	0.068713288
CB4	0.375168	0.125818	0.295523	0.016599	0.254117	0	0.04738705	0.447071	0.041322977	0.041322977
CB5	0.242128	0.095783	0.292434	0.010435	0.339298	0	0.032771185	0.407892	-0.097963886	0.097963886
CB6	0.240082	0.09208	0.275949	0.008568	0.090178	0	0.032625442	0.418075	0.065482834	0.065482834
CB7	0.395978	0.144168	0.290129	0.012584	0.236299	0	0.045305018	0.50464	0.034752033	0.034752033
CB8	0.239483	0.093067	0.322143	0.013377	0.07855	0	0.032063294	0.4161	0.118311029	0.118311029
CB13	0.20011	0.075375	0.274687	0.009412	0.060403	0	0.02596294	0.375991	0.095140549	0.095140549
CB14	0.206198	0.075787	0.255592	0.009003	0.092158	0	0.030439309	0.362762	0.059325387	0.059325387
CB15	0.217576	0.087307	0.277645	0.007366	0.061121	0	0.028398917	0.423293	0.069902137	0.069902137
CB16	0.21538	0.084098	0.269207	0.007366	0.049867	0	0.028919425	0.410938	0.080998552	0.080998552
CB17	0.220121	0.088048	0.269859	0.007903	0.075373	0	0.030709973	0.415057	0.058525302	0.058525302
MW1A	0.072209	0.020407	0.707663	0.011023	0.228299	0	0.063689361	0.237554	0.210136017	0.210136017
MW1B	0.733071	0.138984	0.197392	0.015678	0.665545	0	0.064084947	0.185485	0.084994986	0.084994986
MW2A	0.873247	0.068546	0.182081	0.008236	0.738075	0	0.043160525	0.187008	0.078017958	0.078017958
MW2B	2.385349	0.295248	0.520579	0.021689	2.290012	0	0.05975432	0.160889	0.124218534	0.124218534
MW3A	1.754279	0.13668	0.307354	0.014988	1.710452	0	0.045034354	0.241023	0.051496683	0.051496683
MW3B	2.75363	0.301913	0.384214	0.024963	2.926769	0	0.004247345	0.162356	0.05662442	0.05662442
Pond 1	0.02555	0.101872	0.273513	0.007085	0	0	0.036414741	0.407102	-0.041686039	0.041686039
Lake 1	0.017316	0.051018	0.173164	0.004732	-0.06134	0	0.026191963	0.220404	0.14130347	0.14130347
Lake 4	0.022057	0.083028	0.287084	0.007161	-0.03582	0	0.040037477	0.387555	0.009557471	0.009557471
Lake 5	0.148211	0.068052	0.260681	0.004399	0.009542	0	0.016135748	0.387612	0.076069264	0.076069264
PNA	0.030441	0.074717	0.250329	0.009208	0	0	0.013928795	0.371224	-0.027283689	0.027283689
PNC	0.023504	0.044847	0.106439	0.017494	0.011197	0	0.001894649	0.098356	0.266145944	0.266145944
CB Dam	0.270273	0.103929	0.278646	0.009591	0.101534	0	0.035123881	0.427919	0.079756283	0.079756283
CB Upstrea	0.135935	0.086649	0.279864	0.006957	-0.01731	0	0.026212784	0.413505	0.093358537	0.093358537
CB Pumpin	0.678527	0.239292	1.482051	0.012353	0	0	0.108057464	2.209714	0.019968627	0.019968627
CB Pumpin	0.77943	0.223493	0.72989	0.012533	0	0	0.107495315	1.128734	0.170754227	0.170754227
Sum (ions)	14.11528	3.364246	10.08744	0.322367	10.32071	0	1.14155736	12.74183	0.070742813	
Average	0.486734	0.116008	0.347843	0.011116	0.355887	0	0.039364047	0.439373	0.072523523	0.084036186
Sum (catio	27.88933				24.2041					

May 2023

	mEq/L									
Sample ID	Ca 2+	Mg 2+	Na 1+	K 1+	HCO3 1-	CO3 2-	SO4 2-	Cl -	CBE	CBE ABS
CB 1	0.156452	0.048604	0.17966	0.006185	0.083364		0.031203	0.143762	0.204198432	0.204198432
CB 2	0.157587	0.052276	0.211969	0.007137	0.086009		0.033535	0.154599	0.220200287	0.220200287
CB 3	0.267396	0.118893	0.248493	0.011148	0.378134		0.073121	0.277136	-0.0600008	0.0600008
CB 4	0.289878	0.090403	0.250779	0.012286	0.280292		0.071397	0.304928	-0.01020807	0.01020807
CB 5	0.151505	0.047273	0.187928	0.009892	0.053874		0.029171	0.12498	0.311886153	0.311886153
CB 10	0.136658	0.060594	0.22044	0.00561	0.128376		0.063052	0.300113	-0.07459128	0.07459128
CB 11	0.146552	0.045782	0.200326	0.008463	0.058327		0.029515	0.142566	0.270319516	0.270319516
CB 12	0.144987	0.045049	0.197548	0.00682	0.055639		0.028193	0.138039	0.279961238	0.279961238
CB 14	0.13115	0.045786	0.226872	0.008602	0.039012		0.033918	0.176405	0.246429998	0.246429998
CB 15	0.129457	0.038816	0.170301	0.004996	0.057432		0.022049	0.098725	0.316926596	0.316926596
CB 16	0.135534	0.044427	0.226033	0.008365	0.073001		0.028405	0.13231	0.278736195	0.278736195
Spring 1	0.199972	0.091011	0.212313	0.008219	0.213803		0.053492	0.326147	-0.074145245	0.074145245
Spring 2	0.376704	0.140514	0.191965	0.009597	0.398077		0.052371	0.272363	-0.002797549	0.002797549
Spring 5	0.248362	0.081548	0.228677	0.019882	0.14346		0.03502	0.277723	0.118169532	0.118169532
MW1A	0.062134	0.033404	0.447396	0.015995	0.064579		0.045823	0.433724	0.013419798	0.013419798
MW1B	0.988606	0.170012	0.273249	0.022372	0.639271		0.064476	0.292429	0.186932405	0.186932405
MW2A	1.011139	0.072354	0.209811	0.007681	0.576345		0.03539	0.228714	0.215059516	0.215059516
MW2B	3.232581	0.35738	0.617755	0.024928	1.548716		0.017325	0.187296	0.414185702	0.414185702
MW3A	2.126224	0.150118	0.370374	0.017018	1.118995		0.036746	0.2241	0.317514538	0.317514538
MW3B	2.990952	0.308793	0.421745	0.024474	1.337797		0.001575	0.214552	0.413601189	0.413601189
Pond 1	0.009662	0.025259	0.168581	0.004553	-0.01291		0.018684	0.149423	0.145527409	0.145527409
Lake 1	0.014009	0.035293	0.139904	0.004789	-0.00798		0.007649	0.049705	0.594240177	0.594240177
Lake 5	0.667179	0.070288	0.199536	0.009593	0.797187		0.00842	0.088732	0.028386346	0.028386346
PNA	0.009178	0.023236	0.159026	0.004082	-0.01648		0.014268	0.119005	0.252074502	0.252074502
PNC	0.016594	0.035265	0.096906	0.016491	-0.02519		0.003009	0.105732	0.328371312	0.328371312
CB Dam	0.166386	0.058509	0.282162	0.013557	0.103236		0.036144	0.168759	0.256380255	0.256380255
CB upstrea	0.078281	0.033332	0.178533	0.00901	0.008389		0.052857	0.169667	0.128744082	0.128744082
Sum (ions)	14.04512	2.32422	6.518281	0.301745	8.180755		0.92681	5.301633	0.233523992	
Average	0.52019	0.086082	0.241418	0.011176	0.302991		0.034326	0.196357	0.197019342	0.213444745
Sum (catio	23.18936				14.4092					

July 2023

	mEq/L									
Sample ID	Ca 2+	Mg 2+	Na 1+	K 1+	HCO3 1-	CO3 2-	SO4 2-	Cl -	CBE	CBE ABS
CB1	0.256004	0.122373	0.239244	0.02095	0.22757	0	0.057256	0.163916	0.174586	0.174586
CB2	0.163328	0.053909	0.16714	0.005628	0.074517	0	0.020737	0.108747	0.313135	0.313135
CB3	0.164543	0.057125	0.170872	0.005741	0.238815	0	0.32361	0.225191	-0.3283	0.328304
CB4	0.292533	0.08866	0.218804	0.012086	0.211547	0	0.053889	0.192827	0.14371	0.14371
CB5	0.1522	0.05211	0.158228	0.00541	0.055421	0	0.0205	0.109393	0.330106	0.330106
CB6	0.158937	0.053656	0.169286	0.007481	0.063563	0	0.019996	0.109994	0.335913	0.335913
CB7	0.151848	0.051442	0.162635	0.00493	0.047312	0	0.019142	0.108843	0.358066	0.358066
CB8	0.265466	0.099873	0.211651	0.009869	0.229502	0	0.04375	0.15914	0.151549	0.151549
CB10 (spri	0.127778	0.061762	0.203618	0.006286	0.092096	0	0.040037	0.140163	0.189281	0.189281
CB11 (d/s	0.106329	0.0369	0.127964	0.004223	0.053082	0	0.018851	0.106332	0.214138	0.214138
CB12 (u/s	0.140774	0.048864	0.165221	0.007927	0.045904	0	0.018314	0.104626	0.364809	0.364809
CB14 (righ	0.137224	0.051096	0.172452	0.011917	0.090434	0	0.017039	0.111988	0.258766	0.258766
CB15 (left	0.130784	0.04857	0.182923	0.00767	0.036364	0	0.01593	0.093394	0.43492	0.43492
CB16	0.132683	0.04827	0.155767	0.004752	0.035748	0	0.017518	0.098356	0.385021	0.385021
CB17 (trib	0.0874	0.044727	0.214269	0.007814	0.048274	0	0.03624	0.134623	0.235588	0.235588
CB19	0.128088	0.048274	0.162401	0.005104	0.034584	0	0.015399	0.092714	0.413449	0.413449
Spring 2	0.40809	0.171451	0.197564	0.014459	0.430773	0	0.040949	0.1461	0.123274	0.123274
Spring 6	0.247089	0.118571	0.236299	0.009139	0.226184	0	0.072296	0.191276	0.110225	0.110225
MW1A	0.118341	0.072975	0.221397	0.011923	0.032562	0	0.04608	0.288949	0.072007	0.072007
MW1B	0.71601	0.147976	0.204925	0.017368	0.600433	0	0.061001	0.253485	0.085628	0.085628
WM2A	1.009175	0.084964	0.18778	0.009793	0.775108	0	0.047697	0.245463	0.09468	0.09468
MW2B	2.926284	0.362958	0.538377	0.024982	3.957471	0	0.006221	0.157755	-0.03372	0.033715
MW3A	1.920754	0.147364	0.30964	0.01902	1.618036	0	0.047691	0.250453	0.111431	0.111431
MW3B	3.267857	0.360796	0.462633	0.032839	2.885594	0	0.002927	0.169388	0.148456	0.148456
Pond 1	0.015537	0.037149	0.130965	0.005174	-0.02969	0	0.021312	0.153524	0.130793	0.130793
Pond 2	0.008353	0.022445	0.108947	0.004208	-0.02741	0	0.013569	0.109836	0.199891	0.199891
Lake 5	0.013679	0.020728	0.105743	0.001296	-0.0164	0	0.002626	0.061721	0.493682	0.493682
PNA	0.011496	0.016911	0.12063	0.00482	-0.01139	0	0.001763	0.072456	0.420077	0.420077
PNC	0.015288	0.040444	0.091961	0.019627	-0.03161	0	0.020158	0.128844	0.175369	0.175369
CB Dam	0.165558	0.054088	0.160339	0.006727	0.075587	0	0.020477	0.098745	0.330002	0.330002
CB Upper	0.087674	0.042353	0.186565	0.006423	-0.00624	0	0.014974	0.088004	0.539064	0.539064
Top Precip	0.061758	0.039065	0.024208	0.071726	0.674513	0	0.044472	0.027876	-0.58297	0.582973
Bottom Pr	0.136798	0.087214	0.171487	0.356529	1.352882	0	0.191126	0.158303	-0.38718	0.387185
Pumping \	0.765131	0.305772	1.619922	0.018973	0.469392	0	0.116502	2.83963	-0.11666	0.116657
Pumping \	0.807165	0.253229	0.748998	0.014814	0.530537	0	0.113619	1.153812	0.007244	0.007244
Sum (ions)	15.29795	3.354065	8.710853	0.777629	15.09106	0	1.623669	8.655866	0.051763	
Average	0.437084	0.09583	0.248882	0.022218	0.431173	0	0.046391	0.24731	0.168458	0.246605
Sum (catio	28.1405				25.37059					